Reply to Reviewer comments on
"Extending the Modular Earth Submodel System (MESSy v2.55) model hierarchy: The ECHAM/MESSy idealized (EMIL) model set-up" by Hella Garny et al.

We thank all reviewers for their very valuable reviews of our manuscript, which led to a major revision of the paper, as detailed in our response (blue) to the individual reviewer comments (black, italic) below.

In the process of the revision, we discovered an inadvertently introduced modification to the original equilibrium temperature set-up. In the formulation of the „Held-Suarez" tropospheric equilibrium temperature function, used in all the simulations presented in the manuscript, the modified formulation led to a weaker vertical temperature gradient in the tropics. We corrected the formulation to the standard set-up in the model implementation, and repeated a number of simulations. In particular the benchmark simulations presented in Section 3 are now performed with the standard set-up to ensure comparability to earlier studies. To study the sensitivity of the results on the modified versus standard set-up, a number of additional simulations was performed, and the simulations with the differing set-ups are presented in concert in Section 4.
Most of the results are qualitatively unchanged with the standard versus modified model set-up. One major difference of the two set-ups is the strength of the response of the tropospheric jet to stratospheric polar vortex changes, and we added a new subsection to discuss this result (see new Section 3.3).

Edwin Gerber (Referee)

The authors document a new idealized model configuration within the ECHAM/MESSy modeling framework, and demonstrate how it can be used to investigate open questions in the climate sciences, namely chemistry-transport interactions and the monsoonal circulation. I believe that this work is timely and important, and would be of interest to GMD readers. I therefore recommend publication pending consideration of the comments/suggestions below. As my identify might be obvious given my familiarity with the system, I'm signing this review. Ed Gerber

Thank you, Ed, for your very helpful suggestions to improve our manuscript, that we greatly appreciate.

General comments

1) The authors compare the performance of EMIL against a number of benchmark cases that are in the literature. It would be ideal, however, if we could move beyond the "picture norm" for these comparisons – at least in the future. Could you publish the data for these results (or incorporate it within the ECHAM-MESSy distribution), so that in the future, other groups could check their models against yours? The best standard would be to determine whether your integrations are consistent/inconsistent with other benchmark integrations, within the sampling uncertainty. I believe that data can be archived through Zenodo.org, or other structures. You could just provide the zonal mean time mean data needed for the figures. Another option would be to include the key benchmarks as test cases within ECHAM/MESSy, something that could easily be reproduce by another group. Could you provide a citable link to the model and the required parameter scripts? (That is, a frozen version of the model, as was used to produce this paper, ideally with the same run scripts that you used.) I appreciate that the supplement provides all the parameters, but it would still involve a lot of work (and hence many chances to make a mistake) to reproduce this exactly.

Thank you for this suggestion, we agree that it would be very beneficial to be able to do quantitative comparisons of model simulations in the future, rather than the comparison to published Figures, as we have done in our paper. Indeed, having data for comparison available would have likely prevented us from using the inadvertently modified model set-up for the last 3.5 years, as we likely would have discovered the above mentioned differences much quicker.

Thus, we decided to provide the simulation data as freely available data set (via Zenodo), to enable future users to reproduce the analyses presented in the paper.
The doi to the data set is inserted in the paper in the “data availability” section.

The ECHAM/MESSy code is available upon registration as MESSy user, and the next MESSy release (v2.55) will include the here described implementation of the idealized set-up, together with a sub-set of the namelists for the simulations presented here. Thus, the user will be able to repeat the simulations. Further, to ensure reproducibility, we include now a table with all simulations and information on the set-up (new Table B1), and further the supplement was improved to make the transition from the parameters in the presented Equations to the namelist parameters easier for future users (see improved Tabels 1-3 in supplement, see also answer to comment 3 below).

2) I appreciate that the authors have striven to find a balance between detailing a new model set-up for others to use, and presenting new results. I felt that the test cases that were shown at the end in section 5 were very interesting, but could have been more developed. To provide more space, perhaps the earlier sections could be condensed? (The reader might also be a bit exhausted by the time they reach these really interesting results!) For example, there are a lot of equations and parameters defined in this study, many which are specified in other papers (but also many of which are new). I think some of this detail could best be put in an appendix (e.g., in sections 2.1.1, 2.1.2 and 2.1.3), allowing you to move more quickly to the results.

Thank you for this excellent suggestion, we followed your advice and moved all equations to a new Appendix (Appendix A), and only kept a short description in Section 2, in which we particularly stress which formulations are new.
As we have expanded the results on troposphere-stratosphere coupling, we refrained from adding additional material to Section 5, also because we plan future publications for example on the idealized monsoon circulations.

3) It would help the reader to have a table that defines all the parameters in one place. It would also help you catch any parameters that are multiply defined. One example is k_max, which appears in the equations (8) and (9) with distinct values. k_damp is also defined inconsistently between these two equations (though any reasonable reader would understand what is meant). The parameter \delta\phi also appears in multiple equations, e.g., (5) and (16).
Finally, I noticed that \sigma is sometimes used to refer to a vertical coordinate (p/ps), and at other times used width (where I appreciate the motivation is to connect it to the variance of a Gaussian). It might be good to adopt a consistent notation, where \delta is always used for width parameters – but again watching out to make sure all parameters are uniquely defined. (This said, I know that these parameters came from multiple papers in the literature, where the other authors were not consistent with each other!)

Thank you for spotting the inconsistent naming of the parameters, we realized the parameters were also not assigned to the namelist variables in a straightforward way. To address the comment and clarify parameters, we:
- made sure to name parameters consistently and uniquely by following your advice to use sigma for the vertical coordinate and delta for width parameters, and by adding superscripts to variables used in multiple equations (see equations A1-A16).
- added to the Tables in the Supplement (Table 1 to 3) detailed descriptions of the namelist parameters, including default values and the corresponding symbol in the defining equations A1-A16. Thus, the information on the default values is removed from Appendix A, enhancing the readability of this section.
- added a table with all simulation details as Appendix B.

4) The paragraph spanning from page 3 line 28 to page 4 line 2 is very interesting, but seems out of place in the introduction. I would consider pushing this to final section, where you could present it as the next step in your research program.

Good suggestion, the paragraph is moved to the final paragraph of the paper.

5) Finally, the topic of regimes comes up quite prominently in section 4. I think this is a very interesting (albeit sometimes frustrating) result that could be mentioned in the abstract and introduction. I think these regimes have simmering in idealized models for sometime: as detailed by Gerber and Polvani (2009), the original PK02 result is so dramatic precisely because of a regime switch between their \gamma 2 and 4 integrations. Chan and Plumb (2009, DOI: 10.1175/2009JAS2937.1) and Wang et al. (2012) discuss this in more detail. The presence of regimes is interesting: if such a thing existed in our atmosphere, we could be in for surprises with global warming (or perhaps when the planet enters an ice age). If it is an artifact of these idealized models, however, it's something that the dynamics community should be wary of. It could lead to unphysical parameter sensitivity or results that are qualitatively disconnected from the real atmosphere, breaking the link we'd hope to establish through model hierarchies.

We agree that the regime behavior in the idealized models is a very interesting result, and we agree that it requires careful evaluation whether those regimes are at all relevant for our real atmosphere. Inspired by your comment, we analyzed the regime behavior in our model simulations more closely, which led to the discovery of the modified implementation in the equilibrium temperature (see above). The modified equilibrium temperature, with lower tropical upper tropospheric temperatures, led to an equatorward shift of the tropospheric jet (in agreement with studies prescribing diabatic heating in the upper tropical troposphere), and interestingly the response of the jet location to stratospheric forcing appears to be strongly damped in this set-up compared to the stndard equilibrium temperature (see new Fig. 6 (left)). We added a new subsection (Section 3.3) to the paper to discuss the stratosphere-troposphere coupling and the regime behavior of the tropospheric jet location. The changed tropospheric state in the simulations with modified set-up appears to inhibit the regime-like behavior of the tropospheric jet, possibly because the jet is located further equatorward in the basic state. Thus, while the general result that the tropospheric response is sensitive to the prescribed tropospheric equilibrium temperatures is in line with the study by Chan and Plumb (2009), the reason for the damped response seems to be a different one (in the simulations by Chan and Plumb (2009), the jet was rather located further poleward in the basic state). However, the dynamical reasons for this behavior remain to be analyzed in detail, which is beyond the scope of the present paper.

Moreover, we want to point out that next to the regimes in the location of the near-surface jet, the regimes we had addressed so far in the paper are regimes in the polar vortex strength. We added more discussion on the polar vortex regimes in Sections 4.1-4.2 (including appended Figures of probability distributions, new Figs. C1-3). More detailed analysis of the polar vortex regimes is part of ongoing work that we plan to publish in a follow-on paper.

Overall, the following changes with respect to discussion of the regimes and of stratosphere-troposphere coupling were made:
- added statement to Abstract
- added paragraph to Introduction
- new Section 3.3 and new Fig. 6
- added new Fig. 12, showing relation of tropospheric jet location and stratospheric polar vortex strength, and Figures C1-3 with probability distribution functions of polar vortex strength and free tropospheric and near-surface jet location, and discussion thereof in Sections 4.2 and 4.3
- added paragraph with discussion to Section 6

Specific comments (largely typographical) by page:line number
1:1 Consider "As models of the Earth system grow in complexity, a need emerges to connect them with simplified systems through model hierarchies in order to improve process understanding."
Done
1:3 consider cutting "with the aim"
Done

1:6 Would you consider ECHAM/MESSy a "model", or rather a "framework" which allows you to build many different models.
Good point, MESSy is definitely a framework, ECHAM/MESSy is one instance of this framework. We decided to change „model“ to „framework“ here.
1:10 Consider "Test similations with EMIL reproduce benchmarks provided by earlier dry dynamical core studies."
Done (and changed title of Section 3 accordingly to „Model benchmark tests“).
1:19 What do you mean by "the ability to simulate dynamical systems"? Dynamical systems in the broadest sense is a whole field in mathematics. Perhaps you mean "the ability to simulate qualitatively realistic dynamical variability of the circulation"
True, this was a misnomer, we rephrased to „circulation systems“.
1:22 Consider something like "Earth system models continue to incorporate more processes to enable a more complete simulation of the climate system, and thus produce the best possible climate projections. In practice, this increases the complexity of model codes as new compartments are added to represent new processes." I'm not sure if you need that second sentence; my thought was that the goal is to increase the range of processes that are simulated, and this is effected in practice by adding more compartments, modules, etc..
Done, thanks for the suggestion, we decided to keep the addition on the compartments.
2:9 stray space: "hereafter) ."
Done.
2:13 I think the upper level drag is only in the PK02 set up, and not a part of the original HS94 configuation.
True, removed „and upper level“ here.
2:16 consider a paragraph break before "The functions…"
Done.
2:21 "to idealized heating that mimics the thermal response to CO2 increase" I think "climate change" is the response, not the forcing!
True, and changed.
2:26 "motivates one to include"
Changed to „motivates the expansion of ...“
2:29 Jucker and Gerber (2017) were not the first/only one to do this. Consider also referencing: Merlis, T. M., T. Schneider, S. Bordoni, and I. Eisenman, 2013: Hadley circulation response to orbital precession. Part I: Aquaplanets. J. Climate, 26, 740–753,doi:10.1175/ JCLI-D-11-00716.1. Tan, Z., T. A. Shaw, and O. Lachmy, 2019: The sensitivity of the jet stream response to climate change to radiative assumptions, J. Advan. Mod. Earth Sys.,10.1029/2018MS001492.
Thanks for pointing those references out, we added them here.
2:35 Here and throughout the text, the quotes seem to be reversed. Perhaps this is set by the journal, but I am used to “hello” as opposed to ”hello“
Thanks for spotting this, and corrected.
3:19 consider "allows the creation of model hierarchies"
Done.
3:20 consider "Earth-system model. Any developments…"
Done.
5:9 I found "idealzied localize contrained" to be awkward. Consider just "forced by a simple, localized heating that…"
Done.
eqn (1) In HS94 and other papers, it's usually just T_{eq}
Done, replaced throughout the paper.
5:30 This was a point where I feel you've lost the balance on providing enough technical advice without making the paper too long. Do you need to describe an option that "physicaly of little use" eqns (204) To make the paper more concise, you could refer the reader to HS94. I appreciate that equation (2) is modified by the inclusion of the \epsilon sin(\phi) term; this was documented by equations A3 and A4 in PK02. A happy medium might be to reference past work in the paper, highlighting your modifications, and including equations in an appendix.
As detailed above, the section has been reworked by moving equations and details to the appendix, while only a general description is left in the main part of the paper. Thanks for the suggestions.

5:19 T_{US} isn't defined in the paper. The reference is: U.S. Standard Atmosphere, U.S. Government Printing Office, Washington, D.C., 1976. (Which I appreciate isn't so easy to find!)
Thanks, and added.
eqn (6) Aditi Sheshadri did something like this in her 2015 paper, https://doi.org/10.1175/JAS-D-14-0191.1. There she lowered the start of the vortex to 200 hPa. That said, I appreciate the more thorough investigation of the transition height in this study!
Thanks for pointing this out, we added a sentence in section 4.2.
Figure 3 and surrounding discussion. It is interesting that the jets shift equatorward when you move from the T63L19 to the T42L90 integrations. I suspect the vertical resolution plays a more important role her than you might suspect. This is consistent with the behavior of GFDL's spectral core, where the jets also shift equatorward when the vertical resolution is increased. See Fig. 4 of Gerber et al. (2008), https://doi.org/10.1175/2007MWR2211.1. This doesn't seem to happen in finite difference or finite volume based cores. [This said, I don't mean for you to add another citation; I think you've already been very generous in referencing my past work.]
Interesting that there is a similar behavior in the GFDL model. Newer results of ours also indicate that the vertical resolution might be more important here than we had assumed. We changed the text to „The jets are shifted equatorward in the T42L90MA resolution, and eddy variance is generally reduced. This is likely a combined effect of lower horizontal and higher vertical resolution, in agreement with Wan2008.".
11:13 consider a paragraph break after PK02.
We chose to keep the text in one paragraph as still the same Figure is discussed.
11:14 (namely GFDL's spectral dynamica core)
Done.
Figure 5: the caption on this figure could be expanded to help a reader who's skimming the paper, for instance, defining the key parameters p_{Tw} and \gamma that are being used. I'll admit I had to remind myself what p_{Tw} represented.
Done.
13:16 Along the lines of my general comment on the "picture norm", it would be ideal to be more precise about what you meant by negligible. I think you mean that it is small relative to uncertainties in the cliamatology with resolution (i.e., T63L19 vs. T42L90), but you could also define it relative to sampling uncertainty (i.e., it would take inordinately long integrations for the difference to be significant above sampling noise.)
True, the statement on the differences due to the different sponge set-up was rather vague so far, and not based on a statistical evaluation. We added a significance test on the differences, to clarify whether the differences are negligible with respect to sampling uncertainty. We based the t-test on slices of 30-day means, assuming that there is no correlation between those 30-day time-slices (given a decorrelation time-scale in those simulations of about 30 days, this should be about right). The addition of the significance test revealed a weak (significant) downward extension of zonal wind differences into the troposphere, that we had not noticed so far. We rewrote the description of the differences to be more precise and quantitative.
Figure 6 and discussion. I appreciated this portion of the paper, but a a quick question: is one month of austral hemisphere gravity wave drag enough to nail down the effective damping rate in models? I don't have a good sense how much this rate varies. I assume this includes both orographic and non-orographic drag? Would the effective rate be much different in the boreal hemisphere during winter? I think it would help to expand the caption, to explain that GWD/u provides an effective damping time scale of the winds when using a full gravity wave drag scheme.
True, only one month of data for one hemisphere was a very thin data basis to argue with. The „effective damping time-scales" for both the NH and SH are added to the Figure now, including values from 50 winters in each hemisphere. There is considerable variability between different winters, and the damping is on average stronger in the SH (possibly because of the lower planetary wave activity?). Overall, the chosen damping time-scales in the new sponge layer implementation lie well within the variability. We also added text to the legend to be more clear.
15:4 "cannot"
Done.
Figure 8 and following figures. You could possible color the dashed curves which show the equilibrium profiles, to make the comparison with their respective \gamma's easier. For Figure 8 specifically, please specify the location of this profile. Is it right at the pole?

Done (colored dashed lines for Figures with multiple T_eq values).

16:7 consider a paragraph break after \gamma.

Obsolete due to re-writing of paragraph (emphasizing on vortex regimes).

17:3 In Wang et al. (2012), I think we had to grapple with this same regime behavior. The model switch abruptly from a state with active stratospheric variability and a strong residual mean circulation (which allows the temperature to deviate substantially from T_eq) to a state with an very cold, stable vortex near "radiative" equilibrium. In Wang et al., this regime change was associated with a substantial change in the position of the tropospheric jet. Does that happen here?

Yes, and the tropospheric jet shift is discussed in more detail now in Section 4.2 (new Fig. 12 and discussion thereof). Whether the stratospheric polar vortex regime shift and the tropospheric jet location regimes are (necessarily) connected is, to my understanding, a question to be clarified.

17:28 "these two simulations"

Obsolete, as we removed old Fig. 10 (climatologies), as we felt that they do not add much value, and wanted to compensate for the new additional Figures.

Figure 10 Here you are showing results from integrations which exhibit multiple regimes. Based on past experience (e.g., Wang et al. 2012), regime transitions can introduce very long time scales, as the model switches between states. You can see this of this Figure 5 of your text, which corresponds to pTw=400, gamma 2 integration shown in the right panel (I think.) Therefore, you have to be very careful in establishing convergence. Earlier in the text you suggested that runs were done for 1825 days; it seems that you have longer runs (3000 days are shown in Fig. 5), but I'm not sure that would be sufficient. It would be good to check/comment on the sampling uncertainty in these climatologies.

Agreed, and indeed we find very long time-scales in the simulations with regime transitions (the simulation with gamma = 2 and pTw = 400 presented in old Fig.5 has a decorrelation time scale of ~100 days). We agree that an integration length of 1825 days is thus far too short to establish convergence (indeed, for a simulation with regime transitions, convergence might be never reached). We commented on this issue at the beginning of Section 3, and further in Section 4.2. We have extended the newly simulations (with the standard set-up, see top) to ~10000 days to test for the robustness of the results, but are not able to extend all simulations to this length. However, the new extended simulations do show a generally similar behavior than the old (short) simulations, letting us believe that the sampling uncertainty does not influence our conclusions majorly.

Figure 12 and discussion. I suspect that the strength of the overturning (difference between T and T_eq) near the model top will be dominated by the drag layer. Hence, it's likely to be determined by \gamma: if you force a stronger vortex, you need a stronger drag. At lower layers, the strength of overturning is dominated by "wave pumping", and so the resolved circulation. I worried about this a lot in preparing my 2012 paper, but convinced myself that in the mid-to-upper stratosphere, the differences in the residual circulation in response to changing gamma were still being dominated by the waves, and so not an artifact of the sponge layer. I'm not exactly sure how far down you need to go to be free of the sponge layer, but perhaps 10 hPa would be a better choice than 1 hPa? This would be supported by Figure 7, where you find that the spong layer has a negligible impact below 10 hPa. I'd also be curious to see if the nonlinearity in the vortex shown in Figure 11, bottom left, shows up in the overturning at 10 hPa in the model with heating.

Thanks for pointing this out, and we decided to change the figure to show the 10 hPa results, which also provide more interesting insights – as you suspected, the non-linearity in the vortex is in agreement with the deviation from T_eq at 10 hPa.

22:18 consider a paragraph break after "high."

Done.

22:19 consider "high latitudes (north of 60N), driven by the strong wave dissipation that effected the SSW; see the red line in the top panel of Fig. 13. This transports …"

Done.

22:22 consider "latidues, evident in Fig. 13 ... 15 ms-." (no paratheses). I'd also consider breaking the paragraph after this sentence.

Done.

22:29 Isolated from what? Consider cutting "in an isolated manner," or to be more specific, e.g., "independent of the annual cycle" or "isolated from all other chemical processes".

Moved sentence to the end of the section, and added more specific statement.

Figure 13 Consider reworking the caption, as you first refer to the middle panel. It might also be nice to include a second axis on the top panel, or to make "w[10ˆ-5 hPa]" in red*
Reworked figure, and done.
23:1 Consider a paragraph break after "is steep."
We chose to keep the text in one paragraph as still the same Issue is discussed.
23:3 "downwelling is maxized at the"
Done.
23:4 same as above
Done.
24:10 consider a pargarph break after "state."
Done.
24:17 10ˆ20 J sounds like a lot, but could you provide some context? Say, what is the effective heating rate per square meter (W/mˆ2), which could be more easily compared to solar or precipitation forcing. With hope this number is in the ball park for what you'd expect from monsoon precipitation.
Thank you for this comment. We added the following sentence to the text: „This heating is of the same order of magnitude as the idealized heat source of 6×10^{19}\unit{J} prescribed in Siu and Bowman (2019) to model the North American monsoon anticyclone (see their experiments 5a-5e).” Keeping in mind e.g. that the Asian monsoon anticyclone is clearly more pronounced than the North American monsoon anticyclone, the higher energy input in our study seems reasonable.
24:19 "produced in response to the additional heating"
Done.
24:23 consider a paragraph break after "respectively.)"
Done.
24:26 Perhaps the anticyclonic centers could be marked/labeled in the figure.
Done.
24:30 You could break the paragraph after "2016).
Done.
24:30 Consider. "An example of eastward eddy shedding was observed during the second period, as displayed on the right of Fig. 16. This phenomenon has been previously investigated…"
Done.
25:7 Your summary opens with a hard sentence to parse. Consider from line 8"...model system is documented. The set-up, denoted EMIL (explain the acronym), is shown to perform consistently with established dry dynamical core benchmarks, both earlier configurations of the ECHAM core, and those developed by other modeling centers."
Thanks, and Done.
25:26 "used setups. The polar"
Done.
26:1 This is an interesting result, as we see this coupling in observations (i.e., with the ozone hole, or following an SSW). It is my understanding that the tropospheric state of the Lingren et al. (2018) model is substantially different, and might explain why does not couple to the stratosphere. As you have shown in Figure 10 (right panel), for instance, easterlies are generated in the UTLS region of the winter hemisphere.
We added substantial discussion of the tropospheric jet response in the different set-ups of the model, mentioning also that from observational evidence we expect a vertically coherent response of the tropospheric jet (which is not seen in the „Lindgren“ set-up).
26:3 consider "we present, as a proof-of-concept, a"
Done.

Reviewer Name: Penelope Maher

Summary of the Review

This manuscript describes the implementation of the Held–Suarez configuration, with the Polvani–Kuchner amendment for the stratosphere, within the ECHAM/MESSy modelling framework. From the model description, it seems the model has been implemented in a modular nature which is a credit to the modelling effort (this can be a development nightmare otherwise). The manuscript has a well described parameterisation equation set, and has tested the relevant parameter spaces for the tunable variables and compares their results with the literature. The new model set-up is then used, as a proof of concept, for looking at how CFCs impact the polar vortex and monsoon circulation.

Thank you for the positive description of our modeling efforts.

Unfortunately, we realize that a general misunderstanding arose: in the model version we describe in this paper, it is possible to analyze the impact of dynamical variability and forced changes ON tracer distributions, including diagnostic chemical tracers as shown for the CFC example (Section 5.1), but NOT the impact of e.g. CFCs on dynamics. No feedback of the chemical tracers on dynamics exists currently in the model.

Thanks to your following comments and to avoid this misunderstanding, we reworked the model description and motivation (in Abstract, Introduction and Summary), as detailed below.

In these regards the manuscript is both novel and interesting. There were, however, a number of things that I was confused about and that need further clarification or description. I also feel there are a number of figures that could benefit from further work. This manuscript is well suited for publication in GDM, is written in a way consistent with the journal style and with further revision I believe it will be suitable for publication in GMD. In this review I have used the notation "PxLy" and this should be interpreted as page x and line y.

2 Major Comments

1. The introduction is well motivated in terms of the using idealised models in general (the philosophy of idealised models), however, I think more introductory material is needed for describing the need for adding chemistry into the hierarchy and what these styles of models are used for. For example, it may not be clear to readers if/why chemistry models are needed to investigate the polar vortex or monsoons.

The motivation to implement the idealized model set-up in the framework of a chemistry-climate model system is, for the current set-up, the ability to study the impact of idealized dynamical variability and forced changes on to the distribution of (chemically active) tracers. This model set-up is motivated by a large number of research questions on the distribution of chemical substances in the atmosphere, e.g. the question how changes in the circulation in a changing climate will affect stratospheric ozone, and how important the monsoon systems are in transporting tracers from the troposphere to the stratosphere. As detailed in the paper, it will be the next step to couple the chemistry and dynamics, a task that will be possible to perform within the chemistry-climate model system framework we use. This second step is motivated by the research question on how circulation-induced anomalies in radiative trace gases (e.g. ozone and water vapor) feed back on the dynamics, a question that is relevant both on climate time-scales as well as in intra-seasonal timescales (e.g. during sudden warmings).

We added the motivation for the inclusion of diagnostic (chemical) tracers in the Introduction (see p3, line 16ff), and motivation for the next step in the hierarchy (including the coupling), that we moved to last paragraph of the paper (see also Ed Gerbers major comment 4).

2. I felt the abstract, introduction and conclusions did not sufficiently describe what is currently possible within the ECHAM vs MESSy models. I initially assumed this paper was the first to implement the Held-Suarez test case within ECHAM but realised my mistake on page 10 when the authors described the study of Wan et al 2008. I think what options are (or not) previously

available needs to be said much earlier or more clearly. I understand the RELAX submodel is new (ie implementing the parameterisations of newtonian cooling and drag), but were changes to the dynamical core needed or where they already available (if it was available, is it the same/similar as Wan et al 2008?)? I am confused by what is new and what was existing in ECHAM.
Thank you for pointing out the fact that we need to state much clearer the difference of our model set-up, i.e. using ECHAM as base model within the MESSy framework, to the original ECHAM model. MESSy is a framework that allows to link a base model (i.e. a dynamical core, here ECHAM) to submodels (e.g., physical parameterizations, diagnostics, and among others the chemistry scheme). While Wan et al. (2008) used a dynamical core version of ECHAM in their paper, this version was to our knowledge only used for testing purposes of the model core and is not part of the general model distribution of ECHAM. The implementation we performed here is new in that it was developed within the MESSy framework. One advantage of MESSy is that the implementation of the model was possible simply through the implementation of a new submodel for the relaxation, and the other physical parameterizations could be simply switched off. Thus, no changes to the dynamical core had to be made. Within MESSy, it is now possible to run the dynamical core model with the same executable as more complex versions of the model, and the idealized model set-up is available for all model users. Moreover, the full infrastructure on tracer set-up, transport and chemical reactions, available in the MESSy framework, can be exploited also with the dynamical core model.
We added text on the distinction and motivation of our implementation of the dry dynamical core model within MESSy to the Introduction (p4, l20 ff) and Abstract (p1, line 6-7).

3 Minor Comments

1. The introduction would benefit from a plane language description of ECHAM vs ECHAM/Messy (ie what is the standard GCM, atmosphere only or ECM).
We expanded the description of the MESSy framework in the Introduction, to state that ECHAM is (one possible) dynamical core used within the MESSy framework:
"The MESSy framework couples a base model (dynamical core) to submodels, that contain the physical parametrizations as well as diagnostics. Among other base models, the ECHAM dynamical core is available in MESSy." (p3, line 33)
2. The manuscript would be easier to read to non-ECHAM specialists if there was a table of acronyms with a short description of each model and where if fits in with the other options.
While we do see that the number of Acronyms are confusing (in particular for non-MESSy users), we do not feel like we can omit any of them, as the paper also serves as documentation. However, we did try to reduce the usage of the acronyms in the text as much as possible to increase readability, and explain the model framework in more detail (which we hope serves the purpose more than adding a table).
3. From my perspective, sections 1 through to 4 are describing the implementation and the validation of the code. While in section 5, the model infrastructure is now well justified to use with the chemistry models. I think at the beginning of section 5 this should be more clearly communicated to let the reader that we have reached to point of advertising why a model like this is useful.
Thanks for the suggestion, and we added a sentence at beginning of section 5.
Figures often reflect personal styles and different perspectives. I have listed quite a few changes to the figures. These are separated into changes I would like to see made (below) and suggestions which I feel would help (these can actioned at your discretion, see clarifications section).
Requesting the following changes be made to the figures/captions:
1. Fig 1: Are there four options on the y-axis or more? I found it hard to interpret this figure and I am not sure which set-up has which chemistry option. What does '/...' in the 3D dynamical core mean?
The figure caption was expanded to clarify the meaning of the axis, and the Figure was slightly reworked to emphasize on the model set-ups with /without coupled chemistry.

2. Consistent colour bars are needed. Fig 2, 3, 10 use a yellow-to-red colour bar to describe T , uv and vT. Suggest Fig 3 has different colour bar for the fluxes. The blue-to-red colour bar is used for diffs in Fig7 but for T in Fig 4 and Φ in Fig 15-16. Suggest diffs for blue-to-red, T use yellow-to-red

and another colour option for Φ etc.
We reworked these Figures according to your suggestion to use consistent colour bars (Figs. 3, 4, 15, 16 (now 17, 18))
3. Many subplots all have the colour bar repeated. Suggest only having one colour bar or legend per plot.
Done.
4. Fig 5 caption should explain PT W and y are from the legend and point to relevant equations.
We added the description of p_Tw and gamma in the caption.
5. Fig 13: The jet colour map is generally considered bad practice and I suggest a different colour. I found it hard to interpret the zonal mean zonal wind in white and it look me a while to identify what the breaks were a SSW (also is this surface wind or aloft?). On first reading I thought the top panel was divided by w so the title was confusing for me. Are both u and w essential (could it be described instead as the inverse in general)?. I suggest exploring some other formats for this plot to help draw out the features.
The plot was reworked by changing the color map, and adding an additional y-axis in the upper panel to avoid confusion on the time-series of u and w*. The caption now clarifies that the wind contours in the middle panel are displaying winds at 50 hPa.

.
4 Clarifying Comments

4.1 Figures
Suggestion the following changes be made (optional):
1. Fig 1: The y -axis title 'Chemistry' is floating in a way that it feel out of place (either remove or move). I am not sure what the purpose of the two dotted vertical lines are.
The label „Chemistry" was moved, and the caption expanded to make the purpose of the vertical lines more obvious.
2. Fig 2: The title on the fig is not helpful (suggest removing it).
Done.
3. Fig 3: I find the left plots very hard to see. Suggest moving the left panel to a new plot and then keep the flux plots together. Alternatively you could consider only plotting 0-90 in one hemisphere given they are symmetric in this case. What does the 'MA' in the caption (and text) mean? The fonts are too small (also in other plots).
The plot is redone and resized to make it more visible, The „MA" is omitted from the title to avoid confusion, and explained in the text (MA="Middle Atmosphere", i.e. high-top version of model levels).
4. Fig 4 Suggest subplot titles are larger and also included in bottom panel.
Added titles to subplots, and omitted upper panels to keep balance of number of figures (two new additions).
5. Fig 5: Suggest you use the same seaborn colours as in Fig 8 (matching the values of y in fig 8) – this assumes these are in python though I notice a mix a languages used to generate the plots which is fine.
Well spotted, there is indeed a mixture of languages due to the different habits of the authors. Most figures are reworked now (in python), as is Fig, 5. Colors of Fig. 8 (new Fig. 9) and the time-series in Fig. 5 are consistent now.
6. Fig 6 (but in general): might want to consider skipping either red or green in your line plots so everyone can easy see it. I would prefer you use the same colour choices as in Fig 7.
Usage of Red and Green lines in Fig. 6 (new 7) is omitted now.
7. Fig 7 (and text): add the equilibrium temp to the legend. What do you mean by 'plane' in titles (and text)?
The title „plane surface" is omitted to avoid confusion (without topography was meant) and the equ. temp. line is explained in the caption.
8. Fig 11-12 bottom panels: suggest using colours not already used in the top panels and they are different so as not to confuse latitude, wind speed and temp differences.
Due to the addition of the new experiments, the coloring changed and is unique in each set of panels (top versus bottom).

9. Fig 14, if this image is a a pdf/png/jpg or similar, then I would suggest replacing the error bars with filled upper and lower intervals with lower alpha values (ie shading). If your using ps/eps this won't work.
Decided to leave figure as is (it is an eps file).
10. Fig 14: the line width is not consistent (thinner is nicer) and I suggest removing titles. The choice of black gives this authority (as is commonly done for obs), was this intentional?
Fixed (thinner lines in all panels, title removed). Black was intentional as this is the base case presented in Fig. 13.

4.2 Abstract
1. P1L1: I think it would help to explain why you mean by 'a need emerges'. I know what you mean but it might help to explicitly say it.
Thank you for the suggestion. As the reason for the „emerged need" is detailed in the first sentences in the introduction, we felt that adding it to the Abstract as well would blow up the Abstract too much. Also, we feel that the addition „to improve process understanding" does explain already why we need the model hierarchies.
2. P1L2: I would suggest a more general description instead of 'process understanding', perhaps ' simulations of the climate'
As detailed above, we think that the reason for the simplified models is exactly the seek for process understanding, while the complex models are the ones that are used for the best possible „simulations of the climate". Therefore, we would rather keep the formulation as is. See first paragraph of introduction.
4.3 Introduction
1. P2L8-13: In terms of the Held-Suarez description, a reader could easily get confused about a models dynamical core vs the parameterisation set-up of HS. Suggest rewriting L8-13 to make it clearer that HS was designed as a test for the dynamical core.
True, and reformulated to make it more clear that we mean a „Held-Suarez" type model here, not the particular functions for the equilibrium temperature they propose.
2. P3L2: The sentence starting 'The motivation of the MESSy framework was' is an excellent sentence that helped ground me in the context of the configurations. Could I requestion you add this (word for word is fine) to the abstract (something similar is already in the abstract but not as clear) and something just as cleanly described for the EMIL.
Thanks for the suggestion, we revised the paragraph in the Abstract to describe the MESSy hierarchy and the motivation for the implementation of the dry dynamical core model within this framework more clearly:
"The Modular Earth Submodel System (MESSy) was developed to incorporate chemical processes into an Earth System model. It provides an environment to allow for model configurations and set-ups of varying complexity, and as of now the hierarchy reaches from a chemical box model to a fully coupled Chemistry-Climate model. Here, we present a newly implemented dry dynamical core model set-up within the MESSy framework, denoted as ECHAM/MESSy IdeaLized (EMIL) model set-up. EMIL is developed with the aim to provide an easily accessible idealized model set-up that is consistently integrated in the MESSy model hierarchy. The implementation in MESSy further enables the utilization of diagnostic chemical tracers."
3. L9: Could you include what MECCA stands for? Is MECCA the chemistry model of EMAC or it more subtle?
Yes, MECCA is the chemistry module used in EMAC. The full name is added to the text.
4.4 Model Description
1. What surface conditions are you using? Is it generally an aquaplanet with 'water' mountains or does have a land like surface heat capacity?
As in the dry dynamical core model, the only interaction with the ground is via the prescribed friction, the ground does not actually have any heat capacity (it is implicitly included in the prescribed equilibrium temperature).
2. Equ 2: Worth mentioning the extra term (ϱ sin φ) that is not in the original HS formulation is from PK.
We added the remark that the asymmetry term was added is from the PK study (see equ. A1, moved to appendix in response to Reviewer Ed Gerber).

3. P6L12: suggest replacing (40κa)−1 with 0.025κ−1 s and (4κs) −1 with 0.25κ−1 s
The default values have been omitted from the text, and moved to the new Table 1 in the supplement.
4. Equ 8: Why use σ0 here and σb in equ 3?
As those are two distinct parameters, we chose to keep the distinct labeling to be able to keep them apart.
4.5 Model test cases, sensitivity simulations and application examples
1. Fig 4: titles and caption have inconsistent window for the averages, were they 10 or 11 years?
True, indeed 11 years as on the Figure titles were used. However, as we have chosen to remove the panels showing ERA-Interim climatologies to compensate for the addition of new Figures, this is obsolete.
2. P15L1: might help to define UTLS and what it's acronym is
Thanks and done.
3. P24L5: a key task of what?
Rephrased.
4. P24: I think you should state early in section 5.2 that the monsoon simulations are run with the chemistry scheme. I think you should also say if this is usual, and if not, why is the chemistry scheme is helpful.
In the monsoon simulations presented in the paper, no chemical tracers were included (see clarifications at top of review). However, for future applications, we plan to use diagnostic tracers to study tracer transport in the idealized model framework, one of the major research questions about monsoon circulation systems (see addition to the Introduction, new p3, line 20 ff).
5. Sect 5.2: Is there temporal variability in these simulations? If it was said then I missed it.
The forcing term is set constant, so there is no variability in the forcing. This is described in the second paragraph of Section 5.2.
4.6 Summary and Outlook
1. P25L7: Suggest removing 'In the paper presented here,' (it works better without it).
Done.
2. L2511: suggest replace 'based on the suggestions by HS94 and PK02' with 'as described in HS94 and PK02'. I would then start a new sentence that described what is new in your implementation.
Done.
3. P25L25-27: I found the description of 'climate states' confusing. I also suggest rewriting this sentence (or even multiple sentences) as the grammar has gotten complicated.
Done.
4. Please add in the acknowledgements where the SPARC and Era-I data can be downloaded from.
Done (for SPARC, ERA-I is not used directly anymore).

5 Editorial comments
There were a number of times where latex has compiled with " instead of " (please review).
Done.
5.1 Title and abstract
I think the title is too technical. By their very nature GMD papers are technical but I think you could make your title easier to read/understand (and remove some of the acronyms where possible).
We tried to reduce the usage of acronyms in the text of the paper, including the Abstract, which hopefully is now much more readable also to non-MESSy -users. However, we think the title needs to include the model system/ set-up names (indeed, it is requited by GMD to include version numbers), so we decided to keep it as is.
1. I found the number of acronyms hard to digest. Given the subject matter, I think ECHAM, MESSY and EMIL are probably fine to use but I would suggest removing RELAX and EMAC as they are not essential. I also think referring to the model as only EMIL or ECHAM/Messy idealied model would help readability. There is a lot of switching between model names which makes it hard to read at times for non-ECHAM experts.
We agree, and as said above, we tried to reduce the usage of the acronyms in the text, and hopefully explain the nature of the model framework more clearly now. However, we don't think we can remove any of the acronyms completely, as they are important informations to the model

users.
2. I don't think you need to citations in the abstract. I think it is fine to say Held-Suarez model.
References are omitted.
5.2 Introduction
1. P1L1 'more and more processes and compartments' is awkward, suggest changing to 'increasing complexity' or similar
Rephrased (see Ed Gerbers review).
2. P2L13 (or there abouts) suggest stating that the HS model will be described in detail in section 2.
Done.
3. P2L32: The description 'currently underway' reads as though these models are yet to be released. Suggest rewording as both Isca and CESM are broadly used for idealised studies.
Rephrased to „are aiming to...".
4. P3L3: suggest adding '0d' before box model.
Done.
5. P3L22-27: I very much liked this paragraph. I would suggest moving it earlier in the introduction. Maybe even as the first paragraph.
Thanks, and we moved to paragraph to an earlier place (before the whole MESSY framework is explained, to make it clear why we use it).
6. P3L28: What do you mean by 'consistent' ?
With „consistent", we here refer to a model hierarchy which adds processes in a logical order to study chemistry-dynamics interactions. The paragraph has been moved to the end of the paper, where it is put more in context.
7. P3L28: I like the description of model hierarchy of chemistry-dynamical coupling and I suggest you use this more often (esp in abstract).
See above, the paragraph has been moved to the very end of the paper, to make it more clear that this is an outlook.
8. P3L28-P4L2: Suggest moving this paragraph to outlook section.
Done.
9. P4L5: replace 'to' with 'two' and suggest separating into two sentences, one that talks about section 3 and one for section 4.
Done.
10. P3L6: Suggest joining the two paragraphs that describe what is coming up in the paper.
Done.

5.3 Model description
1. P5L12: Suggest adding convection to the list of parameterisations.
Done.
2. P5L13: suggest you mention Held-Suarez in this sentence.
Done.
3. P5L17-20: Suggest you add these as dot points rather than a list in a sentence.
Done.
4. P5L25: should cite HS in here.
As this is the generic equation for temperature relaxation, we don't think the reference in necessary here – it is cited again two sentences later.
5. P5L27 (and else ware): suggest replace 'local' with 'environmental'.
Changed to „actual temperature"
6. P5L28: suggest adding this paragraph to the one before and list dot points for the ways of implementing κ and Tequ
Obsolete due to restructuring of section.
7. P6L12: The discussion on hf rac should start with a description of ϱ.
Done.
8. P6L14: suggest replacing 'sign' with ±
We keep the „sign" function here, as this function is returning the sign of the given parameter.
9. P8L15: suggest replacing 'employed' with 'added'.
Done.

10. P8L18: suggest replacing 'reads' with 'is given by'
Kept as is to avoid duplication of „given by"

5.4 Sensitivity simulations
1. P16: Fig 11-12 are referred to before 9-10. You might want to consider moving figs or mentioning 9-10 earlier.
Consistent order of Figures is ensured now.
2. P17L6 and Fig 9: Could you explain why there are multiple Lindgren lines on these plots (which variables are changed)?
The differences in the set-up (i.e. in the Equilibrium temperature) are explained in the second paragraph of the section, and in the figure legends.
5.5 Supplementary
The tables would benefit from latex hlines and vlines so they look more like tables. Suggest removing the quotations from all variables. I don't think Fig1-2 are needed but I do not feel strongly about this. Fig 3 is a nice aid to see the call sequence (well done).
The supplement, including tables, has been revised.

Anonymous Referee #3

The authors introduce a new idealized and modular modeling setup and demonstrate its use in a couple of ways. I believe the paper would benefit from some restructuring – the paper goes back and forth between model setup issues (choices of values for various parameters) and scientific results which could potentially be a bit confusing to a reader. Perhaps the authors might wish to consider splitting the manuscript in two?
We thank the reviewer for the suggestion. Following Ed Gerber's review, we restructured the paper to enhance readability (moved considerable part of the technical descriptions to Appendix), and added more scientific discussion on the results (namely, stratosphere-troposphere coupling and dynamical regimes). We agree with the reviewer in that the scientific results might be expandable, and a second paper on the dynamical regimes of the polar vortex, that we find in the parameter sensitivity experiments, is in preparation.

Would it be possible to set up a github with a downloadable version of the model? I have doubts about reproducibility which the availability of the model would help to dispel.
The MESSy model is available upon obtaining a licence (see code availability section), so a freely downloadable version at github is not possible. As detailed in response to Ed Gerber's review, the next model release will contain sample namelists for the experiments conducted in the current study, so that the reproducibility will be ensured. Further, we added a new table with the specifications of the simulations, and the supplement contains now more detailed instructions for setting the parameters. Also, we decided to provide the data of the presented experiments via zenodo to enable future comparisons to other models.

On the science front, I think the authors are up against some regime issues in dynamical core models, which it would be good to clarify. The original PK02 model shows a very large response to stratospheric perturbations in comparison with observations, and in the absence of a quantitative theory of how stratospheric perturbations affect the troposphere, responses of the model when planetary scale waves are forced by topography are not necessarily the "correct" response.
We agree, and added discussion on regimes and stratosphere-troposphere coupling in our simulations (for details, see response to Ed Gerbers general comment 5).

On readability, the manuscript would benefit from some proofreading and fixing of minor typos (in particular, the quotation marks all appear reversed?).
We implemented the suggested changes by the other reviewers, and revised the manuscript with fixing all typos etc. we were able to identify.

Extending the Modular Earth Submodel System (MESSy v2.~~55~~.54) model hierarchy: The ECHAM/MESSy idealized (EMIL) model set-up

Hella Garny[1,2], Roland Walz[1], Matthias Nützel[1], and Thomas Birner[2]

[1]Deutsches Zentrum für Luft- und Raumfahrt (DLR), Institut für Physik der Atmosphäre, Oberpfaffenhofen, Germany
[2]Ludwig Maximilians University of Munich, Meteorological Institute Munich, Munich, Germany

Correspondence: Hella Garny (Hella.Garny@dlr.de)

Abstract. ~~While~~ As models of the Earth system ~~gain more and more~~ grow in complexity, a need emerges to ~~establish model hierarchies and to utilize simplified models to~~ connect them with simplified systems through model hierarchies in order to improve process understanding. The Modular Earth Submodel System (MESSy) was developed ~~with the aim to provide an~~ to incorporate chemical processes into an Earth System model. It provides an environment to allow for model configurations and set-ups of varying complexity, and as of now the hierarchy reaches from a chemical box model to ~~the full coupled ECHAM/MESSy Atmospheric Chemistry (EMAC)~~ a fully coupled Chemistry-Climate model. ~~In the current study~~Here, we present ~~and document the development of a new simplified set-up within the ECHAM/MESSy model, namely the~~ a newly implemented dry dynamical core model set-up within the MESSy framework, denoted as ECHAM/MESSy IdeaLized (EMIL) ~~. The~~ model set-up. EMIL is developed with the aim to provide an easily accessible idealized model set-up that is consistently integrated in the MESSy model hierarchy. The implementation in MESSy further enables the utilization of diagnostic chemical tracers. The set-up is achieved by the implementation of a new submodel for relaxation of temperature and horizontal winds to given background values~~(the RELAX submodel)~~, which replaces all other "physics" submodels in the EMIL set-up. The ~~RELAX~~ submodel incorporates options to set the needed parameters (e.g., equilibrium temperature, relaxation time and damping coefficient) to functions used frequently in the past~~(given by Held and Suarez, 1994; Polvani and Kushner, 2002) .~~. Test simulations with the EMIL model set-up ~~show that results from earlier studies with other~~ reproduce benchmarks provided by earlier dry dynamical core ~~models are reproduced under same set-ups~~studies. Furthermore, modifications to the previously used set-ups are tested, with the following main findings: ~~1) lowering~~ Lowering the equilibrium temperature in the lower stratosphere at winter polar high latitudes to more realistic values (i.e., below observed temperatures) results in high latitudes temperature profiles in the model closer to observations~~, and 2) when~~. We find a non-linear response of the polar vortex strength to the prescribed meridional temperature gradient, that is indicative of a regime change. In agreement with earlier studies, we find that the tropospheric jet moves poleward in response to the increase in the polar vortex strength, but at a rate that strongly depends on the specifics of the set-up. When replacing the idealized topography to generate planetary waves by mid-tropospheric wave-like heating (as suggested in a previous study), the response of the free tropospheric jet to changes in the equilibrium temperature is strongly damped~~, indicating~~. However, the near-surface jet shifts poleward at a higher rate than in the topographically forced simulations. Those results indicate that the wave-like heating ~~has~~ might have to be used with

care ~~. As~~ when studying troposphere-stratosphere coupling. As additional application examples, we present simulations with simplified chemistry to study the impact of dynamical variability and idealized changes on tracer transport, and simulations of idealized monsoon circulations forced by localized heating. The ability to simulate ~~dynamical~~ circulation systems and to incorporate passive and ~~chemical~~ chemically active tracers in the EMIL set-up demonstrates the potential for future studies of tracer transport in the idealized dynamical model.

1 Introduction

Earth system models ~~incorporate more and more processes and compartments to enable the~~ continue to incorporate more processes to enable a more complete simulation of the ~~coupled climate system~~climate system, and thus produce the best possible climate projections. In practice, this increases the complexity of model codes as new compartments are added to represent new processes and interactions. However, with models gaining more and more complexity, it becomes difficult to isolate and understand the role of individual processes. This "gap between simulation and understanding in climate modeling" was pointed out ~~in the paper~~ by Held (2005), and it was suggested that the way forward is to work with a hierarchy of models with reduced to full complexity. Two recent overview papers (Jeevanjee et al., 2017; Maher et al., 2018) give surveys of current concepts and activities in building hierarchical model systems.

The basic concept in constructing a simplified model is to include only those processes, that are (absolutely) relevant for the question to be addressed. Thereby, the behavior of those processes can be isolated in an idealized environment, and the interaction of the limited number of processes chosen can be investigated.

A frequently used idealized model set-up for studying global large-scale dynamics is the dry dynamical core model ~~described~~ proposed by Held and Suarez (1994, HS94 hereafter). While originally developed and used for testing dynamical model cores, the elegance of the model makes it an ideal tool for dynamical process studies, and it is widely used for this purpose (see Maher et al., 2018, for a review of applications). ~~The HS94 model set-up~~ This "Held-Suarez"-type model uses the full dynamical core of a GCM, but replaces all physics by relaxation towards a prescribed equilibrium temperature and by Rayleigh friction to damp winds at the surface ~~and the upper model levels.~~(as described in detail in Sec. 2). Thus, with this model set-up the thermodynamic forcing of the atmosphere can be easily modified and the response of the large-scale circulation to those isolated modifications can be studied. Examples are changes in equilibrium meridional temperature gradient or thermal damping time scale (Gerber and Vallis, 2007), or changes in surface friction (Chen et al., 2007).

The functions for the equilibrium temperature and relaxation coefficients suggested in HS94 are widely used, and the HS94 model set-up was extended to study the dynamics of the stratosphere-troposphere system by modifying the equilibrium temperature of the stratosphere (Polvani and Kushner, 2002, PK02 hereafter) and later by adding topography to include planetary wave generation that is essential for the stratospheric circulation (Gerber and Polvani, 2009). This model set-up was used among others to study stratosphere-troposphere coupling (Gerber and Polvani, 2009), the structure of the Brewer-Dobson circulation (Gerber, 2012), and the circulation's response to idealized heating resembling ~~climate change~~ the thermal response to greenhouse forcing (e.g., Butler et al., 2010; Wang et al., 2012). Recently, it was suggested that the forcing of planetary waves

can also be achieved by inserting diabatic heating in the mid- to upper troposphere (Lindgren et al., 2018), which leads to a similar climatology as the topographically forced simulations, but to changes in the sudden stratospheric warming properties.

While the dry dynamical core model has proven useful in advancing our understanding of the dynamical response to given thermodynamic forcing, the application of the model hinges on a realistic representation of the Earth's atmosphere's behavior of the modeled dynamics. Gerber and Polvani (2009) and Chan and Plumb (2009) showed that the strong response of the surface jet location to stratospheric polar vortex changes found in the original study by PK02 resulted from a regime shift of the tropospheric jet. With a changed set-up, e.g. by including topography (Gerber and Polvani, 2009) , or with enhanced meridional temperature gradients in the winter hemisphere (Chan and Plumb, 2009) , the regime-like behavior of the jet location is suppressed, and thus the response of the jet location to stratospheric polar vortex changes is damped strongly. However, the regime shift can re-emerge for experiments with strong additional forcing (e.g., tropical heating, as shown by Wang et al., 2012) . Overall, those results indicate that the dynamical response to a given forcing is highly (non-linearly) dependent on the basic state of the model. Whether this sensitivity to the basic state due to dynamical regimes is relevant for the real atmosphere will have to be evaluated with care. If the regime behavior proves to be an artifact of the idealized models, this would impede its application to advance the understanding of dynamical processes of the real atmosphere.

Beyond the purely dry dynamical core models, which are useful to study aspects of the global circulation, a question that motivates ~~to include~~ the expansion to another level of complexity, is the interaction of moisture with large-scale dynamics, either by latent heat release or by its role as greenhouse gas. Frierson et al. (2006) expanded the dry dynamical core ("Held-Suarez") model by adding moisture and convection with latent heat release to the model, including simplified (gray) radiation that is insensitive to water vapor, thus tackling the question of the role of latent heat release for large scale dynamics. In a step further, ~~Jucker and Gerber (2017) included a full radiation scheme to capture~~ the role of water vapor as ~~radiative active gas (but neglecting clouds~~radiatively active gas is included by using more comprehensive radiation schemes, as done by e.g. Merlis et al. (2013); Jucker and Gerber (2017); Tan et al. (2019) . In those set-ups, treatment of radiatively relevant fields as clouds, ozone and aerosol forcing ~~in the radiative calculation).~~ is mostly based on simple assumptions such as constant values.

As stated above, the nature of the hierarchy that is to be constructed depends on the scientific question at hand. Our aim is to study the large-scale dynamical variability of the stratosphere-troposphere system and its response to idealized forcings, and in particular the impact of dynamical variability and forced changes on transport of passive and chemically active trace gases. The latter is motivated by a variety of research questions on the distribution of trace species in the atmosphere, for example on how changes in the circulation in a changing climate will affect stratospheric ozone. This question got a lot of attention recently in the light of observed lower stratospheric ozone trends that are not fully understood (Ball et al., 2018) . Another question we aim to tackle with the idealized model is the efficiency of troposphere-stratosphere transport in monsoonal circulation systems via different pathways. The idealized set-up allows to study the role of different transport pathways depending on the details of the forcing of the circulation system. To enable those studies, a well suited model set-up is a dry dynamical core model with the utilities for tracer transport and the possibility to include chosen chemical reactions (simplified to the needs of the user). Therefore, we implement such a model set-up within the Modular Earth Submodel System (MESSy, Jöckel et al., 2005) framework, which provides the needed utilities in a modular manner.

Several initiatives are ~~currently under way~~ aiming to build modeling frameworks with set-ups of varying complexity within the same model system (Vallis et al., 2018; Polvani et al., 2017), an approach that will advance both the usability of idealized models as well as the connectedness of the simple and the more complex model set-ups. In the same spirit, the ~~Modular Earth Submodel System (MESSy, Jöckel et al., 2005)~~ MESSy framework was developed explicitly with the goal to provide ~~"~~"a framework for a standardized, bottom-up implementation of Earth System Models (or parts of those) with flexible complexity~~" ~~" (see https://www.messy-interface.org/). The motivation of the MESSy framework was originally to incorporate chemical processes of varying complexity into an Earth System model. The ~~system~~ MESSy framework couples a base model (dynamical core) to submodels, that contain the physical parametrizations as well as diagnostics. Among other base models, the ECHAM dynamical core is available in MESSy. The MESSy framework includes model configurations ranging from a 0-dimensional box model of atmospheric chemistry (Sander et al., 2019) to the complex chemistry-climate model ECHAM/MESSy Atmsopheric Chemistry (EMAC), coupled to a deep ocean model (Jöckel et al., 2016). An illustration of a selection of available model complexities is shown in Fig. 1, as function of the complexity in physical processes/ compartments included (horizontal axis) and of the complexity of atmospheric chemical processes included (vertical axis). The lowest complexity on the chemical axis are prescribed concentrations for ~~radiative~~ radiatively active species (e.g., ozone), followed by a simplified parametrization to include effects of methane oxidation on stratospheric water vapor. The chemistry module MECCA ~~(Sander et al., 2019)~~ (Module Efficiently Calculating the Chemistry of the Atmosphere, Sander et al., 2019) contains a large set of reactions relevant in the troposphere and stratosphere, but it can be configured to the user's needs by choosing any subset of reactions, thus allowing for simplified to very comprehensive chemical set-ups. The chemical calculations can be performed as a box model ~~(Sander et al., 2019)~~ (denoted CAABA, see Sander et al., 2019) , or within a full general circulation model either without feedback between dynamics and chemistry ~~(the so-called "Quasi Chemistry-Transport Model" (QCTM), see Deckert~~ with feedback, i.e., as full chemistry-climate model (Jöckel et al., 2006; Jöckel et al., 2010, 2016). Besides the prescribed sea surface temperature set-up, a mixed-layer ocean (Dietmüller et al., 2014) or a full ocean model (Pozzer et al., 2011) can be used.

One advantage of the MESSy framework is its modular nature, i.e., individual processes are implemented as independent submodels that can be easily exchanged or complemented by new processes, and each submodel can be easily switched on or off (by namelist choice). Therewith, the hurdle of code modifications to build a model tailored to the necessary complexity is rather low. Moreover, the design of the model system allows ~~to create~~ the creation of model hierarchies in which the same code can be used in a simple model set-up as well as in the full Earth-System model~~, thus any~~ . Any developments in model components can be transferred easily up- and downward in the model hierarchy.

~~As stated above, the nature of the hierarchy that is to be constructed depends on the scientific question at hand. Our aim is to study the large-scale dynamical variability of the stratosphere-troposphere system and its response to idealized forcings, and furthermore the impact of dynamical variability and changes on transport of passive and chemically active trace gases. To achieve this goal, the most suited model~~

In this paper, we document the implementation of the dynamical core set-up ~~is a dry dynamical core model with the utilities for tracer transport and a set of chosen chemical reactions (simplified to~~ within the MESSy framework and its performance.

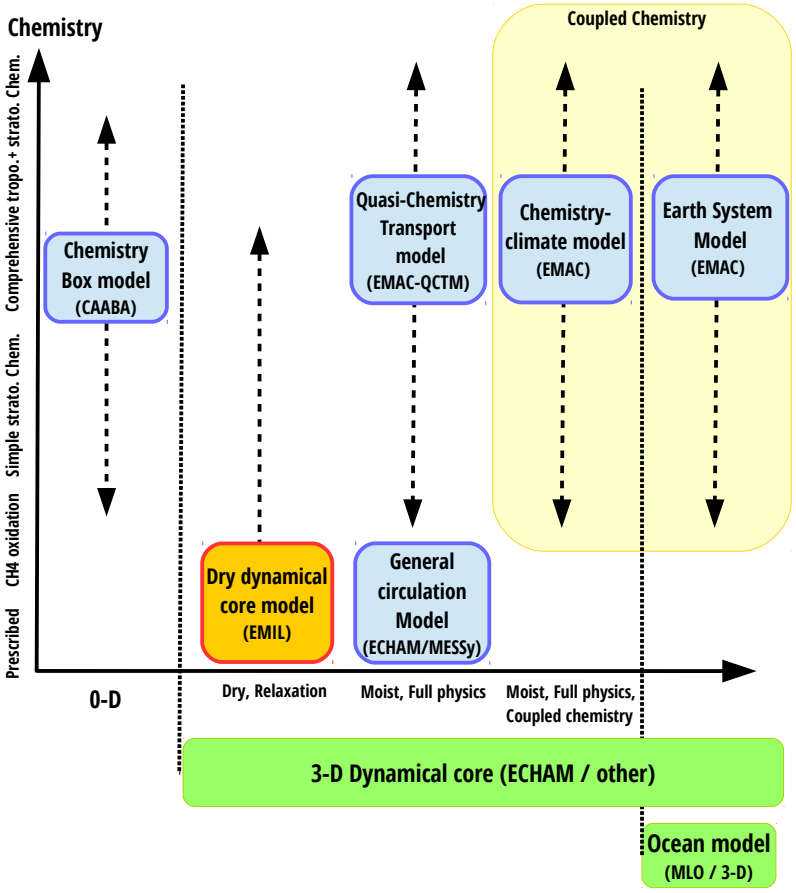

Figure 1. Schematic of the MESSy model hierarchy with existing (blue) model set-ups and the model set-up described in this paper (red). Model set-ups are displayed as function of their complexity in dynamics/physics/compartments (horizontal axis) versus complexity in chemical mechanism (vertical axis). The horizontal axis ranges from (left) a 0-dimensional box model to (middle) models with an atmospheric dynamical core (ECHAM or other implemented dynamical cores in MESSy), but with varying physical complexity, and to (right) models with an additional ocean model (Full 3-d or mixed-layer ocean). The vertical axis displays the chemical complexity, that can gradually be increased from prescribed tracer concentrations for the radiation scheme to a more and more comprehensive set of chemical reactions. The chemistry can be used diagnostically only, or in a coupled manner (yellow box).

While "Held-Suarez" test simulations with the same dynamical core (ECHAM) were previously performed to study the resolution sensitivity of the model core (Wan et al., 2008) , the here presented implementation is new in that it is part of the ~~needs of the user). The implementation of such a model~~ MESSy framework. The implementation within MESSy ensures an easily accessible idealized model set-up ~~within the MESSy framework is documented in the current paper.~~

~~Another step in constructing a consistent model hierarchy of chemistry-dynamical coupling would be to allow the anomalies of chemically and radiative active tracers caused by transport to feedback on the dynamics. This would require radiative calculations depending on the actual tracer concentrations. While this expansion of the idealized set-up will be subject of future work, we note here that all necessary components are available already~~ that is consistently integrated in the MESSy ~~framework: the radiation scheme from the full EMAC model (Dietmüller et al., 2016) can be used with setting the input to either the online simulated values of the trace gas of interest (i.e., ozone), while the other relevant species can be set to climatological values (e.g., water vapor) or zero (e.g., clouds and aerosols). The envisioned model set-up, basically an idealized "chemistry-dynamical model", would thus consist of a dry dynamical core with thermodynamic forcing by an idealized prescribed latent heating and radiative calculations that are dependent on the chemical species of interest (e.g., ozone).~~

~~Schematic of the MESSy model hierarchy with existing (blue) model set-ups and the model set-up described in this paper (red). Model set-ups are displayed as function of their complexity in dynamics/physics/compartments (horizontal axis) versus complexity in chemical mechanism (vertical axis).~~

~~In this paper, we document the implementation of the dynamical core set-up within MESSy and its performance~~model hierarchy, and that enables the use of all tracer utilities, including the utilization of diagnostic chemical tracers. The implementation is achieved by adding a simple submodel for Newtonian cooling and Rayleigh ~~fricitonfriction~~, that replaces the complex physics (see Sec. 2 and the supplement for technical details including a user manual). ~~Next to~~ We present standard test cases with ~~the forcing as in~~ forcings given by Held and Suarez (1994) and its stratospheric extension ~~(Polvani and Kushner, 2002, see Sec. 3)~~ (Pol Sec. 3. Further, we test several modifications to those set-ups, most importantly a modification of the equilibrium temperatures in the winter high latitudes that leads to more realistic temperature profiles in the lower stratosphere (Sec. 4). We further test the sensitivity of the simulated dynamics to the generation of large-scale waves by zonally asymmetric heating instead of idealized topography, as suggested recently by Lindgren et al. (2018).

Finally, we present two application examples of the model: first, we present simulations including a small set of chemical reactions (namely photolysis of Chlorofluorocarbons) and demonstrate the potential of the model to study the role of dynamical variability and idealized changes on tracer transport (Sec. 5.1). Secondly, the simulation of an upper tropospheric anticyclone forced by ~~idealized locally~~ simple, localized constrained heating that resembles the Asian monsoon anticyclone is presented in Sec. 5.2.

2 Model description

The ECHAM/MESSy IdeaLized (EMIL) model set-up is based on MESSy version ~~2.55~~ 2.54 (Jöckel et al., 2006; Jöckel et al., 2010, 2016), and will be available for users in the next release, i.e. version 2.55. In the idealized, "Held-Suarez"-type,

model set-up, all physics (radiation, clouds, convection and surface processes) are switched off, and are replaced by the newly implemented submodel ~~"RELAX"~~"RELAX", that relaxes the variables temperature and horizontal winds to given background values. The submodel RELAX is described in the next subsection. Technical details of the model set-up (namelist choices etc.) and implementation are provided in the supplement.

2.1 The submodel RELAX

The submodel RELAX calculates ~~(1) Newtonian coolingwhich relaxes the temperature~~

1. Newtonian cooling, i.e. temperature relaxation towards a given equilibrium temperature with a given relaxation time scale ~~, (2) Rayleigh frictionwhich relaxes the horizontal wind~~
2. Rayleigh friction, i.e. horizontal wind relaxation towards zero with a given damping coefficient ~~, and (3)~~
3. additional diabatic heating over selected regions ~~.~~

The three processes are switched on/off via namelist parameters (in relax.nml, see Supplement).

The submodel is called from the physics routine *physc* through *messy_physc*. The full call tree including all subroutines is provided in the supplement. In the following, the implemented options in the routines are described, with the full equations given in Appendix A.

2.1.1 ~~Newtonian cooling~~

Newtonian cooling

The temperature tendency calculated by Newtonian cooling is given by $\delta T/\delta t = -\kappa(T - T_{\rm eq})$, where κ is the inverse relaxation time scale, T the ~~local~~ actual temperature calculated by the model, and ~~$T_{\rm equ}$~~ $T_{\rm eq}$ the prescribed equilibrium temperature.

The inverse relaxation time scale ~~κ~~ and the equilibrium temperature ~~$T_{\rm equ}$~~ have to be specified in the model set-up~~via the RELAX namelist file (relax.nml, including the "coupling" (CPL) namelist in which all options are set). There are three options: (1) Set κ and/or $T_{\rm equ}$ to a constant value specified in the namelist. This option is physically of little use and is implemented for test purposes only. (2) Choose one of the implemented functions for κ and/or $T_{\rm equ}$. Those options are described below. (3) Set κ and/or $T_{\rm equ}$ to a field that is~~ , either by setting them to fields imported from an external file~~(via import.nml). The imported fields are interpolated to the current pressure profile at each time step within the RELAX submodel.~~

~~The implemented functions (option (2)) for κ and $T_{\rm equ}$ are either~~ , or by setting them to values given by pre-implemented functions. Currently, the implemented functions for the inverse relaxation time scale and the equilibrium temperature are firstly those given by HS94 (option 'HS'~~), or those given by PK02 (option 'PK'~~, see Eq. A1), but with the possibility ~~of extensions. Note that κ in 'PK' and 'HS' are identical.~~

~~The functions for the 'HS' set-up, as defined by Held and Suarez (1994) , are where ϕ is the geographical latitude and p the local pressure. All constants can be set via namelist entries, with defaults set to the values given in HS94 ($T_{\rm top} = 200\,$K~~to

include hemispheric asymmetry, ~~$T_0 = 315\,\mathrm{K}$ $\delta_y = 60\,\mathrm{K}$, $\delta_z = 10\,\mathrm{K}$, $k = R/c_p = 2/7$, $p_0 = 1013.25\,\mathrm{hPa}$, $\kappa_\mathrm{a} = (40\,\mathrm{days})^{-1}$, $\kappa_\mathrm{s} = (4\,\mathrm{days})^{-1}$ and $\sigma_\mathrm{b} = 0.7$). p_s is the current surface pressure. The parameter h_fac, that is set in the namelist, controls the hemispheric asymmetry: If h_fac is zero, the equilibrium temperature is symmetric between the hemispheres (i.e., $\epsilon = 0$). If $h_\mathrm{fac} \neq 0$, then $\epsilon = \mathrm{sign}(h_\mathrm{fac}) \times 10\,\mathrm{K}$, i.e., the sign of h_fac determines which hemisphere is the winter hemisphere (positive h_fac: northern hemispheric winter, negative h_fac: southern hemispheric winter).~~

~~The equilibrium temperature in the PK set-up is similar to the one of HS in the troposphere, but uses the following function in the stratosphere above a given transition pressure $p_\mathrm{T}(\phi)$~~and, secondly, those given by PK02 (option 'PK', see Eq. A4), but with the following extension: ~~The stratospheric temperature profile is based on the US standard atmosphere temperature profile $T_\mathrm{US}(p)$ in the summer hemisphere and exhibits a temperature decrease with lapse rate γ in the winter hemisphere representing the region of the polar vortex. This transition is performed by the weighting function The smooth transition between tropospheric and stratospheric temperatures is ensured by bounding the tropospheric temperature to the temperature in the transition region $T_\mathrm{US}(p_\mathrm{Ts})$.~~

~~As an extensionto the original PK set-up,~~ we include the possibility to vary the transition pressure between tropospheric and stratospheric temperature from summer to winter hemisphere~~, using the weighting function $W(\phi)$: where p_Ts and p_Tw are the transition pressures over the summer and winter hemisphere, respectively. Again, all constants can be set in the namelist with default values $T_0 = 315\,\mathrm{K}$, $\delta_y = 60\,\mathrm{K}$, $\delta_z = 10\,\mathrm{K}$, $k = R/c_p = 2/7$, $p_0 = 1013.25\,\mathrm{hPa}$, $|\epsilon| = 10\,\mathrm{K}$, $|\phi_0| = 50$, $\delta\phi = 10$, $h_\mathrm{fac} = 1$, $\gamma = 4\,\mathrm{K/km}$, $p_\mathrm{Ts} = 100\,\mathrm{hPa}$ and $p_\mathrm{Tw} = 100\,\mathrm{hPa}$. These default values correspond to the original PK02 set-up with constant transition pressure $p_\mathrm{T}(\phi) \equiv 100\,\mathrm{hPa}$.~~

~~In the following, only the polar vortex lapse rate γ and the transition pressure p_Tw over the~~ . This latitudinal variation is implemented by using the same weighting function as is used for the transition to the polar vortex equilibrium temperatures (see Eqs. A5 and A6). In section 4.2, sensitivity simulations with respect to variations in the transition pressure over winter high latitudes ~~are varied, whereas $p_\mathrm{Ts} = 100\,\mathrm{hPa}$~~ ($p_\mathrm{Tw}$) are presented. The transition pressure in the remaining area is held constant at $p_\mathrm{Ts} = 100\,\mathrm{hPa}$, as in the original 'PK' set-up. Fig. 2 shows ~~the zonally symmetric equilibrium temperature~~ an example of the equilibrium temperature with modified winter transition pressure, here for $p_\mathrm{Tw} = 400\,\mathrm{hPa}$ and $\gamma = 2\,\mathrm{K\,km^{-1}}$.

2.1.1 ~~Rayleigh friction~~

Rayleigh friction

Horizontal winds are relaxed to zero (i.e., damped) with a given damping coefficient k_damp by ~~:~~

$\delta \boldsymbol{v}/\delta t = -k_\mathrm{damp} \boldsymbol{v}$. As for the Newtonian cooling, the damping coefficient can be selected via the namelist with the same ~~three options(i. e., constant, implemented function, or imported externally).~~ options. The implemented functions that can be chosen are ~~:~~

1) ~~Damping of~~ the surface layer damping as specified by HS94 (option *'HS'*~~): with default values $k_\mathrm{max} = 1.16 \times 10^{-5}\,\mathrm{s^{-1}}$, $\sigma_0 = 0.7$ and p_s the current surface pressure.~~

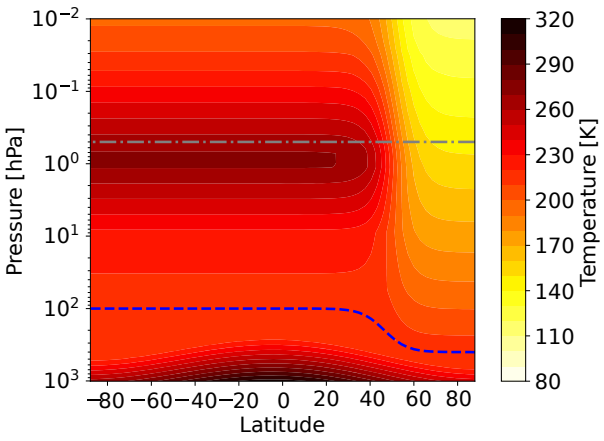

Figure 2. Equilibrium temperature (in K) for $p_{\mathrm{Tw}} = 400\,\mathrm{hPa}$ and $\gamma = 2\,\mathrm{K\,km^{-1}}$ together with the transition pressure $p_{\mathrm{T}}(\phi)$ (blue dashed line) and the pressure above which damping sets in (gray dashed-dotted line).

, see Eq. A7), 2) ~~Damping~~ the damping of a layer at the model top as specified by PK02 (option *'PK'*~~): with default values $k_{\mathrm{max}} = 2.3148 \times 10^{-5}\,\mathrm{s^{-1}}$ and $p_{\mathrm{sp}} = 0.5\,\mathrm{hPa}$.~~

, see Eq. A8), and 3) ~~Damping~~ a different option for damping of a layer at the model top ~~with~~ that is newly introduced here, and that follows the function as implemented in the original ECHAM code (option *'EH'*~~): where i_{lev} is the number of the hybrid level counted from the top of the model for a vertical resolution of L90MA. Thus~~, see Eq. A9). For the *'EH'* option, the drag ~~k_{drag}~~ is enhanced by a ~~factor of c~~ given factor for each level going upward. ~~Default values are $c = 1.5238$, $k_{\mathrm{drag}} = 5.02 \times 10^{-7}\,\mathrm{s^{-1}}$ and $i_{\mathrm{lev}}^{sp} = 10$, corresponding to a pressure of 0.43hPa for the L90MA vertical resolution. If the model is run at a different vertical resolution, the damping coefficients are first calculated according to Eq. A9 for L90MA, and then interpolated to the current vertical levels.~~

~~As~~ Sensitivity simulations with respect to the newly implemented form of the upper level damping are presented in Section 4.1. Note that as damping at the model surface (option 1) and at the upper layers (options 2 or 3) are complementary, more than one option can be chosen~~. In this case, the chosen profiles of k_{damp}~~, in which case the profiles of the damping coefficients are added.

2.1.1 ~~Diabatic heating routines~~

Diabatic heating routines

~~In addition~~ Next to the zonally symmetric temperature tendency calculated by Newtonian cooling, additional temperature tendencies (diabatic heating) can be ~~employed~~added. Currently, three options are implemented, one function for zonal mean heating (*tteh_cc_tropics*), a wave-like heating varying with longitude ~~λ~~ (*tteh_waves*) and a function for localized heating (*tteh_mons*).

The zonal mean diabatic heating (*tteh_cc_tropics*) is one of the tropical heating functions given by Butler et al. (2010), and reads

with p_s being the surface pressure and default values of $q_0 = 0.5\,\mathrm{K/day}$, $\phi_0 = 0°\mathrm{N}$, $\sigma_\phi = 0.4 \cdot 180°/\pi$, $z_0 = 0.3$ and $\sigma_z = 0.11$ as used by Butler et al. (2010) .

with the given heating amplitude decreasing exponentially in latitude and height (see Eq. A10). The temperature tendency *tteh_waves*, used here for the generation of planetary wavesintroduced by Lindgren et al. (2018) , reads

with default values $q_0 = 6\,\mathrm{K/day}$, $m = 2$, $\phi_0 = 45°\mathrm{N}$, $\sigma_\phi = 0.175 \cdot 180°/\pi$, $p_{\mathrm{bot}} = 800\,\mathrm{hPa}$ and $p_{\mathrm{top}} = 200\,\mathrm{hPa}$ as used is the one as introduced by Lindgren et al. (2018) .

The other (see Eq. A11). The third option for an additional temperature tendency, *tteh_mons*, allows to impose a localized heat source. The effect of localized heat sources has been investigated in a couple number of studies (e.g., Gill, 1980; Schubert and Masarik, 2006; Siu and Bowman, 2019) and we will use localized heating will be used here to produce monsoon-like anticyclones in Sec.5.2 (hence the name *tteh_mons*). The function describing formulation for the localized heating field is given as: Here, the individual factors are used to describe the temporal and spatial (horizontal and vertical) dependence of the heating function. The temporal evolution of the heating is given by : To slowly increase the heating after the start of the simulation a spin up factor of $\frac{t}{t_s}$ is included until the end of the spin up time (t_s).After the spin up time (t_s) the temporal variation of the heating is only given by a periodic oscillation (period δt) with amplitude (q_{temp}) around a constant base heating (q_0). is given by Eqs. A12 to A16.

In the vertical the heating is assumed to be of the same form as in Eq. (A11), i.e.: Here, p_{bot} and p_{top} denote the maximum and minimum pressure to which the heating is confined in the vertical. The latitudinal dependence for $\phi \in [-90, 90]$ follows the function suggested by Schubert and Masarik (2006 , their Eq. 4.1), and is given as

Finally, the longitudinal dependence for $\lambda \in [0, 360)$ is given by where $g(\lambda, \lambda_0) = min((\lambda - \lambda_0)\ mod(360), (\lambda_0 - \lambda)\ mod(360))$ and the modulo function $mod(360)$ maps $\mathbb{R}$ to $[0, 360)$, i.e. the function returns the smallest angle between the longitude λ and the central longitude λ_0 with accounting for the crossing of the $0°$ line. Again the longitudinal function is based on the heating described by Schubert and Masarik (2006 , their Eq. 4.1). However, as Schubert and Masarik (2006) were aiming to investigate the Madden-Julian-Oscillation, they included a movement of the localized heat source, which we do not include here (i.e., we use their equation with propagation speed 0). Overall this heating structure is similar to other idealized heatings used for studying monsoon anticyclones (e.g., Siu and Bowman, 2019) .

3 Model test casesbenchmark tests

In this section, results obtained with the EMIL set-up are compared to results of earlier studies with identical set-ups (both with the Held-Suarez set up, Sec. 3.1 and the Polvani-Kushner set-up, Sec. 3.2) to test whether the EMIL implementation is able to reproduce the results of those earlier studies. If not mentioned otherwise, the simulations are performed for In Sec. 3.3, the stratospheric influence on the tropospheric jet location as shown by PK02 is analyzed in the EMIL model, and further the sensitivity of this coupling to the tropospheric basic state is discussed. For the latter, sensitivity simulations are utilized in which

the tropical vertical temperature gradient is reduced. This modified set-up was inadvertently implemented in an earlier version of the model. While we choose the standard set-up to enable comparisons to former studies, the modified set-up provides valuable results on the models sensitivity, and thus the standard and modified ("log10") set-up are contrasted in Sec. 3.3, 4.2 and 4.3.

The simulations are performed for at least 1825 days, ~~with the first 300 daysconsidered as spin-up and not included in the analysis.~~and a number of simulations is extended up to 10950 days. The simulation length is specified for each simulation in the following (see Figure captions and Table B1). It would be favorable to extend each simulation until convergence of the climatologies is reached, however, in particular for simulations in which multiple dynamical regimes are present, this would require very long integration times. To reduce computational and data storage costs, we used the strategy of variable simulation length, i.e. we extended only a chosen set of simulations to test for the robustness of the results (in particular for the sensitivity simulations in Sec. 4.2 and 4.3). Details on the simulation set-up and integration length can be found in Table B1.

3.1 Held-Suarez forcing

~~Results of idealized ECHAM5~~ "Held-Suarez" test simulations with the ~~Held-Suarez set-up were previously presented in the study by Wan et al. (2008)~~ same dynamical core (ECHAM) as used in EMIL were previously performed (Wan et al., 2008) . We ran a simulation with identical set-up and resolution (T63L19) to test whether our implementation of the Held-Suarez set-up with the same base model can reproduce the results of Wan et al. (2008). As shown in Fig. 3 the climatologies of zonal wind, temperature and eddy fluxes are closely reproduced when compared to Fig. 1 of Wan et al. (2008). ~~The~~ In both model set-ups, the wind jet maxima are ~~identical at 28~~ around 30 ms^{-1}, ~~as well as the eddy variance maxima (at 40 K^2)~~the eddy heat flux maxima around 20 K m s^{-1}, and the eddy momentum flux maxima around 70 $\mathrm{m}^2\mathrm{s}^{-2}$.

In the remainder of the paper, a vertical resolution with high top (0.01 hPa) and with 90 levels (L90MA, where MA=Middle Atmosphere) will be used together with T42 as spectral resolution (one of the standard resolutions of EMAC, see Jöckel et al., 2016). The differences in the climatologies between the T42L90MA and the T63L19 simulation (for the HS set-up) are shown in Fig. 3 (bottom). ~~In agreement with results presented by Wan et al. (2008) , there are shifts in the jet and a general reduction of eddy variance with lower horizontal resolution (which likely dominates over the effect of changed~~ The jets are shifted equatorward in the T42L90MA resolution, and eddy variance is generally reduced. This is likely a combined effect of lower horizontal and higher vertical resolution, ~~see Wan et al. , 2008)~~in agreement with Wan et al. (2008) . The issue of resolution sensitivity will not be touched further as it is not the subject of this paper, but it should be kept in mind that the T42 spectral resolution is below the resolution of convergence (estimated to be T85L31 by Wan et al., 2008) for tropospheric eddy dynamics.

3.2 Polvani-Kushner set-up

In the study by PK02, an equilibrium temperature is introduced that enables the simulation of an active stratosphere with a polar vortex in the winter hemisphere.

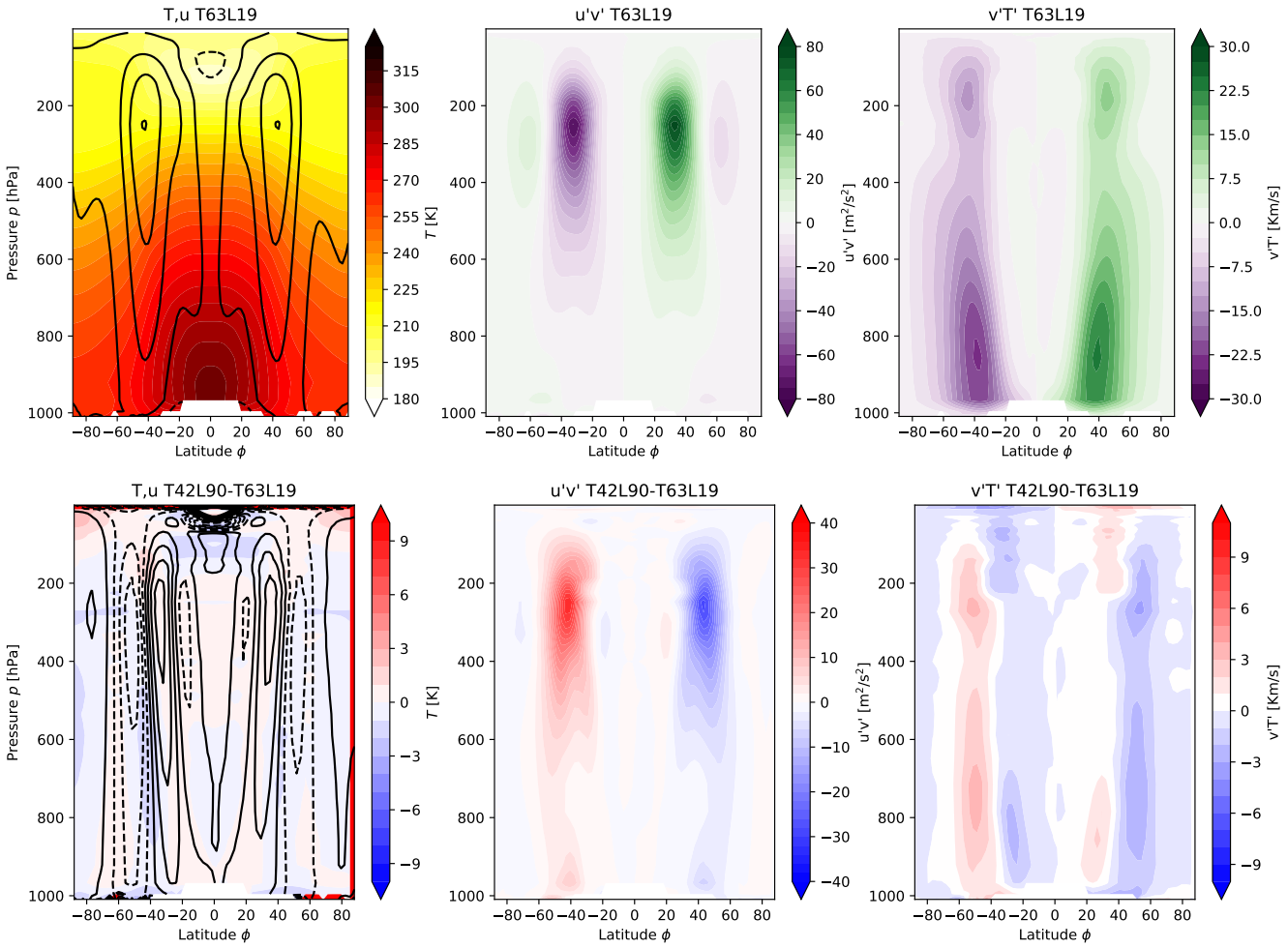

Figure 3. Top: Results from a HS simulation at T63L19 resolution, showing mean temperature [K] and zonal mean zonal wind [m s^{-1}, contour interval 10 m s^{-1}] (left), mean eddy momentum fluxes [m^2 s^{-2}] (middle) and mean eddy heat fluxes [~~mK~~ K m s^{-1}] (right) averaged over ~~1000~~ 1500 days (after spin-up of ~~450~~ 325 days). Bottom: As above, but difference of a simulation at T42L90MA resolution ~~to~~ minus the T63L19 simulation (with wind contour interval 2 m s^{-1}).

As a test case, EMIL simulations are performed with identical forcing as in PK02, i.e., with the same choice of the prescribed equilibrium temperature and the damping layer at the top of the model. The results for simulations with the polar temperature lapse rate γ set to 4~~K~~ K km^{-1} are shown in Fig. 4 (~~bottom~~ left). The polar vortex strength maximizes at around ~~around~~ 90 ms^{-1} for ~~$\gamma = 4$~~γ=4 K km^{-1}, and at 30 ms^{-1} for ~~$\gamma = 1$~~γ=1 K km^{-1} (not shown), similar to the wind maxima shown in PK02. Also the structure of the polar vortex, and the subtropical jets agree well between our simulation and the ones presented by PK02. Based on the same model as used by PK02 (namely ~~GFDL~~GFDL's spectral dynamical core), Jucker et al. (2013) show climatologies of wind and temperature for the PK02 set-up with ~~$\gamma = 4$~~γ=4 K km^{-1}. The temperature climatology of the EMIL

simulation with ~~$\gamma = 4$~~ γ=4 K km^{-1} agrees well with the one shown by Jucker et al. (2013), with both models simulating a tropical lower stratospheric temperature minimum of 210 K and a pronounced minimum in temperature (T $<$ 180 K) at the winter pole around 10 hPa. ~~Note that when compared to the southern winter climatologies from ERA-Interim Reanalysis (Dee et al., 2011) , as shown in Fig. 4 (top left), the winter high latitude temperature minimum is both too pronounced and too confined in altitude in the model. This issue that will be further discussed in Sec. 4.2.~~

For a second test case, we include the generation of planetary waves by an idealized topography, as proposed by Gerber and Polvani (2009). Fig. 4 (~~bottom~~ right) shows the simulated climatologies with a wavenumber 2 (WN2) mountain with amplitude h = 3 km and ~~$\gamma = 4$~~γ=4 K km^{-1}. Following Gerber and Polvani (2009), the mountain is centered at 45°N and falls off to zero at 25°N and 65°N. This set-up of the mountain was found to lead to most realistic simulation of the mean state of the polar vortex and its variability by Gerber and Polvani (2009). The resulting climatologies of zonal wind, with a polar vortex strength of about 50 ms^{-1}, and of temperature, with a minimum temperature over the winter pole at 10 hPa of around 180 K again closely reproduce the results by Gerber and Polvani (2009) and the equivalent simulation shown by Jucker et al. (2013). ~~As in the case without topography, the winter high latitude temperature minimum is too pronounced and too confined in altitude when compared to northern winter climatologies in ERA-Interim (see Fig. 4, top right).~~

The variability of the polar vortex is diagnosed by the time-series of the zonal mean zonal wind at 10 hPa and 60N for the PK simulation with ~~$\gamma = 4$~~ γ=4 K km^{-1} and a WN2 mountain amplitude of h=3 km in Fig. 5 (black line). The polar vortex is highly variable with winds between -10 to 60 ms^{-1}, with sudden decreases in the wind speeds, known as sudden stratospheric warmings. The time series of the EMIL simulation presented here closely resembles that shown by Gerber and Polvani (2009) in terms of variability.

Overall, the results of this section show that the EMIL set-up is able to reproduce earlier results of simulations performed with dynamical core models under ~~same set-ups of T_{equ}~~identical set-up of equilibrium temperature, relaxation time, the damping layer and topographically generated planetary waves.

3.3 Stratosphere-troposphere coupling

In the study by PK02 it was shown that an increased polar vortex strength, forced by an enhanced stratospheric meridional temperature gradient (i.e., via parameter γ), induces a poleward shift of the tropospheric jet. As discussed in the Introduction, the strength of this response was shown to depend on the details of the prescribed tropospheric equilibrium temperature (Chan and Plumb, 2009) .

As shown in Fig. 6 (left), EMIL model simulations with the same set-up as in the PK02 study reproduce the behavior of the poleward jet shift with increasing polar vortex strength (compare also to Fig. 2 of Gerber and Polvani, 2009) . As has been discussed before, the strong poleward jet displacement between the simulations with γ=2 K km^{-1} and γ=4 K km^{-1} has been shown to be associated with a regime shift between a regime with a subtropical and a poleward located near-surface jet Chan and Plumb (2009) . While we do not find the bimodal distribution of the near-surface jet location as shown by Chan and Plumb (2009) , a broadening of the probability distribution of the tropospheric jet location in the simulation with γ=3 K km^{-1}, and a change in skewness of the distributions (from positive to negative between γ=3 K km^{-1} and γ=4 K km^{-1})

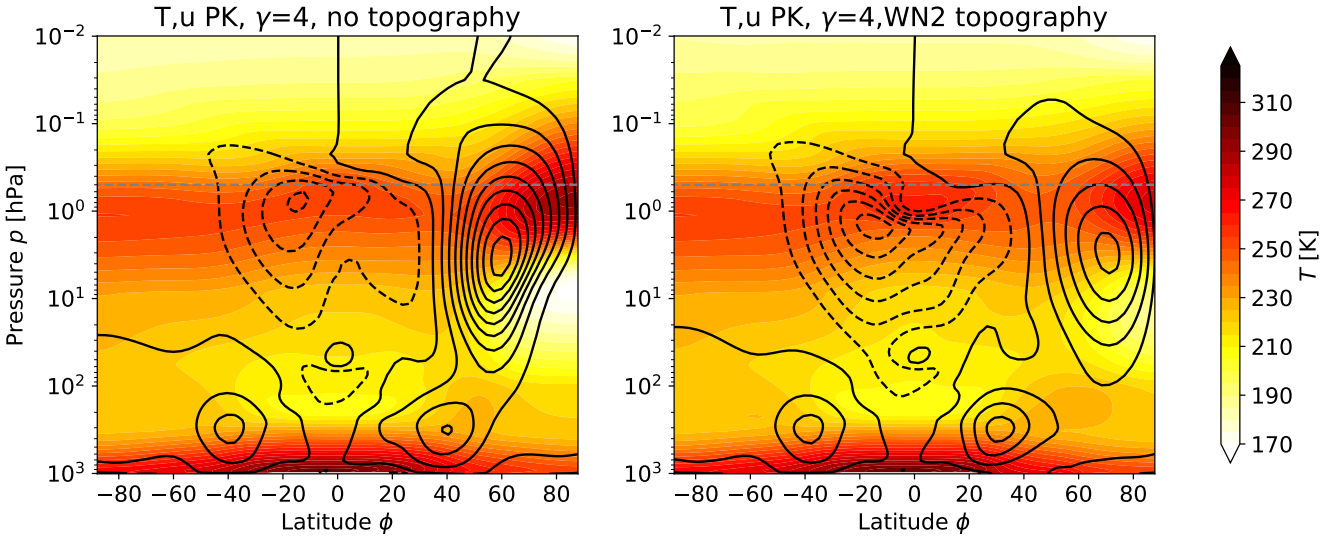

Figure 4. Climatologies of wind (black contours, contour interval 10 ms^{-1}, solid positive, dashed negative) and temperature [K] (colored contours) of (~~top~~ left) ~~July 1995 to 2004 of ERA-Interim, (top right) January 1995 to 2004 of ERA-Interim, (bottom left)~~ an EMIL simulation with the PK02 set-up with ~~$\gamma = 4$~~γ=4 K km^{-1}, and (~~bottom~~ right) an EMIL simulation with the PK02 set-up with ~~$\gamma = 4$~~ γ=4 K km^{-1} and with WN2 topography with h=3 km. The gray dashed horizontal lines in the EMIL climatologies mark the lower boundary of the damping layer. Averages are performed over 10000 days.

indicates a regime shift in the jet location also in our simulations (the properties indicative of regime shifts are detailed in Scheffer et al., 20 The probability distributions are appended for reference, see Fig. C1.

Next to the simulations with identical set-up as in PK02, Fig. 6 shows results from simulations with a modified prescribed tropospheric equilibrium temperature, differing in the strength of the tropical tropospheric vertical temperature gradient (dashed lines). In this set of simulations, in the formulation for the tropospheric equilibrium temperature, the logarithmic decrease of T_{eq} with height in the tropics was implemented as a logarithm with base 10 instead of the natural logarithm (see Eq. B1, 4th term; the simulations are thus referred to as "log10" simulations). The resulting difference in the equilibrium temperature, as displayed in Fig. 6 (right), maximizes at around 5.5 K in the tropical upper troposphere. The simulated temperatures in the same region are about 3.5 K lower, and the upper tropospheric cooling results in an equatorward shift of the tropospheric jet (see Fig. 6, left), as expected from previous simulations that included upper tropospheric heating (e.g., Butler et al., 2010) . The "log10" sensitivity simulations, even though produced inadvertently by an implementation oversight, provide an interesting sensitivity to the original PK set-up: while the change in the stratospheric vortex strength with increased γ is similar in the original set-up and the "log10" set-up (this also applies to variability, as evident from probability distributions, see Fig. C1), the response of the tropospheric jet is strongly damped compared to the original PK02 set-up. At 300 hPa, the maximum wind location shifts only by a few degrees from the simulation without polar vortex to the one with γ=5 K km^{-1}, while in the

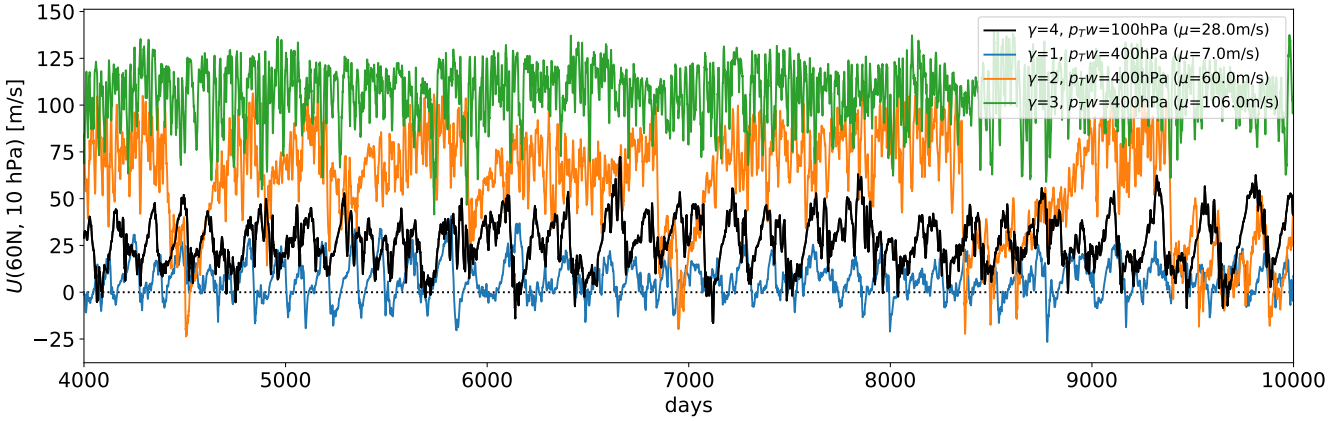

Figure 5. Timeseries of zonal mean zonal wind [ms^{-1}] at 10 hPa and 60°N for different configurations of the PK set-up with a WN2 topography with h=3 km. The black line displays the reference simulation with γ =4 K km^{-1} as in Fig. 4 (right). The colored lines display the sensitivity simulations discussed in Sec. 4.2, with lowered winter transition pressure p_{Tw} and for γ =1, 2 and 3 K km^{-1} (see ~~label~~legend). In the legend, the average value μ over the whole simulation is given.

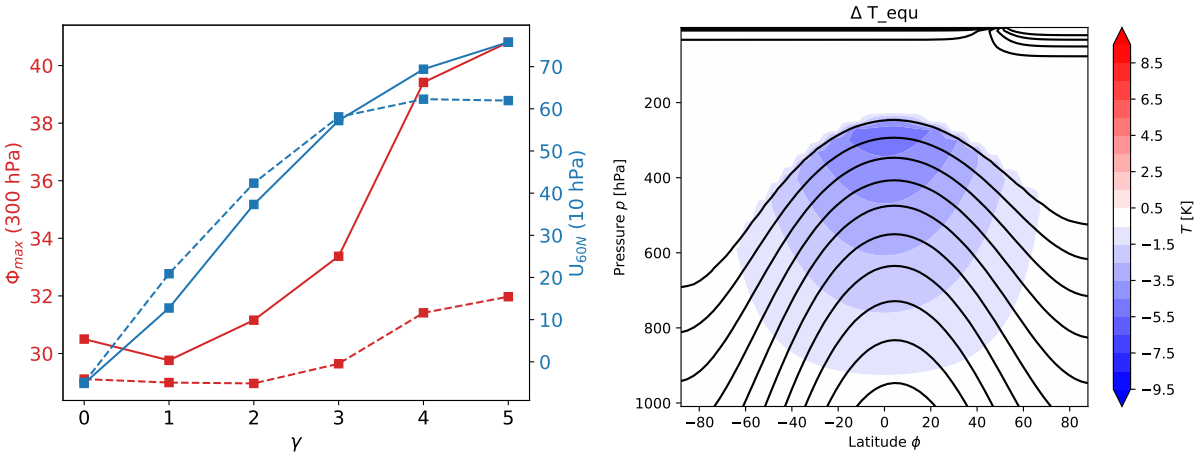

Figure 6. Left: Strength of polar vortex (as measured by zonal mean zonal wind at 10 hPa and 60°N, blue lines) and position of tropospheric jet (measured by zonal wind maximum at 300 hPa, red lines) as a function of γ for simulations with the original PK set-up without topography (solid lines) and the modified set-up with T_{eq} using "log10" (dashed lines). For γ=0, the equilibrium temperature of the summer stratosphere is prescribed also in the entire winter hemisphere. The time means for the original PK simulations are based on 10000 days, the ones for the "log10" simulations on 3300 days. Right: T_{eq} as given by the original PK02 implementation (black contours) and difference in T_{eq} between simulations with "log10" implementation and with standard implementation (colors).

original PK02 set-up this shift amounts to more than 10 degrees latitude. Near the surface (at 850 hPa), the location of the jet even remains almost constant in all "log10" simulations, while in the original PK02 set-up, the near-surface wind maximum shifts by about as much as in the free troposphere (see Fig. C1).

We presume that the more equatorward location of the tropospheric jet in the basic state inhibits the regime transition to a poleward located tropospheric jet in the "log10"-simulations in response to the stratospheric forcing. In the study by Chan and Plumb (2009) , the surface equilibrium temperature equator-to-pole gradient was increased in a set of sensitivity experiments. Despite the different nature of the change in tropospheric equilibrium temperatures in our and their sensitivity simulations, in both cases, the response of the tropospheric jet location to the stratospheric forcing is strongly damped. In the simulations by Chan and Plumb (2009) , the jet was shifted to higher latitudes in the simulations with a weak response, i.e. contrary to our "log10" sensitivity simulations. Thus, while in our simulations the tropospheric jet remains in the "subtropical regime" even under strong forcing, in the sensitivity simulations in Chan and Plumb (2009) , the jet remains in the higher latitude regime. Whether the jet would move to the higher-latitude regime in our "log10" simulations under stronger stratospheric forcing remains to be investigated.

4 Sensitivity simulations

In this Section, the response of the simulated climate to three different types of modifications are tested: (1) modifications in the shape of the upper atmospheric sponge layer, (2) modifications in the winter high-latitude equilibrium temperature profile, and (3) planetary wave generation by wave-like heating instead of topography.

4.1 Sensitivity to the shape of the upper atmospheric damping layer

The damping layer at levels above 0.5 hPa is included to account for the strong damping of winds that in the real atmosphere (or the full model) is due to drag by breaking gravity waves (GW). The simplified manner of damping the entire horizontal wind fields introduces a non-physical sink of momentum. When analyzing results obtained with the model, this has to be kept in mind.

The damping layer as introduced by PK02 uses a damping coefficient that increases quadratically with decreasing pressure. The profile of the PK02 damping coefficient is shown in Fig. 7 together with the profile of zonal mean zonal wind tendencies due to parametrized gravity waves divided by the zonal mean wind (averaged over 40-60°N/S) from a model simulation with the full atmospheric EMAC set-up, i.e., an equivalent damping coefficient of the zonal mean wind by the parametrized GW drag. The "damping" by GW drag ~~increases with height~~ varies between years and hemispheres, but generally increases with decreasing pressure exponentially rather than quadratically. Therefore, we argue that a damping coefficient with exponential increase mimics the net effects of parametrized GW drag better.

A sensitivity simulation is performed in which the damping coefficient in the upper model domain follows the exponential function given by Eq. (A9) (option *EH*; this is the shape of the "sponge" layer originally implemented in the ECHAM model). The damping coefficient of this sensitivity simulation is shown in Fig. 7 as ~~green~~ red line.

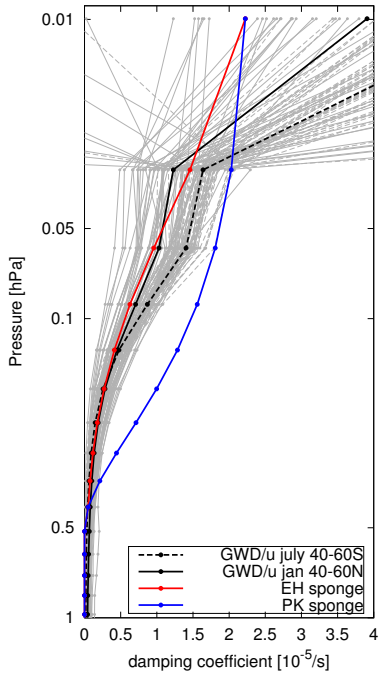

Figure 7. Damping coefficient [s^{-1}] of the sponge layer in the "EH~~"~~" (~~green~~red) and in the PK02 set-up (blue) together with the "effective damping ~~"~~ time scale of the zonal winds by ~~GWD~~ gravity wave drag (i.e., -GWD/u) from an ECHAM simulation with a non-orographic and orographic GW scheme, averaged over 40-60°S in July ~~2000~~ 1960 to 2010 (gray dashed, average over all years shown as black dashed) and averaged over 40-60° ~~S~~ N in January 1960 to 2010 (~~red~~gray solid, average over all years shown as black solid).

The simulated climate states with the two different set-ups of the sponge layer differ within the sponge layer, with maximum differences in zonal winds of 30 $\mathrm{m\,s^{-1}}$ around 0.5 hPa (see Fig. 8)~~, and~~ . Considerable differences in wind and temperature extend below the damping layer ~~, but are negligible outside the winter high latitudesand below about~~ in particular at high latitudes. Differences are mostly insignificant below 10 hPa~~. At high latitudes, an upward shift of the temperature maximum at the stratopause is found, as well as an~~ , however small (significant) differences in zonal winds of 2 $\mathrm{m\,s^{-1}}$ extend down into the troposphere. The increase in zonal winds, which maximizes at the lower bound of the damping layer, is accompanied by an upward shift of the temperature maximum at the stratopause. Since the *EH* sponge is weaker, the increase in zonal mean winds within the damping layer can be expected. The weaker sponge and changed zonal wind structure modifies planetary wave propagation (stronger upward propagation between from about 3 hPa upward, not shown), thus influencing the mean climate also below the damping layer (decreased wave driving, leading to stronger zonal winds and lower polar temperatures). The effect of the modified damping coefficients is similar in simulations with WN2 topography (albeit with weaker absolute differences~~).~~ , not shown).

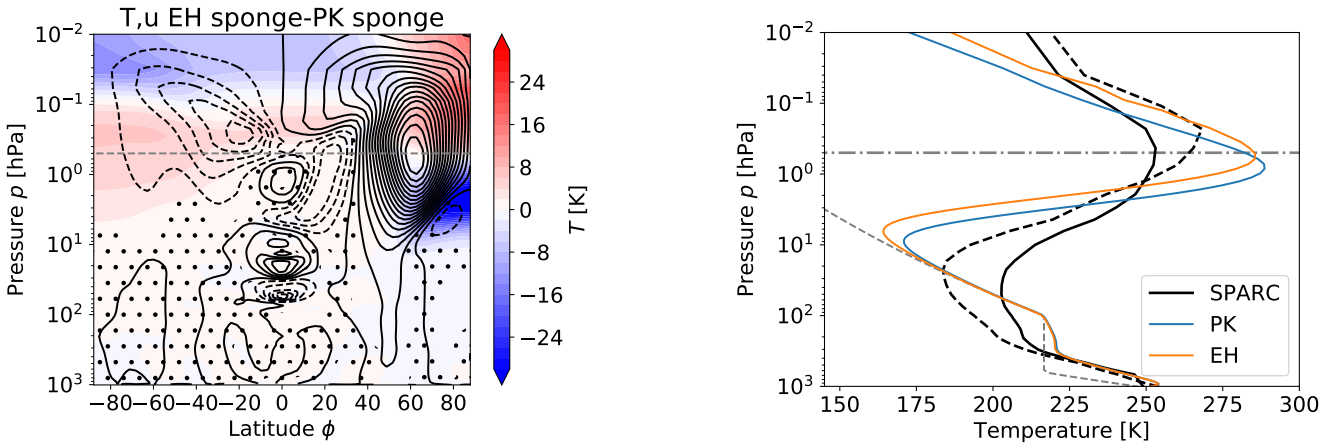

Figure 8. Left: Differences in zonal mean temperature (contour interval is 2 K) and zonal mean zonal wind ~~ms^{-1}~~(contour interval is 2 $\mathrm{m\,s}^{-1}$) between a model simulation with exponentially increasing damping coefficient (*EH*) and a model simulation with quadratically increasing damping coefficient (*PK*) for $p_{\mathrm{Tw}} = 100\,\mathrm{hPa}$ and $\gamma = 4\,\mathrm{K\,km}^{-1}$ without topography. ~~The temperature contour interval is 2K~~Averages are performed over 1500 days of simulation. ~~The~~ Stippling indicates non-significant wind ~~contour interval is $5\,\mathrm{m\,s}^{-1}$~~differences (on a 95% level, based on a T-test performed on 30-day means). Right: Polar winter temperature profiles of same model simulations averaged from 70°N to 90°N, with temperature profiles from the SPARC climatology in northern hemispheric winter conditions (black solid line) and southern hemispheric winter conditions (black dashed line) as well as the equilibrium temperature profile (gray dashed line). The dash-dotted line marks the lower boundary of the sponge layer.

As the exponentially increasing damping coefficient (*EH*) resembles the vertical structure of GW drag, and since for both, plane surface and idealized topography, the height at which the polar winter temperature profile reaches its maximum is more realistic in case of the *EH* damping layer (see Fig. 8 right), we chose to use the exponentially increasing damping coefficient (*EH*) in the following as our reference set-up.

4.2 Sensitivity to modification of the equilibrium temperature in the winter high latitude lower stratosphere

The simulated winter high-latitude temperature profiles for EMIL simulations with *PK* set-up and WN2 topography are shown in Fig. 9 (left) for varying γ, compared to temperature profiles from the "SPARC" climatology (Randel et al., 2004; SPARC, 2002) for northern winter. The comparison of the simulations to the SPARC climatology reveals a positive temperature bias in the ~~UTLS~~ upper troposphere / lower stratosphere (UTLS) region of the winter high latitudes (70°N to 90°N), when using the standard *PK* set-up with a constant transition pressure of $p_{\mathrm{T}}(\phi) \equiv 100\,\mathrm{hPa}$. The positive temperature bias remains unchanged for different polar vortex lapse rates γ. Even for strong decreases of the equilibrium temperature above the $100\,\mathrm{hPa}$ level, the positive temperature bias in the UTLS region ~~can not~~ cannot be compensated. This is essentially because the equilibrium temperature ~~(shown in gray)~~ already exceeds the temperatures obtained from SPARC in that region. Due to the general-circulation transport of heat from the tropics to polar regions throughout the troposphere and stratosphere, the temperature bias even in-

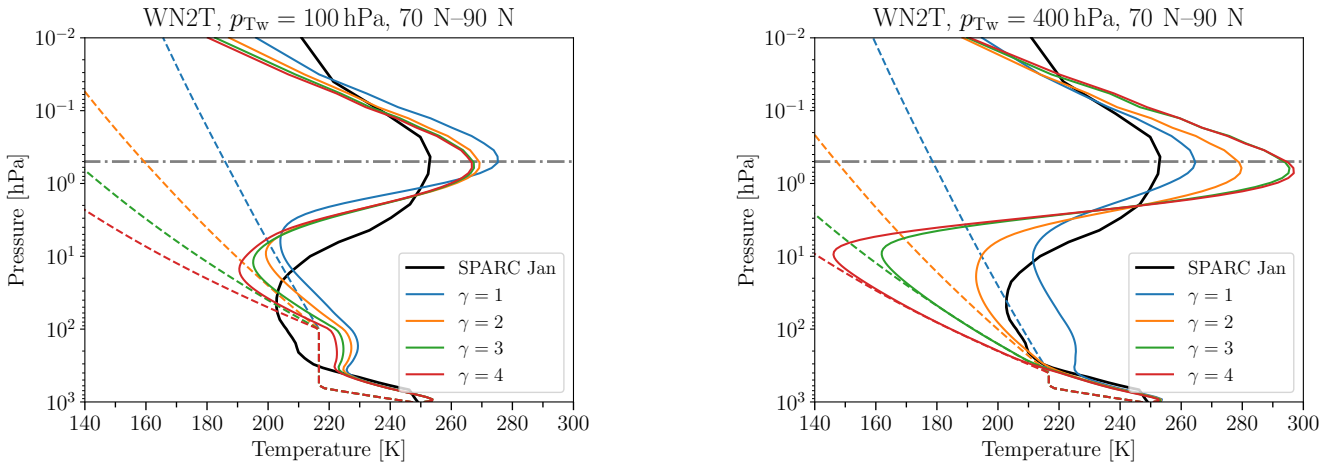

Figure 9. Polar winter temperature profiles of model simulations with WN2 topography of height $h = 3\,\mathrm{km}$ and different polar vortex lapse rates γ for $p_{\mathrm{Tw}} = 100\,\mathrm{hPa}$ (left) and $p_{\mathrm{Tw}} = 400\,\mathrm{hPa}$ (right), together with the temperature profiles obtained from the SPARC climatology (black line) as well as the equilibrium temperature profiles (~~gray~~ colored dashed lines). Averages are based on about 10000 days.

creases. Therefore, every simulation with $p_{\mathrm{Tw}} = 100\,\mathrm{hPa}$ necessarily has a too warm UTLS region in the winter high latitudes compared to the SPARC climatology~~(and compared to ERA-Interim reanalysis, see Fig. 4).~~. The warm bias is associated with an unrealistic "step" in the temperature profile, forced by the constant equilibrium temperature profile in the UTLS up to 100 hPa.

In order to approach a more realistic temperature profile in the UTLS region of the winter high latitudes, the transition pressure p_{Tw} is increased. ~~The parameters p_{Tw} and γ are varied~~ A similar approach was used by Sheshadri et al. (2015) , who lowered the transition pressure globally to 200 hPa and showed that this led to an improvement in lower stratospheric zonal winds. Here, we systematically vary the the transition pressure in polar winter high latitudes only across $p_{\mathrm{Tw}} = 100$ to $450\,\mathrm{hPa}$ ~~and~~ as well as γ across $\gamma = 1$ to $4\,\mathrm{K\,km^{-1}}$ ~~. At~~ (see Table B1).

As noted in Sec. 3.3, in a former version of the model, a modified version of the tropospheric equilibrium temperature function was implemented, resulting in a reduced vertical temperature gradient (see Fig. 6, right). The whole parameter sweep was performed in this modified model set-up, and we repeated simulations for $p_{\mathrm{Tw}} = 100\,\mathrm{hPa}$ and $400\,\mathrm{hPa}$ with the standard set-up to test the sensitivity of the results to the changed tropical tropospheric equilibrium temperature. In Figs. 10 and 11, the results of both set-ups are shown, with the modified simulations labeled as "log10"-simulations. The "log10" simulations are performed for 1825 days (with the first 300 days considered as spin-up), while the simulations under standard set-up were extended to 10950 days (with 1000 days of spin-up). While the 1825-day simulations are mostly too short to establish convergence of the climatologies, the qualitative behavior in those simulations is in general in agreement with the results from the extended simulations (as presented in the following).

The polar temperature profiles shown in Fig. 9 for the simulations with standard set-up are very similar to those for the simulations with the modified "log10" set-up (not shown). In both set-ups, at $p_{\mathrm{Tw}} = 400\,\mathrm{hPa}$, all equilibrium temperatures in the polar winter UTLS region fall below the corresponding temperatures obtained from SPARC except the one for $\gamma = 1\,\mathrm{K\,km^{-1}}$ (see the right panel of Fig. 9). For the simulations with $\gamma = 3\,\mathrm{K\,km^{-1}}$ and $\gamma = 4\,\mathrm{K\,km^{-1}}$, the winter high-latitude temperatures are lower than the SPARC temperatures throughout the UTLS region, and follow the equilibrium temperature up to about 30 hPa. Above, the temperature increases strongly, reaching a maximum at around 0.7 hPa. In contrast, the UTLS temperature in the simulation with $\gamma = 1\,\mathrm{K\,km^{-1}}$ is well above the corresponding equilibrium temperature in the UTLS, and the temperature maximum at around 0.5 hPa is weaker. The simulation with $\gamma = 2\,\mathrm{K\,km^{-1}}$ lies in between: Its temperature in the UTLS is higher than the equilibrium temperature, but less so than for $\gamma = 1\,\mathrm{K\,km^{-1}}$.

The non-linear behavior of the deviation from the equilibrium temperature is illustrated for a variety of values of γ and p_{Tw} in Fig. 10~~: in the lower stratosphere, $T - T_{\mathrm{equ}}$ is larger for lower~~. The deviation of temperature from the equilibrium temperature is a valid measure of the strength of the residual meridional circulation in the idealized model (see e.g., Jucker et al., 2013) . We choose to average this temperature difference from 40°N to 90°N, as this is the region of diabatic heating associated with downwelling. Larger values of this temperature difference therefore imply a stronger circulation. In Fig. 10, these temperature differences are displayed for 10 hPa and 100 hPa to represent the strength of the circulation in the middle and lower stratosphere, respectively. For low values of γ, we find an increase in $T - T_{\mathrm{eq}}$ with γ in the mid-stratosphere, but a decrease in the lower stratosphere, in agreement with the result of Gerber (2012) that a stronger polar vortex leads to a strengthened circulation in the upper stratosphere and to a weakened circulation in the lower stratosphere (see Fig. 3 of Gerber, 2012, for comparison) . However, ~~the response to lowering p_{Tw} reverses from low to high values of~~ above a certain threshold of γ, the circulation strength decreases with γ and then stagnates also in the mid-stratosphere (10 hPa). This critical value of γ depends on p_{Tw}, in line with lower polar T_{eq} values for higher values of p_{Tw}. In the upper stratosphere ~~, the deviation in temperature increases nearly linearly, both for enhancing~~ (1 hPa), a monotonic increase in $T - T_{\mathrm{eq}}$ both with larger γ and p_{Tw} ~~. At the same time, the~~ is found (not shown), but we exclude this analysis because of the likely influence of the upper damping layer.

The strength of the polar vortex increases for larger γ and p_{Tw} values, as expected from the stronger meridional temperature gradient ~~induced by larger γ and p_{Tw}~~ (see Fig. 11 top right, here the polar vortex is measured by the zonal mean wind speed at 60°N and 10 hPa)~~, but this increase is again not linear in~~ . The polar vortex increase is non-linear with increasing γ~~. The modified strength~~ : In line with the change in behavior of $T - T_{\mathrm{eq}}$ at 10 hPa when reaching a critical value of γ, the polar vortex accelerates more strongly with γ above this critical value (e.g., for $p_{\mathrm{Tw}} = 400\,\mathrm{hPa}$, between $\gamma = 2\,\mathrm{K\,km^{-1}}$ to $2.5\,\mathrm{K\,km^{-1}}$ in the "log10" set-up). Thus, for increases in the prescribed meridional temperature gradient in the polar stratosphere below a certain threshold, the polar vortex strength increases only very weakly. At the same time, mid-to high-latitude temperatures increase above the corresponding equilibrium temperature (i.e., $T - T_{\mathrm{eq}}$ increases with γ). Thus, the residual circulation is strengthened, and the associated high-latitude warming counteracts the increase in the meridional temperature gradient, explaining the weak changes of the polar vortex~~is~~ . However, when a certain threshold in the prescribed meridional equilibrium temperature is reached, the polar vortex increases strongly, and at the same time $T - T_{\mathrm{eq}}$ decreases, indicating a reduction in wave driving and thus additional dynamical strengthening of the meridional temperature gradient.

The sudden change in the polar vortex strength is indicative of a regime shift, a result that is also reflected in changes in ~~its~~ the polar vortex variability, as shown in Fig. 5 for the simulations with $p_{\mathrm{Tw}} = 400\,\mathrm{hPa}$ and $\gamma = 1$, 2, and $3\,\mathrm{K\,km^{-1}}$. While the simulation with the weakest polar vortex ($\gamma = 1\,\mathrm{K\,km^{-1}}$) exhibits large variability with frequent crossings of the zero-wind line (indicative of sudden stratospheric warmings), in the simulation with $\gamma = 3\,\mathrm{K\,km^{-1}}$ the wind oscillates around its large mean value without crossing the zero wind line. In the simulation with $\gamma = 2\,\mathrm{K\,km^{-1}}$, episodes with strong stable winds are disrupted by sudden decelerations, and the polar vortex remains in a weak state for ~~up to 500 daysthereafter. This behavior indicates that~~ an extended period (up to a few hundred days) thereafter, i.e. the vortex alternates between a strong and a weak regime. The regime behavior is further supported by the shape of the probability distribution of the maximum wind at 10 hPa for those three simulations (see Fig. C2): while in the simulation with $\gamma = 1\,\mathrm{K\,km^{-1}}$, the polar vortex strength is bound below $50\,\mathrm{m\,s^{-1}}$, and in the simulation with $\gamma = 3\,\mathrm{K\,km^{-1}}$, the vortex strength is always above $75\,\mathrm{m\,s^{-1}}$, for $\gamma = 2\,\mathrm{K\,km^{-1}}$ a broad, nearly bimodal, distribution is found. The distribution functions for the "log10" simulations (not shown) are noisier due to the shorter simulation length, but show a similar behavior than those shown in Fig. C2.

As has been shown by Gerber and Polvani (2009) , the response of the tropospheric jet location to stratospheric forcing is strongly damped in the simulations with idealized topography compared to those without topography. The EMIL model simulations presented here reproduce the dampened response to stratospheric forcing (changes in γ) under same set-up as in Gerber and Polvani (2009) : In Fig. 11, next to the strength of the polar vortex, the latitude of the zonal mean zonal wind speed maximum of the tropospheric jet at 500 hPa for varying polar lapse rates γ and transition pressures p_{Tw} are shown. For the stronger stratospheric forcing in the simulations with increased p_{Tw}, the tropospheric jet shifts poleward more strongly, both in the free troposphere and near the surface (see Fig. 11 and 12). This poleward shift is found both in the "log10"-set-up and in the standard set-up, with a similar rate (see Fig. 12).

As discussed in Sec. 3.3, in the simulations without topography, the poleward shift of the jet is much more pronounced in the standard than in the "log10" simulation (see also Fig. 12). Thus, in the presence of planetary wave forcing, the different tropospheric equilibrium temperatures appear to play a smaller role for the stratosphere-troposphere coupling. The poleward shift of the jet for a given polar vortex change in the topography simulations with $p_{\mathrm{Tw}} = 400\,\mathrm{hPa}$ is still smaller than in the original PK02 simulations (compare "WN0, ln" and "WN2T400, ln"/"WN2T400, log10" in Fig. 12). Whether the poleward shift of the tropospheric jet in the $p_{\mathrm{Tw}} = 400\,\mathrm{hPa}$ simulations is associated with a regime shift of the jet location as in the PK02 simulations is not entirely clear: the probability distribution functions of the tropospheric jet location (see Fig. C2) are broadening in the transition from lower to higher latitudes in both cases, but less so in the $p_{\mathrm{Tw}} = 400\,\mathrm{hPa}$ simulations.

Overall, the stratospheric circulation responds non-linearly to modifications of the winter equilibrium temperature profile. Lowering the height at which the equilibrium temperature starts to decrease can diminish the high-latitude lower stratospheric temperature bias. To more or less completely remove the warm bias and the associated unrealistic "step", p_{Tw} has to be ~~lowered~~ increased to $400\,\mathrm{hPa}$. In the simulation set-up with $p_{\mathrm{Tw}} = 400\,\mathrm{hPa}$ and $\gamma = 2\,\mathrm{K\,km^{-1}}$, the winter high-latitude temperature profile is close to reanalysis data (SPARC climatology and ERA-Interim, the latter not shown) in the UTLS region and a moderate oscillation of the temperature in the upper atmosphere is simulated. ~~The corresponding climatologies of zonal mean temperature and zonal mean zonal wind of this simulation are displayed in the left panel of Fig. ??.~~ As discussed above, the

polar vortex transitions from a weak state to a strong state when increasing γ and/or p_{Tw}. In between, vortex states are found that appear to alternate between those two states, indicative of a ~~regime-like behavior~~transition between two vortex regimes. The dynamical reasons for this regime-like behavior, as well as the question whether the regimes of the stratospheric vortex strength are connected to the regimes of the tropospheric jet location, will be investigated in future studies.

4.3 Planetary wave generation with topography versus heating

In the experiments presented in the preceding subsection 4.2, an idealized topography was used to generate planetary waves. Recently, Lindgren et al. (2018) suggested an alternative method to generate planetary waves: they introduced a tropospheric wave-like thermal forcing of the form of Eq. (A11), which is added to the temperature tendency ~~(Eq.)~~ of Newtonian cooling.

For the equilibrium temperature, Lindgren et al. (2018) employ a constant transition pressure of $p_{\mathrm{T}}(\phi) = 200\,\mathrm{hPa}$, i.e. $p_{\mathrm{Ts}} = p_{\mathrm{Tw}} = 200\,\mathrm{hPa}$, and $\epsilon = 0$, i.e., a hemispherically symmetric temperature distribution in the troposphere. Fig. 13 shows the temperature profiles in the winter high latitudes for different simulations that were thermally forced by Eq. (A11). The model simulation with the original Lindgren set-up exhibits a too high temperature in the winter high-latitude UTLS region compared to the SPARC climatology for the same reason as was explained for the topographically forced simulations with $p_{\mathrm{T}}(\phi) = 100\,\mathrm{hPa}$ (~~original PK02~~ "PK" set-up) in the previous subsection: the decrease of the equilibrium temperature due to γ starts too high to be able to compensate the warm bias. This motivated the investigation of model simulations with a larger transition pressure p_{Tw} in the winter high latitudes for the thermally forced simulations as well.

In our model simulations with WN2 tropospheric heating, we similarly use $\epsilon = 0$, but return to $p_{\mathrm{Ts}} = 100\,\mathrm{hPa}$ and vary p_{Tw}.[1] In addition to the profile obtained from the Lindgren set-up, Fig. 13 contains the winter high-latitude temperature profiles for different polar vortex lapse rates, γ ~~,~~ and for $p_{\mathrm{Tw}} = 400\,\mathrm{hPa}$~~(left panel) and $p_{\mathrm{Tw}} = 450\,\mathrm{hPa}$ (right panel).Besides the SPARC temperature profile for January conditions, both panels show the reference model simulation for WN2 topography (with $\gamma = 2\,\mathrm{K\,km^{-1}}$ and $p_{\mathrm{Tw}} = 400\,\mathrm{hPa}$, labeled EMILSUBSCRIPTNB400SUBSCRIPTNB2). For $p_{\mathrm{Tw}} = 400\,\mathrm{hPa}$, two circulation regimes are found. One regime is found in the model runs with $\gamma = 1$–$3\,\mathrm{K\,km^{-1}}$, manifesting~~.

Fig. 10 and Fig. 11 show results from the simulations with thermally forced planetary waves, and again both the modified "log10" simulations as well as simulations with the standard tropospheric equilibrium temperatures are included. As discussed for the topographically forced simulations, we also find a regime-like behavior of stratospheric circulation in the thermally forced simulations: The weak polar vortex regime (for γ smaller than about $3\,\mathrm{K\,km^{-1}}$, see Fig. 11 bottom right) manifests in a positive temperature bias in the UTLS region of the winter high latitudes ~~, with enhanced temperature compared to~~ (Fig. 13), and increasing temperature deviation from the equilibrium temperature ~~(see~~ with increasing γ (Fig. 10 bottom right)~~and a weak polar vortex (see~~. The strong polar vortex regime arises for $\gamma \geq 3$ to $3.5\,\mathrm{K\,km^{-1}}$ (Fig. 11 bottom right)~~. The other regime arises for $\gamma \geq 3.5\,\mathrm{K\,km^{-1}}$~~, with temperature following the equilibrium temperature very closely in the UTLS region (see Fig. 10 bottom right), and with a strong polar vortex (see Fig. 11 bottom right).

[1] The difference in the equilibrium temperature between $p_{\mathrm{Ts}} = 100\,\mathrm{hPa}$ and $p_{\mathrm{Ts}} = 200\,\mathrm{hPa}$ is marginal since the US standard atmosphere between ~~$\sim 55\,\mathrm{hPa}$~~ about $55\,\mathrm{hPa}$ and ~~$\sim 226\,\mathrm{hPa}$~~ $226\,\mathrm{hPa}$ is isothermal at 216.65 K. Thus, for different values of p_{Tw} only the lower region of the polar vortex lapse rate around $\phi_0 = 50°\,\mathrm{N}$ experiences a slight change when employing $p_{\mathrm{Ts}} = 100\,\mathrm{hPa}$ instead of $p_{\mathrm{Ts}} = 200\,\mathrm{hPa}$.

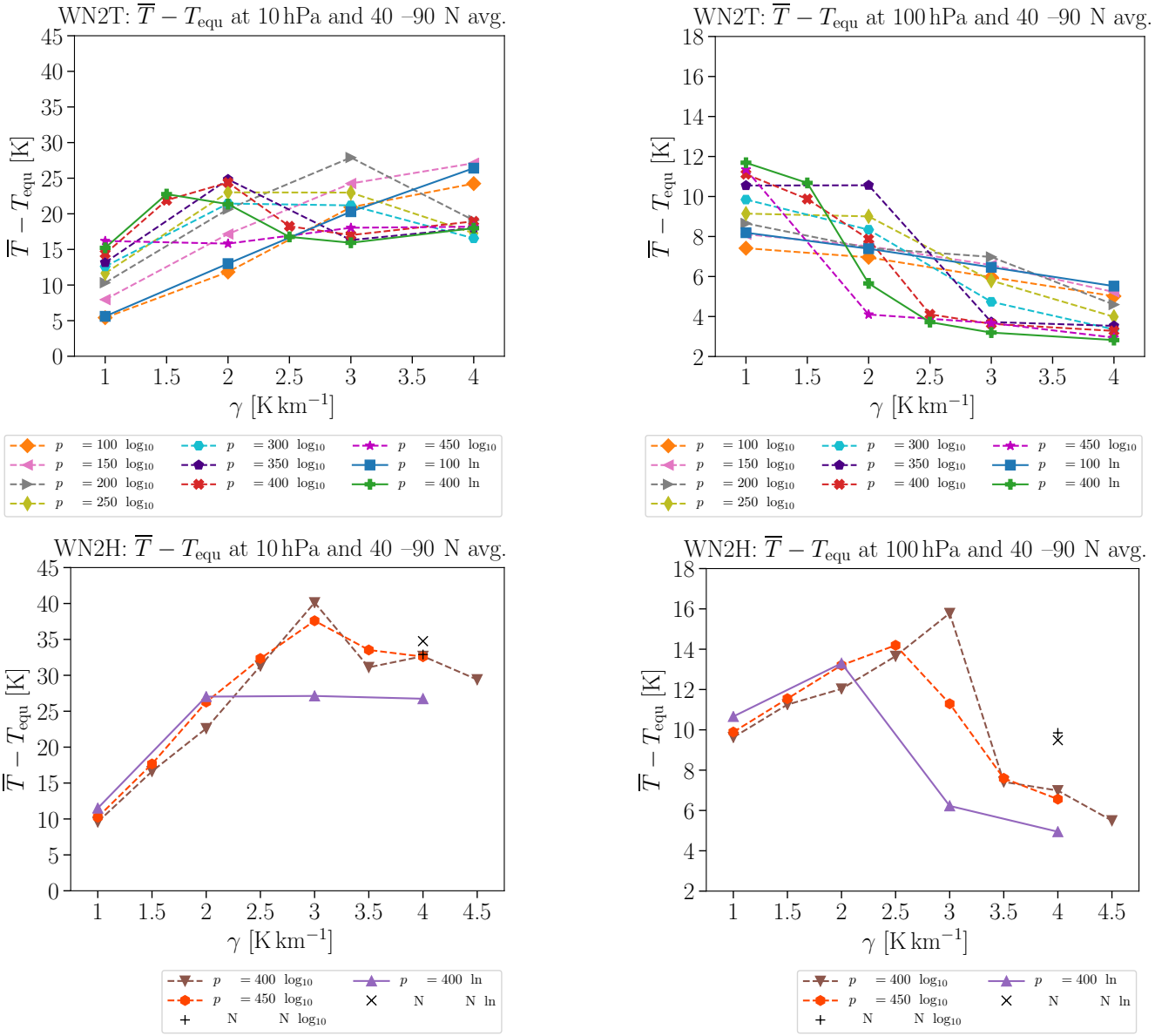

Figure 10. Difference of temperature and equilibrium temperature $T - T_{\mathrm{eq}}$ averaged from 40°N to 90°N at 10 hPa (left panels) and 100 hPa (right panels) for model simulations with WN2 topography of height $h = 3$ km (upper panels) and WN2 tropospheric heating of amplitude $q_0 = 6\,\mathrm{K\,day^{-1}}$ (lower panels).

~~For $p_{\mathrm{Tw}} = 450$ hPa, these two regimes exist for $\gamma = 1$–$2.5\,\mathrm{K\,km^{-1}}$ and $\gamma \geq 3.5\,\mathrm{K\,km^{-1}}$, respectively (~~The probability distribution functions of the polar vortex strength changes strongly between the weak and strong vortex state (e.g., change in sign of skewness, see Fig. ~~13 right panel). However, the resulting circulation for $\gamma = 3\,\mathrm{K\,km^{-1}}$ can not be assigned to one of~~

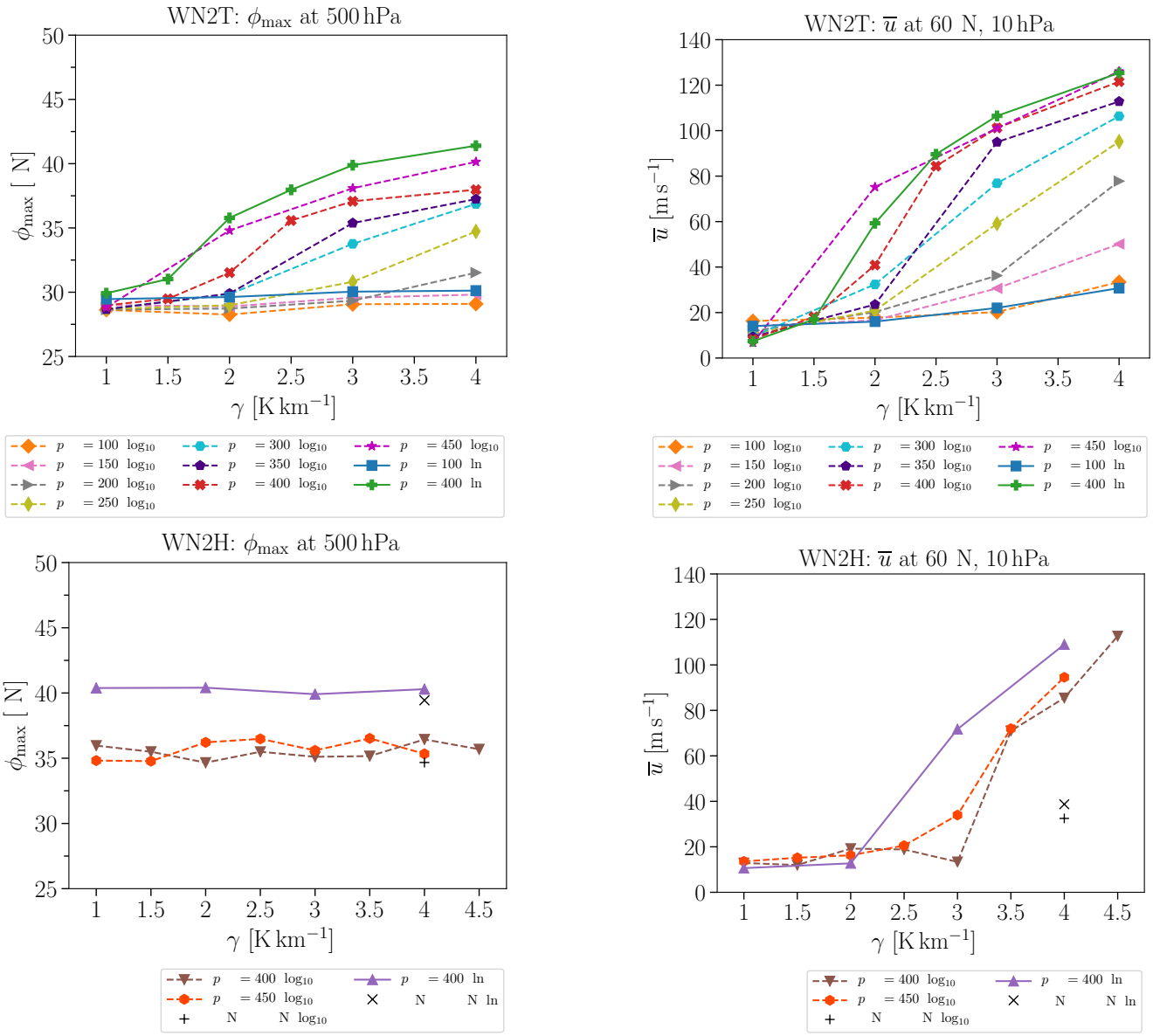

Figure 11. Latitude $\phi_{\max}$ of the zonal mean zonal wind speed maximum of the tropospheric subtropical jet stream (left panels) and zonal mean zonal wind speed u at 60°N and 10 hPa (right panels) for model simulations with WN2 topography of height $h = 3$ km (upper panels) and WN2 tropospheric heating of amplitude $q_0 = 6$ K day^{-1} (lower panels).

~~the regimes, since the temperature in the UTLS region is neither too warm nor follows its equilibrium temperature, i. e., with a similar behavior as the topographically-forced simulation with $p_{\mathrm{Tw}} = 400$ hPa and $\gamma \geq 2$ K km^{-1}. The climatologies of those two simulations are shown in Fig. ??.~~ C3), supporting further that we see a regime transition. In terms of polar vortex changes

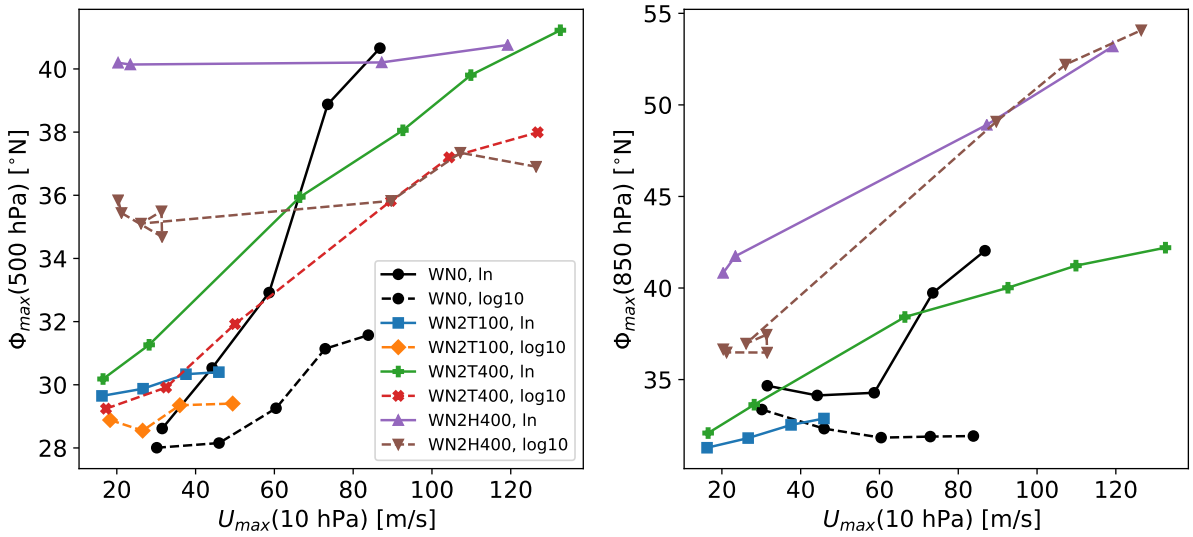

Figure 12. Maximal zonal mean zonal wind speed u at 10 hPa displayed against the latitude $\phi_{\max}$ of the zonal mean zonal wind speed maximum at 500 hPa (left) and 850 hPa (right) for various simulation set-ups: simulations under PK set-up without topography (black, see also Fig. 6), and with WN2 planetary waves forced topographically (labeled WN2T) and diabatically (labeled WN2H) for various values of the winter transition pressure p_{Tw} (see legend, colors follow Figs. 10 and 11). Each symbol displays the simulation-average value for simulations with varying polar vortex lapse rate γ. The values for the "WN2T log10" simulations are not shown on the right, because data at 850 hPa was not saved appropriately.

with increasing prescribed polar stratospheric temperature gradient, the simulations with the different tropospheric equilibrium temperatures ("log10" versus standard) show only minor differences.

~~Temperature K and zonal wind ms^{-1} climatologies of model simulations with idealized topography of height $h = 3\,\mathrm{km}$ (left panel) and the simulations with idealized tropospheric heating of amplitude $q_0 = 6\,\mathrm{K\,day^{-1}}$ (right panel). The winter high latitude transition pressures and polar vortex lapse rates are $p_{\mathrm{Tw}} = 400\,\mathrm{hPa}$ and $\gamma = 2\,\mathrm{K\,km^{-1}}$ for the topographically forced model simulation and $p_{\mathrm{Tw}} = 450\,\mathrm{hPa}$ and $\gamma = 3\,\mathrm{K\,km^{-1}}$ for the thermally forced model simulation, respectively.~~

~~The~~ Furthermore, the response of the polar vortex to changes in the equilibrium temperature is similar between the topographically versus thermally forced model simulations in that a regime shift from a weak to a strong polar vortex is found for both cases. However, other aspects of the circulation response show distinct differences. ~~The response of the residual meridional circulation is examined in terms of the difference of temperature and equilibrium temperature, a valid measure of the strength of this circulation in the idealized model (see e.g., Jucker et al., 2013) . We choose to average this temperature difference from 40°N to 90°N to have a positive quantity due to the diabatic heating in that region. Larger values of this temperature difference therefore imply a stronger circulation. In Fig. 10, these temperature differences are displayed for 1 hPa and 100 hPa to represent the strength of the circulation in the lower and upper stratosphere, respectively. Again, in case of a topographically forced circulation, the result of Gerber (2012) is reproduced, according to which a stronger polar~~

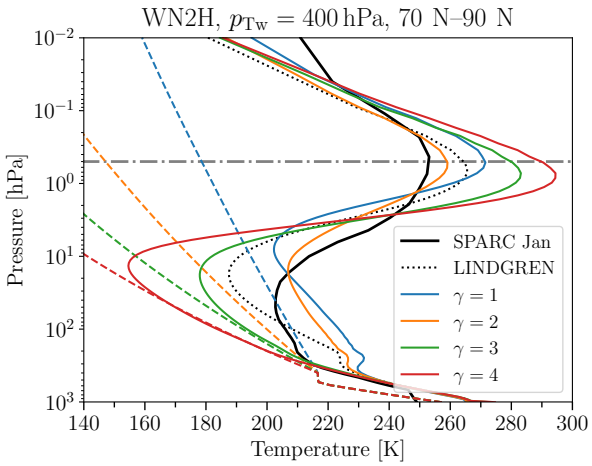

Figure 13. Same as Fig. 9, but for model simulations with WN2 tropospheric heating of amplitude $q_0 = 6\,\mathrm{K\,day^{-1}}$ and different polar vortex lapse rates γ for $p_{\mathrm{Tw}} = 400\,\mathrm{hPa}$ ~~(left) and $p_{\mathrm{Tw}} = 450\,\mathrm{hPa}$ (right)~~. The temperature profiles obtained from a simulation with ~~WN2 topography, $\gamma = 2\,\mathrm{K\,km^{-1}}$ and $p_{\mathrm{Tw}} = 400\,\mathrm{hPa}$ (black dashed line) and from~~ the original Lindgren set-up (black dotted line) are added for comparison.

~~vortex leads to a strengthened circulation in the upper stratosphere and to a weakened circulation in the lower stratosphere (see Fig. 3 of Gerber, 2012, for comparison) .~~

Thermally forced model simulations ~~show the same~~ also show an increase of the strength of the meridional circulation at ~~1 hPa, although the polar vortex increases in strength only for larger γ. However, at 100 hPa, a nonlinear behavior in the strength of the meridional circulation is observed. For low values of the polar vortex lapse rate γ, the circulation strengthens, but for higher values, the circulation weakens as expected from the topographically forced model simulations~~ 10 hPa up to a certain threshold of γ, similar than for the topographically forced simulations. Note, however, that the threshold is higher for the thermally forced simulations for identical equilibrium temperature. The change in the behavior of the meridional circulation in the model simulations with ~~$p_{\mathrm{Tw}} = 400\,\mathrm{hPa}$ and~~ $p_{\mathrm{Tw}} = 450\,\mathrm{hPa}$ and $p_{\mathrm{Tw}} = 400\,\mathrm{hPa}$ (both for the "log10" and standard set-up) appears at the same polar vortex lapse rates, at which the polar vortex starts to strengthen. At 100 hPa, the topographically forced simulations show a (non-linear) decrease of the circulation strength with increasing γ for all values of p_{Tw}, while in the thermally forced simulations the circulation in the lower stratosphere responds in a similar non-linear way as at 10 hPa.

Further, we compare the response of the tropospheric jet to changed equilibrium temperatures in topographically forced simulations to the response in the thermally forced simulations. ~~In Fig. 11, next to the strength of the polar vortex, the latitude of the zonal mean zonal wind speed maximum of the tropospheric jet for varying polar lapse rates γ and transition pressures p_{Tw} are shown. Both, for the topographically and thermally forced simulations, the polar vortex strength generally increases with larger polar lapse rate γ and a transition pressure at lower heights (higher p_{Tw}), as expected. However, the increase is not linear, in particular in the thermally forced simulations, where the polar vortex increases in strength only for $\gamma > 3\,\mathrm{K\,km^{-1}}$. In~~ As discussed in the last section, in case of the topographically forced model simulations~~(upper panels), the~~

result of Gerber and Polvani (2009) is reproduced according to which , the location of the free tropospheric jet shifts poleward in the simulations with a stronger stratospheric polar vortexcauses a northward shift of the tropospheric jet stream (see their Fig.2 for comparison, as does the location of the near-surface jet (see Fig. 12). However, when the circulation is planetary waves are thermally forced, this behavior is not observed the free tropospheric jet maximum remains at a constant latitudinal location (see lower panels of Fig. 11 and Fig. 12). Even strong increases in the stratospheric polar vortex for $\gamma > 3\,\mathrm{K\,km^{-1}}$ at $p_{\mathrm{Tw}} = 400\,\mathrm{hPa}$ and for $\gamma > 2.5\,\mathrm{K\,km^{-1}}$ at $p_{\mathrm{Tw}} = 450\,\mathrm{hPa}$,respectively, are not accompanied by a northward shift of the free tropospheric jet maximum. On the contrary, a slight southward shift is observed.However, for those strong increases in the polar vortex strength, the near-surface jet is shifted to the north, even with a higher rate than in the topographically forced simulations (see Fig. 12). For intermediate values of γ, the near-surface jet location shows signs of bimodality (see Fig. C3, here for $\gamma = 3.5\,\mathrm{K\,km^{-1}}$). The behavior of the near-surface jet in our simulations with thermally forced planetary waves thus seems to show a regime-like behavior as found in other set-ups in earlier studies (Chan and Plumb, 2009; Wang et al., 2012) , despite the free tropospheric jet remaining at a constant latitude.

Latitude ϕ_{max} of the zonal mean zonal wind speed maximum of the tropospheric subtropical jet stream (left panels) and zonal mean zonal wind speed u at $60°\mathrm{N}$ and $10\,\mathrm{hPa}$ (right panels) for model simulations with WN2 topography of height $h = 3\,\mathrm{km}$ (upper panels) and WN2 tropospheric heating of amplitude $q_0 = 6\,\mathrm{K\,day^{-1}}$ (lower panels).

Difference of temperature and equilibrium temperature $T - T_{\mathrm{equ}}$ averaged from $40°\mathrm{N}$ to $90°\mathrm{N}$ at $1\,\mathrm{hPa}$ (left panels) and $100\,\mathrm{hPa}$ (right panels) for model simulations with WN2 topography of height $h = 3\,\mathrm{km}$ (upper panels) and WN2 tropospheric heating of amplitude $q_0 = 6\,\mathrm{K\,day^{-1}}$ (lower panels).

The Overall, the different behavior of model simulations with topographically and thermally forced circulations outlined here indicates that the thermally forced simulations will might have to be used with caution, in particular for studying troposphere-stratosphere coupling.

5 Application examples

In the previous sections, the implementation of the EMIL model was documented and tested, and modified set-ups were introduced, showing that the model is well suited for further applications. In the following, two examples of research applications with the dynamical core model are shown. First, variability and changes in tracer transport in response to changes in the polar vortex are analyzed, using the simulation set-up with the modified equilibrium temperature (see Sec. 4.2). Secondly, the localized heating routine (see Sec. 2.1.1) is used to force an idealized monsoon circulation system.

5.1 Chemistry and tracer transport

With the implementation of the idealized model set-up in the MESSy framework, all tracer utility and chemistry submodels can be easily used to study the tracer transport in the idealized model. Within the chemistry submodel MECCA (Sander et al., 2019), tailor made chemical mechanisms can be selected to the users' needs, allowing for the set-up selection of simplified

chemistry set-ups. As a proof of concept, we present results from simulations where the only selected chemical reactions are the photolysis of Chlorofluorocarbons (CFCs, namely CFC-11 and CFC-12).

Technically, this simulation set-up requires, in addition to the "standard" EMIL set-up, to switch on submodels for solving chemical kinetics (MECCA, Sander et al., 2019), for calculating photolysis rates (JVAL, Sander et al., 2014), for determining orbital parameters (ORBIT, Dietmüller et al., 2016) and submodels for tracer definition (TRACER and PTRAC, Jöckel et al., 2008) and tracer boundary condition nudging (TNUDGE, Kerkweg et al., 2006). CFC mixing ratios were set to values representative of year 2000 at the surface, and tracers were initialized with a mean distribution from an earlier EMAC simulation. To obtain constant January conditions of solar irradiance (compatible with the idealized thermodynamical forcing of the dynamics), in the ~~"TIMER "~~ TIMER namelist, a perpetual month simulation can be selected.

With the given model set-up including chemical tracers, the influence of idealized dynamical variability on chemically active species can be studied. Shown in Fig. 14 are zonal mean CFC-11 mixing ratios at 50 hPa as function of latitude and time in a simulation with *PK* set-up[2] with p_{Tw}=400 hPa and γ=2 K km^{-1}. The polar vortex variability leads to variability in CFC-11 mixing ratios in particular at high latitudes. As diagnosed from the time series of zonal mean zonal wind at 60°N and 10 hPa (top panel in Fig. 14, black line) sudden stratospheric warming (SSW) events occur at around day 600 and day 1350 (defined as zero-crossing of the zonal wind, see dashed gray lines), both followed by an extended period with a weak polar vortex. For both events, the CFC-11 mixing ratios drop at high latitudes simultaneously with the drop of zonal winds at 10 hPa. However, around 200 days after the SSW events, mixing ratios are anomalously high.

This behavior can be explained as follows: simultaneously with the SSW, strong downwelling occurs at high latitudes (north of 60°N~~, and)~~, driven by the strong wave dissipation that ~~causes SSWs,~~ effected the SSW (see red line in top panel in Fig. 14)~~,~~ ~~thus transporting~~ . The enhanced downwelling transports CFC-depleted air from higher altitudes downward. However, due to the diminished vortex in the period after the SSW, air from mid-latitudes with higher CFC mixing ratios can be mixed towards the pole, thus leading to an enhancement of CFC mixing ratios at high latitudes~~(~~. This is evident in Fig. 14 around days 800-1000 and days 1500-1700, when zonal winds are below 15 ms^{-1}~~). Those~~ .

The transport anomalies are evident in the latitudinal profiles of CFC-11 mixing ratios, as shown in the right panel of Fig. 14: during episodes with a strong polar vortex (solid line), there is a local minimum in mixing ratios close to the polar vortex edge (in agreement with strongest downwelling at the vortex edge, see Fig. 15, third panel), denoting the separation between mid-latitude and high-latitude air by the vortex. Just at and after the SSW events, CFC mixing ratios drop at high latitudes (dashed line), while in the episodes with eroded vortex, CFC-11 mixing ratios are enhanced at mid- to high latitude and no mixing barrier can be identified (dotted line). ~~As demonstrated here, the idealized set-up of the simulation allows to study the role of vortex variability on tracer mixing ratios in an isolated manner.~~

Two additional simulations were performed with idealized changes in the polar vortex (intermediate: $\gamma = 2$, weak vortex: $\gamma = 1$, strong vortex $\gamma = 3$). The resulting climatological mean CFC-11 mixing ratios at 50 hPa are shown in Fig. 15 (top). The differing dynamical states of the three simulations are clearly reflected in the tracer mixing ratios: The simulation with the weak vortex ($\gamma = 1$, red) shows highest CFC-11 mixing ratios in the tropics to mid-latitudes, with a smooth transition from tropics

[2] This simulation, and the following presented in this subsection were performed with the modified "log10" implementation.

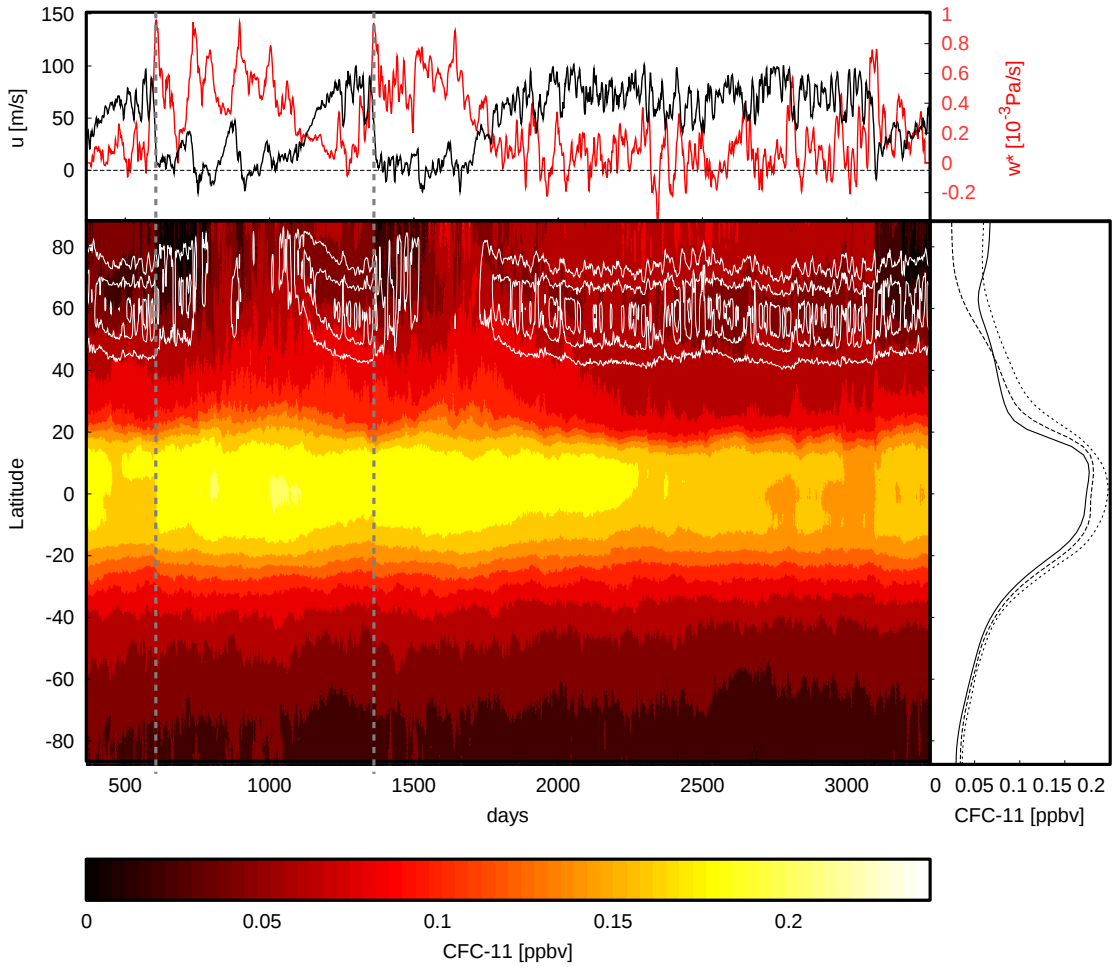

Figure 14. ~~Zonal~~ Top: time series of zonal mean zonal wind u at 60°N and 10 hPa (black) and mean $\overline{w^*}$ at 50 hPa and 60°-90°N (red). Middle panel: zonal-mean CFC-11 mixing ratios (color, in ppbv) at 50 hPa as function of simulated day and latitude~~(color)~~, and zonal mean zonal wind at 50 hPa (white contours, interval 15 ms^{-1}). ~~Top: time series~~ Vertical gray lines mark dates of ~~zonal mean zonal wind at 60N and 10hPa (black) and mean $\overline{w^*}$ at 50hPa and 60-90N (red, in 10^{-5}Pa/s)~~sudden polar vortex decelerations. Right: time-mean CFC-11 mixing ratios as function of latitude over days with strong vortex (days 400-600; 1200-1350; 2000-3000, black solid), over days following SSW with strong downwelling (day 600-780; 1380-1500; 3100-3280, dashed) and over days with eroded polar vortex (day 800-1000 and 1580-1700, dotted).

to high-latitudes, in line with strongest upwelling (see Fig. 15c; see also results in Sec. 4.2) and strong mid-latitudes wave driving that results in mixing (see Fig. 15d). In the simulation with a strong vortex ($\gamma = 3$, blue), mixing ratios in the tropics are ~~weaker~~lower, due to weaker upwelling in the lower stratosphere (see also Fig. 10), and the gradient to mid-latitudes is steep.

This can be explained both due to weaker mixing (see Fig. 15d) as well as stronger downwelling within the mid-latitudes (see Fig. 15c). Indeed, downwelling ~~maximizes~~ is maximized at the equatorward flank of the polar vortex (both in the $\gamma = 3$ and 2 simulations), and is weak within the vortex, in contrast to the $\gamma = 1$ simulation, where downwelling ~~maximizes~~ is maximized more poleward and is stronger also at high latitudes. The maximum of downwelling in the mid-latitudes as well as the high isolation of vortex air in the strong vortex case likely explains why CFC-11 mixing ratios are elevated within the vortex. The intermediate simulation with $\gamma = 2$ lies in between the other two simulations, but shows highest variability (largest standard deviation) in most quantities, as expected, since this simulation ~~transitions~~ oscillates between states with a weak and strong vortex (see Fig. 14 and Sec.4.2).

As demonstrated here, the idealized set-up of the simulation allows to study the role of vortex variability or specifically forced polar vortex strength changes on tracer mixing ratios in an isolated manner, i.e., the absence of other chemical processes or variability like the annual cycle.

5.2 Monsoon anticyclone forced by localized idealized heating

~~Understanding the monsoon systems~~ The Asian summer monsoon system is a key ~~task (Turner and Annamalai, 2012) and idealized~~ circulation feature in northern summer, and its understanding is an important task (Turner and Annamalai, 2012) . Idealized models have been widely used to understand the basic processes occuring in the monsoon regions (e.g., Gill, 1980; Yano and L. McBride, 1998; Bordoni and Schneider, 2008). In particular, also the development and dynamics of the monsoon anticyclones over Asia ~~(e.g., Gill, 1980; Hoskins and Rodwell, 1995; Liu et al., 2007; Wei et al., 2014, 2015; Hsu and Plumb, 2000; Amen~~ North America (Siu and Bowman, 2019) have been investigated using simplified modelling approaches. Here we impose an idealized heating field to divert the circulation from the basic state.

In the following we show results from a T42L90MA simulation with the standard *'HS'* set-up of equilibrium temperature and NH summer constellation, i.e., hemispheric asymmetry is caused by setting the asymmetry factor ϵ to ~~10.~~ -10 K. The first two years of this simulation have been neglected and here results from the third simulation year are presented. On top of the basic state a regionally confined heating source is imposed in the NH tropics to subtropics (following Eqs. A12-A16 with ~~$\phi_0 = 20°$~~ $\phi_0^m = 20°$ N, ~~$\lambda_0 = 90°$~~ $\lambda_0^m = 90°$ E, ~~$\delta\phi = 10°$, $\delta\lambda = 30°$). Vertically the~~ $\delta\phi^m = 10°$, $\delta\lambda^m = 30°$). In the vertical, the heating extends from ~~$p_{bot} = 800$~~ $p^m_{bot} = 800$ hPa to ~~$p_{top} = 100$~~ $p^m_{top} = 100$ hPa. The heating is turned on at day 0 of the simulation with a spin up of ~~$t_s = 20$~~ $t_s^m = 20$ days. Other temporal variations are not considered as ~~$q_{temp} = 0$~~ $q^m_{temp} = 0\,\mathrm{K\,day^{-1}}$. The temporally constant (neglecting the spin-up period) heating is imposed with ~~$q_0 = 8$~~ $q_0^m = 8\,\mathrm{K\,day^{-1}}$. After the spin-up period, the average total energy per day that is added into the model due to this additional heat source (deduced from 6 h model output) is slightly below 21×10^{19} J. This heating is of the same order of magnitude as the idealized heat source of 6×10^{19} J prescribed in Siu and Bowman (2019) to model the North American monsoon anticyclone (see their experiments 5a-5e).

The mean geopotential height field at 100 hPa for this T42L90MA simulation with the described idealized heating is shown in Fig. 16(a). A clear anticyclone is produced ~~from~~ in response to the additional heating. This anticyclone is similar to the Asian monsoon anticyclone (e.g., Hoskins and Rodwell, 1995; Zhang et al., 2002; Randel and Park, 2006; Nützel et al., 2016). Fig. 16(b) shows a latitude vs. pressure cross section of zonal winds averaged over all longitudes. The zonal winds averaged

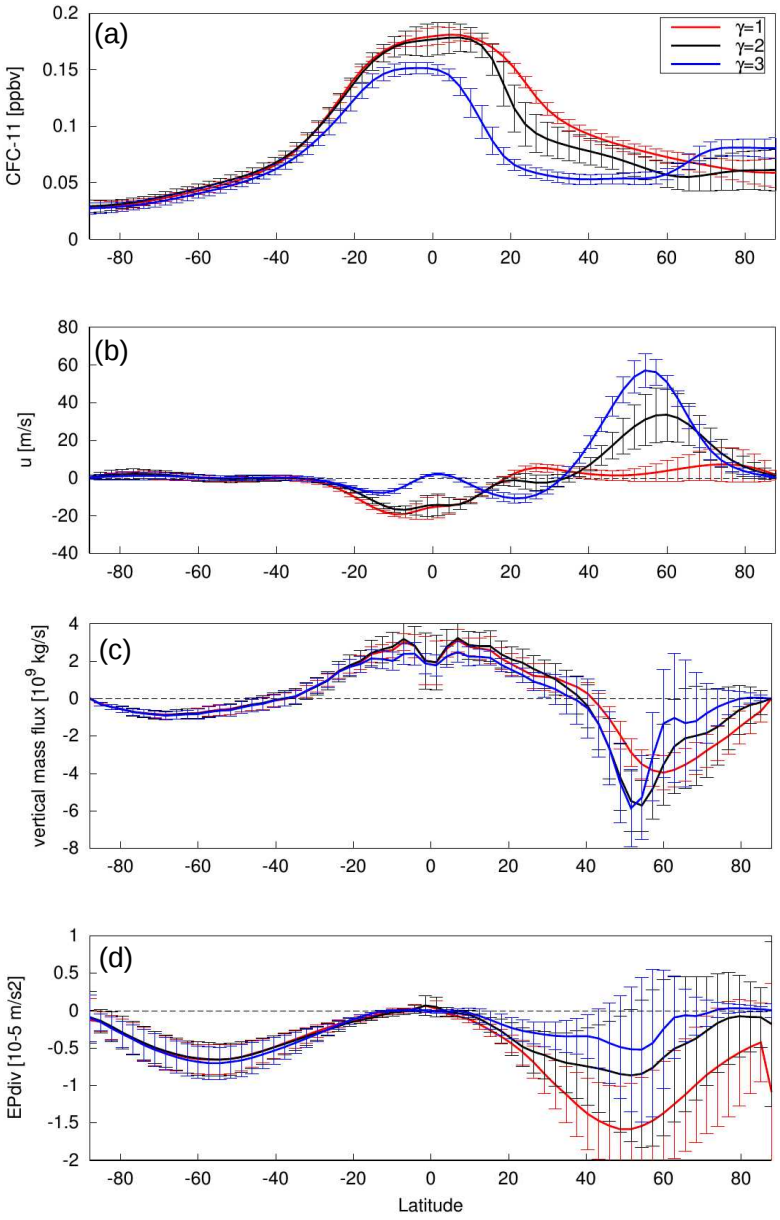

Figure 15. a) Zonal mean CFC-11 mixing ratios , b) zonal mean zonal wind , c) mean vertical mass flux and d) EP flux divergence, all at 50 hPa as function of latitude for EMIL simulations with *PK* set-up with p_{Tw}=400 hPa and $\gamma = 1$ (red) , 2 (black) and 3 (blue), b) zonal mean zonal wind , c) mean vertical mass flux and d) EP flux divergence.

over the anticyclone region are overlayed in black contours. The positive wind speed in the north and the negative wind speeds towards the equator marking the edges of the anticyclone are clearly visible (cf. Figs. 2 and 1 in Randel and Park, 2006; Garny and Randel, 2016, respectively).

Fig. 17 shows the temporal variation of the ~~anticyclone during two periods~~ monsoon anticyclone during a 5-day period of the simulation. ~~On the left of Figure~~The daily geopotential height fields in Fig. 17 ~~,~~ show an example of a splitting event of the anticyclone~~is shown~~. On the first day of the depicted period, the anticyclone is elongated ~~.~~ (Fig. 17a). After that the anticyclone splits and two ~~and four~~ days later two anticyclone centers can be identified ~~. Six~~ (red dots in Fig. 17b). Four days after the elongated phase, the western center has decayed and the eastern center has moved ~~back~~ slightly westwards to roughly 90° E ~~.~~ (Fig. 17c). Such splitting events (sometimes also denoted westward eddy sheddings, Figs. 15 and 16 in Hsu and Plumb, 2000), as shown in Fig. 17 are (typical) features during the monsoon period ~~in observations~~ (e.g., Fig. 13 in Garny and Randel, 2013; Vogel et al., 2015; Nützel et al., 2016; Pan et al., 2016). ~~Also~~

An example of eastward eddy shedding ~~as~~ was found during the ~~second period as displayed on the right of~~ same 5-day period and is indicated via arrows in Fig. 17. This phenomenon has been previously ~~noted~~ investigated in a couple of publications (e.g., Dethof et al., 1999; Garny and Randel, 2013; Vogel et al., 2014; Nützel et al., 2016) and ~~consitutes~~ constitutes a major mode of variability observed in the monsoon anticyclone. During the depicted period on the eastern edge of the anticyclone a filament is torn off. On the first day the anticyclone ~~is nearly unperturbed, while two days later the anticyclone extends clearly to the west~~ stretches to the east (Fig. 17a). Two days later this development is even more pronounced (Fig. 17b) and again two days later a filament is separated from the main anticyclone ~~.~~ (Fig. 17c).

Those examples show that ~~by imposing an idealized monsoon-like heating in the dynamical core model , the monsoon anticyclone can be simulated~~ the EMIL model implementation is suited to simulate a monsoon-like anticyclone with realistic mean state and variability by imposing an idealized localized heating. The variability of the anticyclone under constant versus time-varying forcing, and its impact on troposphere-stratosphere tracer transport will be the subject of future studies.

6 Summary and Outlook

~~In the paper presented here, the~~ The implementation of a dry dynamical core model set-up within the MESSy framework is documented. This set-up, denoted EMIL (ECHAM~~/MESSy model system, the ECHAM~~/MESSy IdeaLized~~(EMIL)model set-up is documented. It is shown that earlier~~), is shown to perform consistently with established dry dynamical core ~~model simulation with ECHAM5 and other models are closely reproduced by EMIL simulations with same set-ups~~benchmarks, both earlier configurations of the ECHAM core, and those developed by other modeling centers.

The implementation of the submodel ~~RELAX~~for temperature and wind relaxation (submodel RELAX), necessary for the dynamical core set-up, includes pre-implemented functions for the parameters for Newtonian cooling and Rayleigh friction ~~based on the suggestions by~~ as described in HS94 and PK02~~, but with extensions, and further~~ . Extensions to those functions are added, namely the option to ~~set the parameters to arbitrarily defined fields, which are read from external files~~change the transition pressure between tropospheric to stratospheric equilibrium temperatures in the winter hemisphere. Further, ~~it~~ the

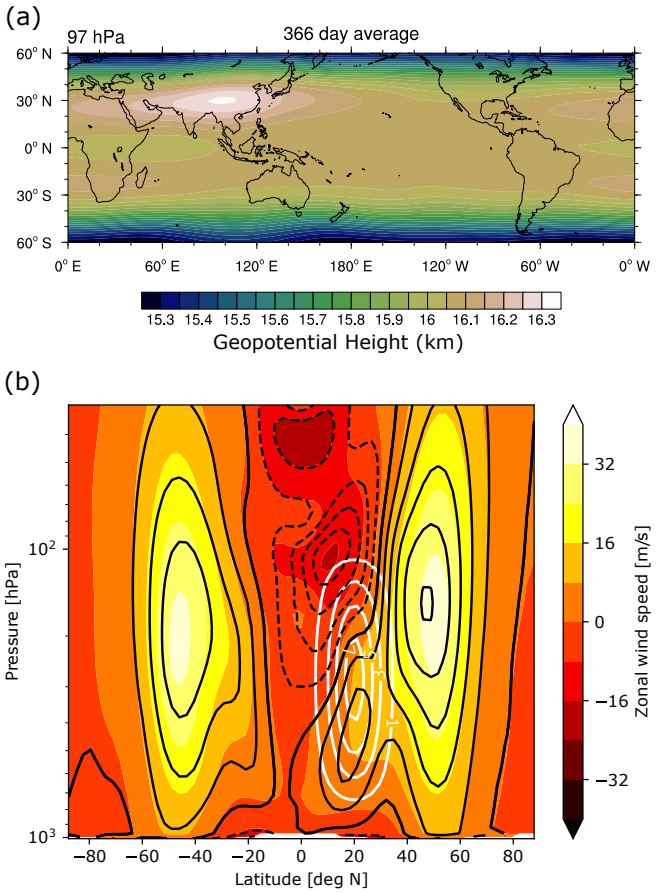

Figure 16. ~~Top:~~ **(a)** Mean anticyclone structure via geopotential height (km) at ∼100 hPa from ~~150~~ 366 days of the ~~integration~~ simulation (map included for orientation and scale purposes only; i.e., the simulation features no orography etc.). ~~Bottom:~~ **(b)** Vertical cross section of zonal mean wind (colour-coded) and wind in the anticyclone region ~~(~~averaged over 60-120°E ~~:~~ (black contours; in steps of 8 m s^{-1}; negative values dashed). White contours show the maximum along the longitudes of the implied heating function (in K ~~/~~day^{-1}).

submodel includes the possibility to include additional diabatic heating either by pre-implemented functions for zonal mean, localized or wave-like heating, or by externally read files. Thus, the implementation provides a tool-kit for the users to chose model set-ups to their needs.

Modifications to the set-up by PK02 and Gerber and Polvani (2009), which were used frequently in the past, are presented with respect to the shape of the upper sponge layer and with respect to the equilibrium temperature profile in the winter stratosphere. The damping coefficient of the upper sponge layer is set to increase exponentially with height instead of quadratically, resembling more closely parametrized drag by GW in the full model and leading to more realistic temperature profiles in the stratopause region. However, the impact outside the sponge layer is ~~limited to~~ considerable only above 10 hPa ~~and to~~ at high latitudes. Modifications of the equilibrium temperature in the high latitude UTLS region are performed by increasing the

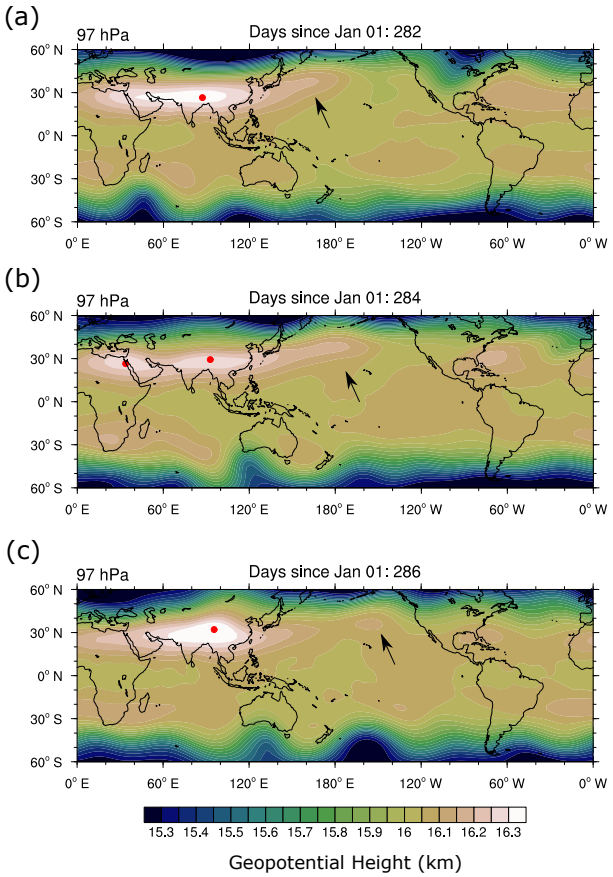

Figure 17. Evolution of geopotential height at ∼100 hPa showing an example of a splitting event ~~(left, over the period of 7 days),~~ and an eastward shedding event ~~(right,~~ over a ~~5 day~~ 5-day period~~)~~. Red dots are idicating the approximate positions of the anticyclone centers, while arrows highlight the eddy shedding event.

transition pressure (p_{Tw}) between troposphere and stratosphere at high-latitudes (thus, the decrease of temperatures forming the polar vortex starts at lower altitudes). We find that increasing the transition pressure from 100 hPa to 400 hPa results in a realistic mean temperature profile (with the polar lapse rate ~~$\gamma = 2$~~γ=2 K km^{-1}), thus correcting for the UTLS warm bias of the PK02/ Gerber and Polvani (2009) simulations. ~~The~~ With the increased transition pressure~~causes climate states, in which~~ , we find a regime-like behavior ~~becomes more pronounced than in the previously used set-ups: the polar vortex~~of the polar vortex. The polar vortex appears to transition from a weak to a strong regime ~~, and the~~ with increasing stratospheric polar lapse rate (i.e. increasing γ and p_{Tw}). The simulation with the most realistic mean temperature profile is at the transition point between those regimes. While we presented evidence here that the polar vortex changes reflect a regime transition, we will address the polar vortex regimes in more detail in a follow-up study.

In the past, regime behavior of the near-surface jets has been discussed (Chan and Plumb, 2009; Gerber and Polvani, 2009; Wang et al., 2
that led to a very strong response of the tropospheric jet to changes in the polar vortex in the original work by PK02. We find

a similarly strong response of the near-surface jet to stratospheric forcing in our model under same set-up as in PK02. In line with previous results, that have shown sensitivity of the tropospheric jet response to the tropospheric equilibrium temperatures (Chan and Plumb, 2009) , we found a strongly damped poleward shift of the tropospheric jets in response to stratospheric forcing under a set-up with lower tropical upper tropospheric temperatures. We hypothesize that the more equatorward position of the tropospheric jet in those simulations leads to the dampened response, but this remains to be analyzed in more detail. In simulations with topographically forced planetary waves, we find a similar tropospheric jet response to stratospheric forcing than in Gerber and Polvani (2009) , as can be expected from the previously shown robustness of the tropospheric jet behavior in different model configurations (resolution, and different dynamical cores, see Wang et al., 2012) . The sensitivity of the jet response to the tropospheric equilibrium temperatures is lower in the topographically forced simulations, possibly because the basic state jet location does not differ by as much as in the simulations without topography (see Fig. 12). In general, it remains to be understood in how far the regime changes of the polar vortex are connected to regime changes of the near-surface jet, and whether those regime changes found in the idealized models are also relevant for the real atmosphere. If this behavior occurs only in idealized models, this would put their application to advance the understanding of our atmosphere into question.

Simulations with planetary wave generation by topography and by wave-like heating (as suggested by Lindgren et al., 2018) are contrasted. Generally, similar basic states can be simulated with the two different set-ups, and in both cases increases in γ lead to increases in the polar vortex strength~~and mid-stratospheric downwelling~~. However, the heating-forced simulations ~~react more non-linear~~ respond more non-linearly to increases in γ both in terms of polar vortex strength and lower stratospheric downwelling. Furthermore, while in the topographically forced simulations~~the tropospheric jet moves~~ , both the free tropospheric jet and the near-surface jet move poleward with a stronger polar vortex (in agreement with Gerber and Polvani, 2009), the free tropospheric jet remains at ~~a fixed~~ an almost constant latitude in the simulations with wave-like heating. ~~These results indicate that the~~ Despite the almost constant location of the free tropospheric jet, the near-surface jet is strongly displaced poleward in response to stratospheric forcing, transitioning from a subtropical regime to a mid-to-high-latitude regime for strong polar vortex increases (similar to previously reported regime transitions, e.g. by Chan and Plumb, 2009) . The prescribed wave-like heating ~~does not allow for stratospheric influences on the tropospheric jet. Further~~ extends throughout the free troposphere and into the lower stratosphere, leading to the hypothesis that the prescribed heating damps the ability of the free tropospheric jet to shift. Another possible explanation of the constant location of the free tropospheric jet is that it is located already at far higher latitudes than in the topographically forced simulations for weak polar vortices (see Fig. 12). Available observational evidence on troposphere-stratosphere coupling indicates that zonal wind anomalies usually occur in a vertically coherent manner, for example due to thermal forcing by stratospheric ozone depletion (e.g., Son et al., 2010) , or in connection with SSW events (e.g., Baldwin and Dunkerton, 1999) . This puts the behavior of the wave-like heating experiments into question, and further work will be necessary to understand ~~this behavior~~ the different behavior of troposphere-stratosphere coupling in the different model versions and set-ups. Overall, we recommend to use the thermally forced wave generation with caution.

As a first application example of the dry dynamical core model we present, as a proof-of-concept, a simulation with very basic chemistry (here only photolysis of CFCs), and the potential of such simulation set-ups to study the impact of dynamical

variability and changes on tracer transport in an idealized fashion is shown. The set of chemical reactions can be expanded to the user's needs to study transport of more complex chemical tracers, such as ozone.

Secondly, we present a simulation of a monsoon-like upper tropospheric anticyclonic circulation with realistic variability forced by imposed localized heating. Such a set-up can be used to study the dynamics of diabatically forced circulation systems such as monsoon anticyclones under different forcings and background states.

With the dry dynamical core model set-up, the model hierarchy within the ~~ECHAM/MESSy model system~~ MESSy framework is extended by a commonly used model set-up for studying dynamical ~~and transport processes,~~ processes. With the implementation in MESSy, the tracer utilities including the possibility to consider diagnostic chemically active tracers are available in the dry dynamical core model. As a next step, we envision an expansion to account for chemistry-dynamics interaction in a simplified manner as an intermediate step between the dry dynamical core model and the full ~~CCM.~~ Chemistry-Climate model. This next step in constructing a consistent model hierarchy of chemistry-dynamical coupling is motivated by the research question on how circulation-induced anomalies in radiative trace gases (e.g., ozone) feed back on the dynamics. This question is relevant both on climate time-scales as well as on intra-seasonal timescales (e.g. during sudden stratospheric warmings). This extended set-up would require radiative calculations depending on the actual tracer concentrations. While this expansion of the coupled idealized set-up will be subject of future work, we note here that all necessary components are available already in the MESSy framework: the radiation scheme from the full EMAC model (Dietmüller et al., 2016) can be used with setting the input to either the online simulated values of the trace gas of interest (i.e., ozone), while the other relevant species can be set to climatological values (e.g., water vapor) or zero (e.g., clouds and aerosols). The envisioned model set-up, basically an idealized "chemistry-dynamical model", would thus consist of a dry dynamical core with thermodynamic forcing by an idealized prescribed latent heating and radiative calculations that depend on the chemical species of interest (e.g., ozone).

Code and data availability. The Modular Earth Submodel System (MESSy) is continuously further developed and applied by a consortium of institutions. The usage of MESSy and access to the source code is licenced to all affiliates of institutions which are members of the MESSy Consortium. Institutions can become a member of the MESSy Consortium by signing the MESSy Memorandum of Understanding. More information can be found on the MESSy Consortium Website (http://www.messy-interface.org). The code presented here has been based on MESSy version 2.54 and will be available in the next official release (version 2.55).

The data of the simulations presented in this study is freely available under http://doi.org/10.5281/zenodo.3768731

Appendix A: Implemented functions in the RELAX submodel

A1 Newtonian cooling

The inverse relaxation time scale κ and the equilibrium temperature $T_{\rm eq}$ have to be specified in the model set-up via the RELAX namelist file (see Supplement). The following pre-implemented functions are available:

The functions for the 'HS' set-up, as defined by Held and Suarez (1994) but including the option of hemispheric asymmetry (as introduced by PK02), are

$$T_{\rm eq}^{\rm HS} = \max\left\{T_0, \left[T_1 - \delta_y \sin^2\phi - \epsilon\sin\phi - \delta_z \log\left(\frac{p}{p_0}\right)\cos^2\phi\right]\left(\frac{p}{p_0}\right)^k\right\}, \tag{A1}$$

$$\kappa = \kappa_{\rm a} + (\kappa_{\rm s} - \kappa_{\rm a})\max\left(0, \frac{p/p_s - \sigma_{\rm b}}{1-\sigma_{\rm b}}\right)\cos^4\phi \tag{A2}$$

where ϕ is the geographical latitude, p is the actual pressure, p_s is the current surface pressure and $k = R/c_p = 2/7$. All constants can be set via namelist entries, with defaults set to the values given in HS94 (see Supplement, Table 1 for description of parameters and default values). The parameter ϵ sets the hemispheric asymmetry, and its sign is controlled by the namelist parameter $h_{\rm fac}$. If $h_{\rm fac}$ is zero, the equilibrium temperature is symmetric between the hemispheres (i.e., $\epsilon = 0$). If $h_{\rm fac} \neq 0$, then

$$\epsilon = \mathrm{sign}(h_{\rm fac}) * |\epsilon| \tag{A3}$$

i.e., the sign of $h_{\rm fac}$ determines which hemisphere is the winter hemisphere (positive $h_{\rm fac}$: northern hemispheric winter, negative $h_{\rm fac}$: southern hemispheric winter).

The inverse relaxation time scale in the PK set-up is identical to that in 'HS' set-up. The equilibrium temperature in the PK set-up is similar to the one of HS in the troposphere, but uses the following function in the stratosphere above a given transition pressure $p_{\rm T}(\phi)$:

$$T_{\rm equ}^{\rm PK}(\phi,p) = \begin{cases} \max\left\{T_{\rm US}(p_{\rm Ts}), \left[T_1 - \delta_y \sin^2(\phi) - \epsilon\sin(\phi) - \delta_z \log\left(\frac{p}{p_0}\right)\cos^2(\phi)\right]\left(\frac{p}{p_0}\right)^k\right\} & \text{for } p \geq p_{\rm T}(\phi) \\ [1 - W(\phi)]\,T_{\rm US}(p) + W(\phi)\,T_{\rm US}(p_{\rm Ts})\left(\frac{p}{p_{\rm T}(\phi)}\right)^{\frac{R\gamma}{g}} & \text{for } p < p_{\rm T}(\phi) \end{cases} \tag{A4}$$

The stratospheric temperature profile is based on the US standard atmosphere temperature profile $T_{\mathrm{US}}(p)$ in the summer hemisphere (USA, 1976) and exhibits a temperature decrease with lapse rate γ in the winter hemisphere representing the region of the polar vortex. This transition is performed by the weighting function

$$W(\phi) = \frac{1}{2}\left[1 + \mathrm{sign}(h_{\mathrm{fac}}) \tanh\left(\frac{\phi - \phi_0}{\delta\phi}\right)\right]. \tag{A5}$$

The transition latitude ϕ_0 is set, similar to ϵ, to $\phi_0 = \mathrm{sign}(h_{\mathrm{fac}}) * |\phi_0|$. The smooth transition between tropospheric and stratospheric temperatures is ensured by bounding the tropospheric temperature to the temperature in the transition region $T_{\mathrm{US}}(p_{\mathrm{Ts}})$.

As an extension to the original PK set-up, we include the possibility to vary the transition pressure from summer to winter hemisphere, using the weighting function $W(\phi)$:

$$p_{\mathrm{T}}(\phi) = (p_{\mathrm{Tw}} - p_{\mathrm{Ts}})W(\phi) + p_{\mathrm{Ts}} \tag{A6}$$

where p_{Ts} and p_{Tw} are the transition pressures over the summer and winter hemisphere, respectively. Again, all constants can be set in the namelist with default values that correspond to the original PK02 set-up (i.e. with constant transition pressure $p_{\mathrm{T}}(\phi) \equiv 100\,\mathrm{hPa}$), as detailed in the Supplement (Table 1).

A2 Rayleigh Friction

The following implemented functions are available for setting the horizontal wind damping coefficient k_{damp}:

1) Damping of the surface layer as specified by HS94 (option *'HS'*):

$$k_{\mathrm{damp}} = k_{\mathrm{max}}^{\mathrm{HS}} \max\left(0, \frac{\frac{p}{p_s} - \sigma_0}{1 - \sigma_0}\right) \tag{A7}$$

with default values $k_{\mathrm{max}}^{\mathrm{HS}} = 1.16 \times 10^{-5}\,\mathrm{s}^{-1}$, $\sigma_0 = 0.7$ and p_s the current surface pressure.

2) Damping of a layer at the model top as specified by PK02 (option *'PK'*):

$$k_{\mathrm{damp}} = \begin{cases} 0 & \text{for } p > p_{\mathrm{sp}} \\ k_{\mathrm{max}}^{\mathrm{PK}}\left(1.0 - \frac{p}{p_{\mathrm{sp}}}\right)^2 & \text{for } p \le p_{\mathrm{sp}} \end{cases} \tag{A8}$$

with default values $k_{\mathrm{max}}^{\mathrm{PK}} = 2.3148 \times 10^{-5}\,\mathrm{s}^{-1}$ and $p_{\mathrm{sp}} = 0.5\,\mathrm{hPa}$.

3) Damping of a layer at the model top with the function as implemented in the original ECHAM code (option *'EH'*):

$$k_{\mathrm{damp}} = \begin{cases} 0 & \text{for } i_{\mathrm{lev}} > i_{\mathrm{lev}}^{sp} \\ k_{\mathrm{drag}} c^{i_{\mathrm{lev}}^{sp} - i_{\mathrm{lev}}} & \text{for } i_{\mathrm{lev}} \le i_{\mathrm{lev}}^{sp} \end{cases} \tag{A9}$$

where i_{lev} is the number of the hybrid level counted from the top of the model for a vertical resolution of L90MA. Thus, the drag k_{drag} is enhanced by a factor of c for each level going upward. Default values are $c = 1.5238$, $k_{\mathrm{drag}} = 5.02 \times 10^{-7}\,\mathrm{s}^{-1}$

and $i_{\rm lev}^{sp} = 10$, corresponding to a pressure of 0.43 hPa for the L90MA vertical resolution. If the model is run at a different vertical resolution, the damping coefficients are first calculated according to Eq. A9 for L90MA, and then interpolated to the current vertical levels.

A3 Diabatic heating

The implemented heating function for the zonal mean heating (*tteh* *SUBSCRIPTNBcc* *SUBSCRIPTNBtropics*), as given by (Butler et al., 2010) reads

$$Q_0(\lambda,\phi,p) = q_0^{cc} \exp\left[-\frac{1}{2}\left(\frac{\phi-\phi_0^{cc}}{\delta_\phi^{cc}}\right)^2 - \frac{1}{2}\left(\frac{p/p_s-\sigma_z^{cc}}{\delta_z^{cc}}\right)^2\right] \tag{A10}$$

with p_s being the surface pressure and default values are set to those by Butler et al. (2010) (see Supplement, Table 3).

The temperature tendency *tteh* *SUBSCRIPTNBwaves*, used here for the generation of planetary waves introduced by Lindgren et al. (2018) , reads

$$Q_0(\lambda,\phi,p) = \begin{cases} q_0^w \sin(m\lambda) \exp\left[-\frac{1}{2}\left(\frac{\phi-\phi_0^w}{\delta_\phi^w}\right)^2\right] \sin\left(\pi \frac{\log(p/p_{\rm bot})}{\log(p_{\rm top}/p_{\rm bot})}\right) & \text{for } p_{\rm top} \le p \le p_{\rm bot}, \\ 0 & \text{otherwise} \end{cases} \tag{A11}$$

where λ is the geographical longitude, and all parameters are set to default values as used by Lindgren et al. (2018) , see Supplement Table 3.

The function describing the localized heating field, *tteh* *SUBSCRIPTNBmons*, is given as:

$$Q_{\rm loc}(\lambda,\phi,p,t) = Q_{\rm temp}(t) Q_{\rm pres}(p) Q_{\rm lat}(\phi) Q_{\rm lon}(\lambda). \tag{A12}$$

Here, the individual factors are used to describe the temporal and spatial (horizontal and vertical) dependence of the heating function. The temporal evolution of the heating is given by:

$$Q_{\rm temp}(t) = \begin{cases} \frac{t}{t_s^m} \times (q_0^m + q_{\rm temp}^m sin(2\pi \frac{t}{\delta t^m})) & \text{for } 0 \le t \le t_s^m, \\ 1 \times (q_0^m + q_{\rm temp}^m sin(2\pi \frac{t}{\delta t^m})) & \text{otherwise.} \end{cases} \tag{A13}$$

To slowly increase the heating after the start of the simulation a spin up factor of $\frac{t}{t_s^m}$ is included until the end of the spin up time (t_s^m). After the spin up time (t_s^m) the temporal variation of the heating is only given by a periodic oscillation (period δt^m) with amplitude (q_{temp}^m) around a constant base heating (q_0^m).

In the vertical the heating is assumed to be of the same form as in Eq. (A11), i.e.:

$$Q_{\mathrm{pres}}(p) = \begin{cases} sin(\pi \frac{log(p/p^m_{\mathrm{bot}})}{log(p^m_{\mathrm{top}}/p^m_{\mathrm{bot}})}) & \text{for } p^m_{\mathrm{top}} \leq p \leq p^m_{\mathrm{bot}}, \\ 0 & \text{otherwise.} \end{cases} \tag{A14}$$

Here, p^m_{bot} and p^m_{top} denote the maximum and minimum pressure to which the heating is confined in the vertical. The latitudinal dependence for $\phi \in [-90, 90]$ follows the function suggested by Schubert and Masarik (2006 , their Eq. 4.1), and is given as

$$Q_{\mathrm{lat}}(\phi) = exp\left(-\left(\frac{\phi - \phi^m_0}{\delta\phi^m}\right)^2\right) \tag{A15}$$

Finally, the longitudinal dependence for $\lambda \in [0, 360)$ is given by

$$Q_{\mathrm{lon}}(\lambda) = \begin{cases} 0.5(1 + cos(\pi \frac{g(\lambda,\lambda^m_0)}{\delta\lambda^m})) & \text{if } g(\lambda, \lambda^m_0) \leq \delta\lambda \\ 0 & \text{otherwise} \end{cases} \tag{A16}$$

where $g(\lambda, \lambda^m_0) = min((\lambda - \lambda^m_0)\ mod(360), (\lambda^m_0 - \lambda)\ mod(360))$ and the modulo function $mod(360)$ maps $\mathbb{R}$ to $[0, 360)$, i.e. the function returns the smallest angle between the longitude λ and the central longitude λ^m_0 with accounting for the crossing of the $0°$ line. Again the longitudinal function is based on the heating described by Schubert and Masarik (2006 , their Eq. 4.1). However, as Schubert and Masarik (2006) were aiming to investigate the Madden-Julian-Oscillation, they included a movement of the localized heat source, which we do not include here (i.e., we use their equation with propagation speed 0). Overall this heating structure is similar to other idealized heatings used for studying monsoon anticyclones (e.g., Siu and Bowman, 2019) .

Appendix B: List of simulations

In Table B1, a list of all simulations presented in this study is given with details on their set-up, resolution and simulation length. The simulations without planetary wave forcing are labeled "WN0", the ones with topographic wavenumber 2 wave-forcing with "WN2T", the ones with diabatic wave forcing with "WN2H". The values of the winter transition pressure p_{Tw} are given in hPa, and the values of the polar vortex lapse rate γ in K km-1. "npv" refers to simulations with "no polar vortex", i.e. the sumemr stratospheric equilibrium temperature is extended to the winter pole.

The label "ln" refers to the standard set-up of tropospheric equilibrium temperatures according to Eq. A1, the label "log10" to simulations, in which the tropospheric equilibrium temperatures were set to:

$$T^{\log 10}_{\mathrm{eq}} = \max\left\{T_0, \left[T_1 - \delta_y \sin^2\phi - \epsilon \sin\phi - \delta_z \log_{10}\left(\frac{p}{p_0}\right)\cos^2\phi\right]\left(\frac{p}{p_0}\right)^k\right\}. \tag{B1}$$

The upper atmospheric damping coefficients are set to the formulation by PK (see Eq. A8) or to the formulation EH (see Eq. A9). The total length of the simulations is given in the table in days, with the number of analyzed days given in the Figure captions.

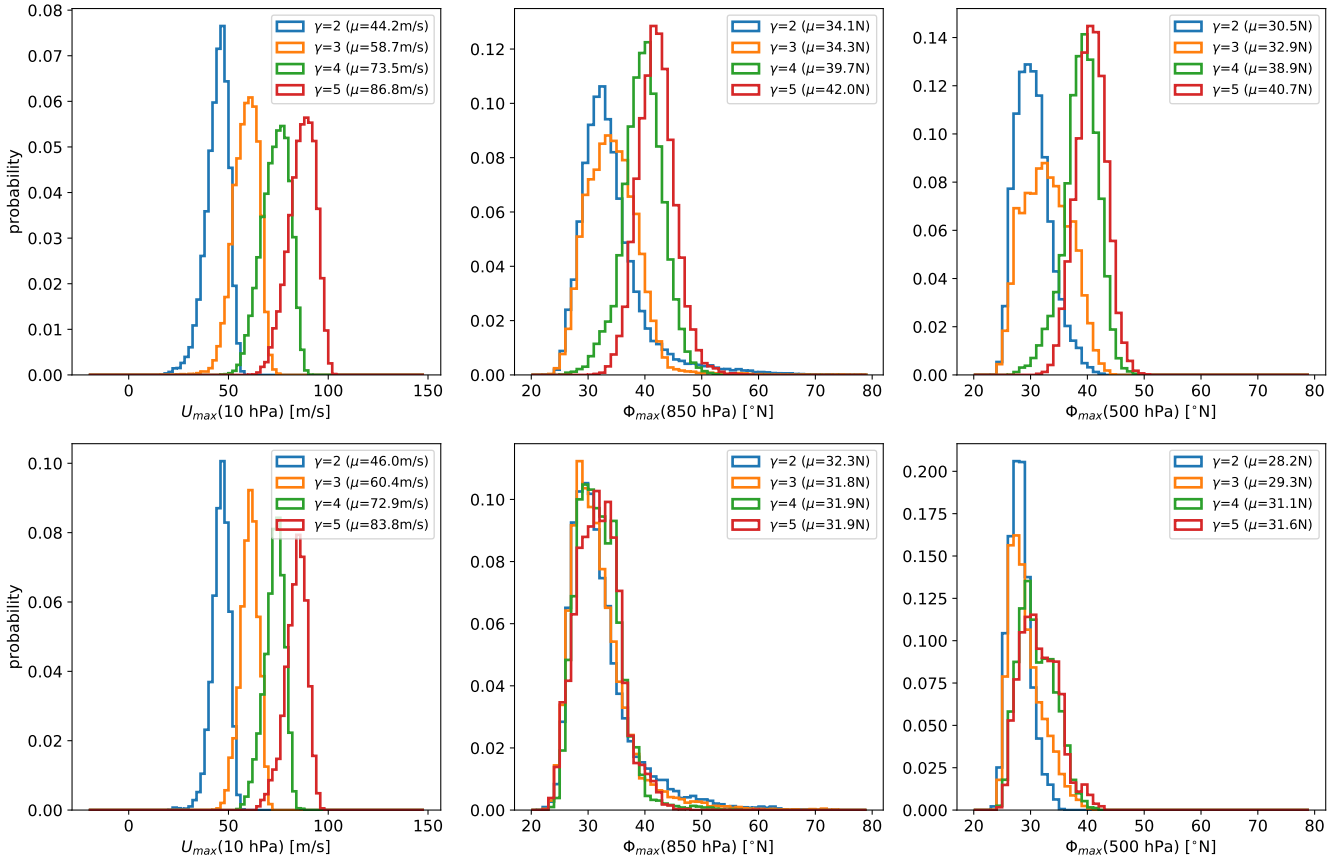

Figure C1. Probability distributions of (left) the maximal zonal mean zonal wind at 10 hPa, (middle) the latitude of the maximum of zonal mean zonal winds at 850 hPa, and (right) at 500 hPa for simulations without planetary wave forcing and (top) for the original PK02 set-up, and (bottom) for the modified "log10" simulations.

Appendix C: Probability distributions of polar vortex strength and tropospheric jet location

The probability distributions of the polar vortex strength (maximum zonal mean zonal wind at 10 hPa) and the position of the tropospheric jet (latitude of zonal mean zonal wind maximum at 850 hPa and 500 hPa) are shown for a number of selected experiments: for the original PK02 set-up, and the equivalent modified "log10" set-up (Fig. C1), for the simulations with a WN2 topography with differing p_{Tw} (Fig. C2), and for simulations with a WN2 diabatic heating for the standard and "log10" set-up (Fig. C3).

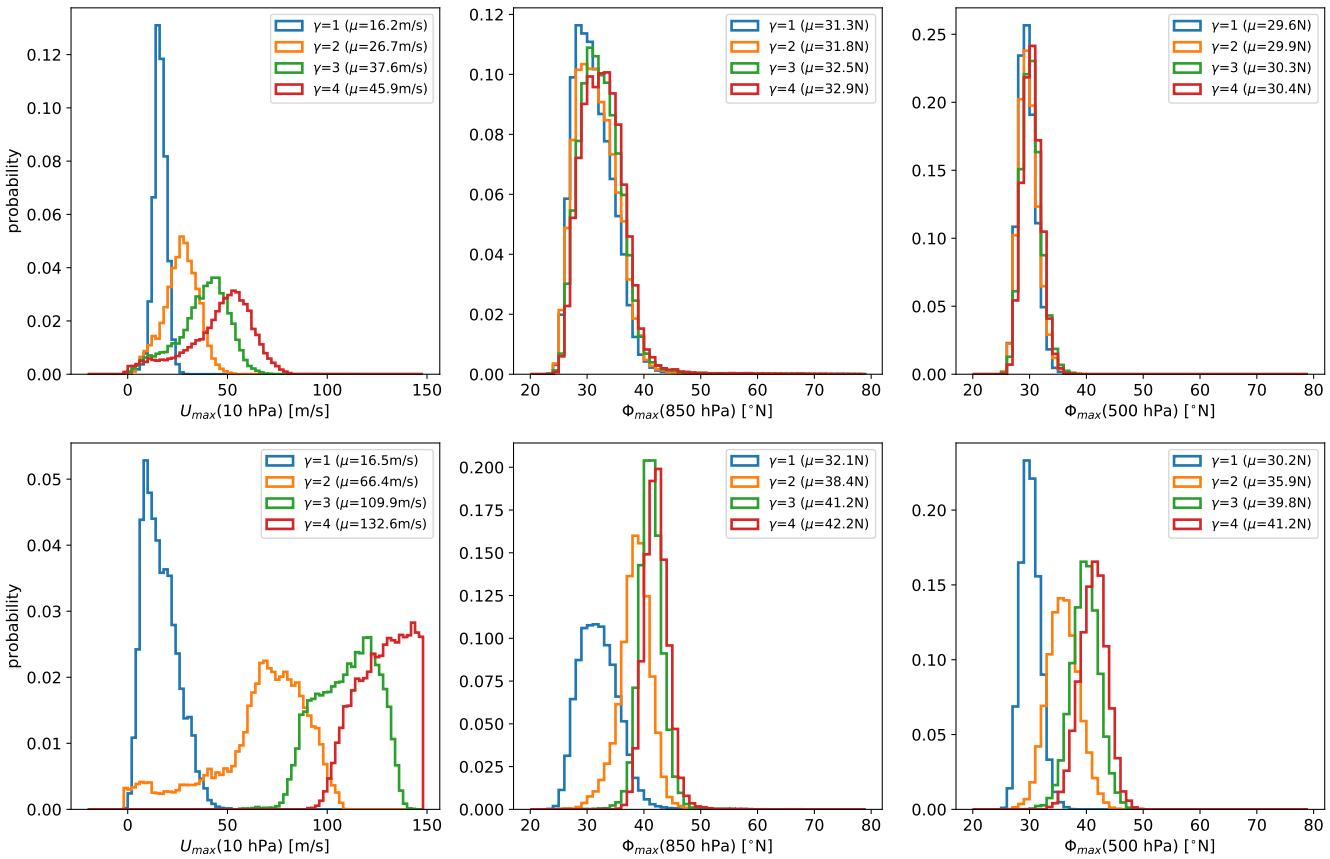

Figure C2. As Fig. C1, but for simulations with standard PK set-up and WN2 topography (top) for p_{Tw}= 100 hPa, and (bottom) for p_{Tw}= 400 hPa.

Table B1. List of all simulations presented in this study, with information on all relevant parameter settings and variations, and simulation length in days (see text for details). Simulations with multiple values of γ are listed in one row for brevity. *) also p_{Ts}=200 hPa; #) Including additional localized heating with parameter settings given in Sec. 5.2.

Section/ Figure	WN	PK/HS	p_{Tw}	γ	ln/log10	upper sponge	length	resolution
3.1 / 3	WN0	HS ($\epsilon = 0$)	-	-	ln	-	1825	T63L19
3.1 / 3	WN0	HS ($\epsilon = 0$)	-	-	ln	-	1825	T42L90MA
3.2 / 4, 8	WN0	PK ($\epsilon = 10$)	100	4	ln	PK	10957	T42L90MA
3.2 / 4, 5	WN2T	PK ($\epsilon = 10$)	100	4	ln	PK	10534	T42L90MA
3.3 / 6, 12, C1	WN0	PK ($\epsilon = 10$)	100	[npv,1,2,3,4,5]	ln	PK	10957	T42L90MA
3.3 / 6, 12, C1	WN0	PK ($\epsilon = 10$)	100	[npv,1,2,3,4,5]	log10	PK	3652	T42L90MA
4.1 / 8	WN0	PK ($\epsilon = 10$)	100	4	ln	EH	1825	T42L90MA
4.2 / 10-12	WN2T	PK ($\epsilon = 10$)	100	[1,2,3,4]	log10	EH	1825	T42L90MA
4.2 / 10, 11	WN2T	PK ($\epsilon = 10$)	150	[1,2,3,4]	log10	EH	1825	T42L90MA
4.2 / 10, 11	WN2T	PK ($\epsilon = 10$)	200	[1,2,3,4]	log10	EH	1825	T42L90MA
4.2 / 10, 11	WN2T	PK ($\epsilon = 10$)	250	[1,2,3,4]	log10	EH	1825	T42L90MA
4.2 / 10, 11	WN2T	PK ($\epsilon = 10$)	300	[1,2,3,4]	log10	EH	1825	T42L90MA
4.2 / 10, 11	WN2T	PK ($\epsilon = 10$)	350	[1,2,3,4]	log10	EH	1825	T42L90MA
4.2 / 10-12	WN2T	PK ($\epsilon = 10$)	400	[1,1.5,2,2.5,3,4]	log10	EH	1825	T42L90MA
4.2 / 10, 11	WN2T	PK ($\epsilon = 10$)	450	[1,2,3,4]	log10	EH	1825	T42L90MA
4.2 / 9-12, C2	WN2T	PK ($\epsilon = 10$)	100	[1,2,3,4]	ln	EH	10957	T42L90MA
4.2 / 5, 9-12, C2	WN2T	PK ($\epsilon = 10$)	400	[1,1.5,2,2.5,3,4]	ln	EH	10957	T42L90MA
4.3 / 10, 11	WN2H	PK ($\epsilon = 0$)	200*	4	log10	EH	1825	T42L90MA
4.3 / 10, 11, C3	WN2H	PK ($\epsilon = 0$)	400	[1,1.5,2,2.5,3,3.5,4,4.5]	log10	EH	1825	T42L90MA
4.3 / 10, 11	WN2H	PK ($\epsilon = 0$)	450	[1,1.5,2,2.5,3,3.5,4,4.5]	log10	EH	1825	T42L90MA
4.3 / 10-13	WN2H	PK ($\epsilon = 0$)	200*	4	ln	EH	10957	T42L90MA
4.3 / 10-13, C3	WN2H	PK ($\epsilon = 0$)	400	[1,2,3,4]	ln	EH	10957	T42L90MA
5.1 / 14, 15	WN2T	PK ($\epsilon = 10$)	400	[1,2,3]	log10	EH	3285	T42L90MA
5.2 / 16, 17	WN0 #	HS ($\epsilon = -10$)	-	-	ln	-	1095	T42L90MA

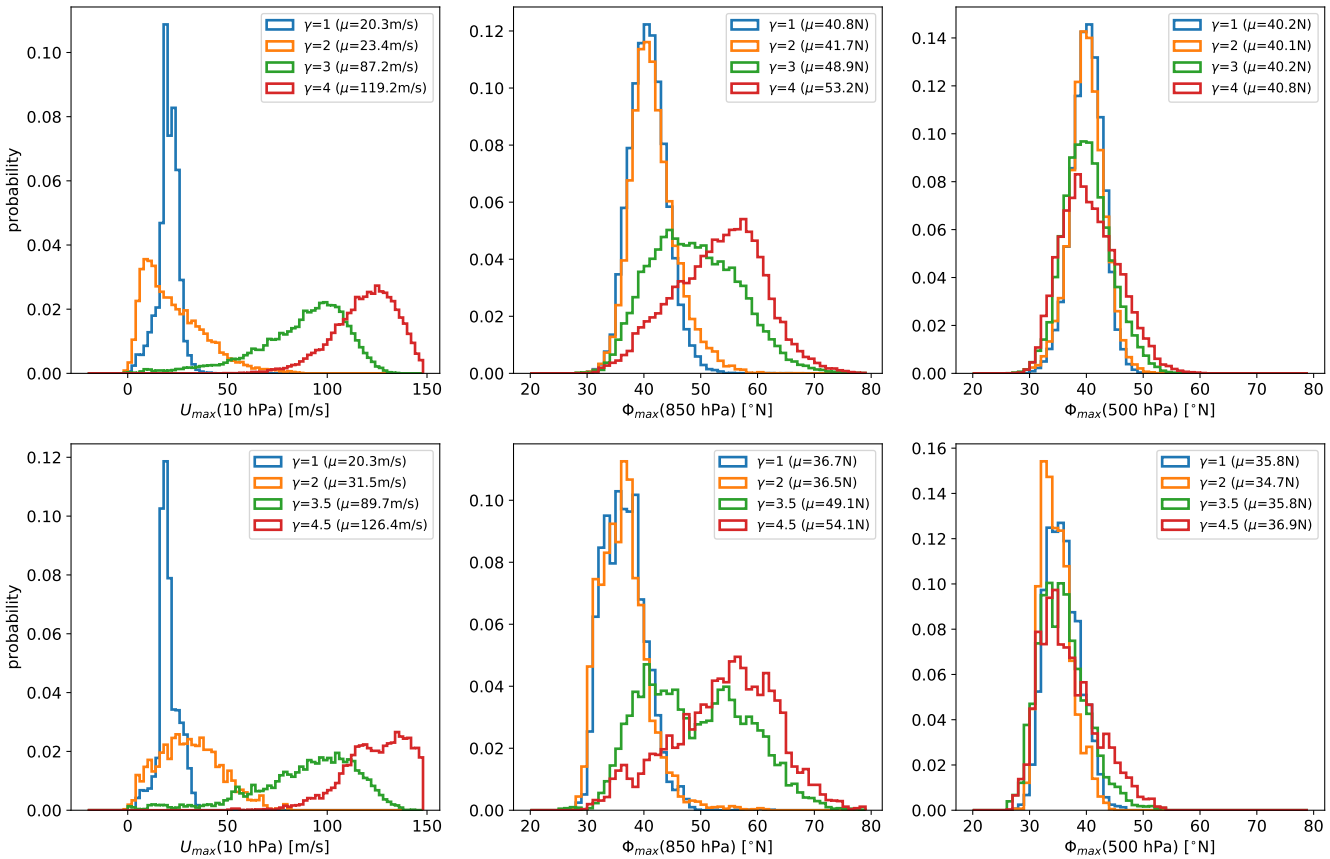

Figure C3. As Fig. C1, but for simulations with WN2 heating and p_{Tw}= 400 hPa for (top) the standard set-up and (bottom) the modified "log10" set-up.

Author contributions. HG designed and performed the implementation of the submodel RELAX, performed the test simulations and wrote large parts of the paper. RW strongly contributed to the implementation and conducted, analyzed and described the sensitivity experiments. MN implemented the localized heating function and analyzed and described the monsoon experiments. TB initiated the design of the sensitivity simulations. All authors contributed to the writing of the paper.

Competing interests. The authors hereby declare that they do not have conflicting interests.

Acknowledgements. HG and RW were funded by the Helmholtz Association under grant VH-NG-1014 (Helmholtz-Hochschul- Nachwuchsforschergruppe MACClim). MN received funding from the Initiative and Networking Fund of the Helmholtz Association through the project "Advanced Earth System Modelling Capacity (ESM). The simulations have been performed at the German Climate Computing Centre DKRZ through support from the Bundesministerium für Bildung und Forschung (BMBF). Data was processed using CDO (Climate Data Operators; Schulzweida, 2019). For parts of the data analysis and plotting NCL (NCAR Command Language; NCL, 2018) has been used. The SPARC climatologies are available at ftp://sparc-ftp1.ceda.ac.uk/sparc/ref SUBSCRIPTNBclim/randel/temp SUBSCRIPTNBwind/. We thank Patrick Jöckel for useful discussion and comments, and Philip Rupp for helpful discussions on idealized modelling of monsoon anticyclones. We thank Ed Gerber, Penelope Maher and an anonymous reviewer for very their valuable comments on the previous manuscript version.

References

U.S. Standard Atmosphere, U.S. Government Printing Office, Washington, D.C, 1976.

NCL: The NCAR Command Language (Version 6.5.0) [Software], Boulder, Colorado, UCAR/NCAR/CISL/TDD, 2018.

Amemiya, A. and Sato, K.: A Two-Dimensional Dynamical Model for the Subseasonal Variability of the Asian Monsoon Anticyclone, Journal of the Atmospheric Sciences, 75, 3597–3612, https://doi.org/10.1175/JAS-D-17-0208.1, 2018.

Baldwin, M. and Dunkerton, T.: Downward propagation of the Arctic Oscillation from the stratosphere to the troposphere, J. Geophys. Res., 104, 937–946, 1999.

Ball, W. T., Alsing, J., Mortlock, D. J., Staehelin, J., Haigh, J. D., Peter, T., Tummon, F., Stübi, R., Stenke, A., Anderson, J., Bourassa, A., Davis, S. M., Degenstein, D., Frith, S., Froidevaux, L., Roth, C., Sofieva, V., Wang, R., Wild, J., Yu, P., Ziemke, J. R., and Rozanov, E. V.: Evidence for a continuous decline in lower stratospheric ozone offsetting ozone layer recovery, Atmospheric Chemistry and Physics, 18, 1379–1394, https://www.atmos-chem-phys.net/18/1379/2018/, 2018.

Bordoni, S. and Schneider, T.: Monsoons as eddy-mediated regime transitions of the tropical overturning circulation, Nature Geosci, 1, 515–519, http://dx.doi.org/10.1038/ngeo248, 2008.

Butler, A. H., Thompson, D. W. J., and Heikes, R.: The Steady-State Atmospheric Circulation Response to Climate Change-like Thermal Forcings in a Simple General Circulation Model, Journal of Climate, 23, 3474–3496, https://doi.org/10.1175/2010JCLI3228.1, 2010.

Chan, C. J. and Plumb, R. A.: The Response to Stratospheric Forcing and Its Dependence on the State of the Troposphere, Journal of the Atmospheric Sciences, 66, 2107–2115, https://doi.org/10.1175/2009JAS2937.1, 2009.

Chen, G., Held, I. M., and Robinson, W. A.: Sensitivity of the Latitude of the Surface Westerlies to Surface Friction, Journal of Atmospheric Sciences, 64, 2899, 2007.

Deckert, R., Jöckel, P., Grewe, V., Gottschaldt, K.-D., and Hoor, P.: A quasi chemistry-transport model mode for EMAC, Geoscientific Model Development, 4, 195–206, https://www.geosci-model-dev.net/4/195/2011/, 2011.

Dee, D. P., Uppala, S. M., Simmons, A. J., Berrisford, P., Poli, P., Kobayashi, S., Andrae, U., Balmaseda, M. A., Balsamo, G., Bauer, P., Bechtold, P., Beljaars, A. C. M., van de Berg, L., Bidlot, J., Bormann, N., Delsol, C., Dragani, R., Fuentes, M., Geer, A. J., Haimberger, L., Healy, S. B., Hersbach, H., Holm, E. V., Isaksen, L., Kållberg, P., Köhler, M., Matricardi, M., McNally, A. P., Monge-Sanz, B. M., Morcrette, J.-J., Park, B.-K., Peubey, C., de Rosnay, P., Tavolato, C., Thepaut, J.-N., and Vitart, F.: The ERA-Interim reanalysis: configuration and performance of the data assimilation system, Q J Roy. Meterol. Soc., 137, 553–597, 2011.

Dethof, A., O'Neill, A., Slingo, J. M., and Smit, H. G. J.: A mechanism for moistening the lower stratosphere involving the Asian summer monsoon, Q. J. R. Meteorol. Soc., 125, 1079–1106, 1999.

Dietmüller, S., Ponater, M., and Sausen, R.: Interactive ozone induces a negative feedback in CO2-driven climate change simulations, Journal of Geophysical Research: Atmospheres, 119, 1796–1805, https://agupubs.onlinelibrary.wiley.com/doi/abs/10.1002/2013JD020575, 2014.

Dietmüller, S., Jöckel, P., Tost, H., Kunze, M., Gellhorn, C., Brinkop, S., Frömming, C., Ponater, M., Steil, B., Lauer, A., and Hendricks, J.: A new radiation infrastructure for the Modular Earth Submodel System (MESSy, based on version 2.51), Geoscientific Model Development, 9, 2209–2222, https://www.geosci-model-dev.net/9/2209/2016/, 2016.

Frierson, D. M. W., Held, I. M., and Zurita-Gotor, P.: A Gray-Radiation Aquaplanet Moist GCM. Part I: Static Stability and Eddy Scale, Journal of the Atmospheric Sciences, 63, 2548–2566, https://doi.org/10.1175/JAS3753.1, 2006.

Garny, H. and Randel, W.: Dynamical variability in the Asian monsoon anticyclone observed in potential vorticity and correlations with tracer distributions, J. Geophys. Res. Atmos., 118, 1–13, 2013.

Garny, H. and Randel, W. J.: Transport pathways from the Asian monsoon anticyclone to the stratosphere, Atmospheric Chemistry and Physics, 16, 2703–2718, http://www.atmos-chem-phys.net/16/2703/2016/, 2016.

Gerber, E. P.: Stratospheric versus Tropospheric Control of the Strength and Structure of the Brewer-Dobson Circulation, J. Atmos. Sci., 69, 2857–2877, 2012.

Gerber, E. P. and Polvani, L.: Stratosphere-Troposphere Coupling in a Relatively Simple AGCM: The Importance of Stratospheric Variability, Journal of Climate, 22, 1920–1933, 2009.

Gerber, E. P. and Vallis, G. K.: Eddy-Zonal Flow Interactions and the Persistence of the Zonal Index, J. Atmos. Sci., 64, 2007.

Gill, A. E.: Some simple solutions for heat-induced tropical circulation, Q. J. R. Meteorol. Soc., 106, 447–462, 1980.

Held, I. I. M. and Suarez, M. M. J.: A proposal for the intercomparison of the dynamical cores of atmospheric general circulation models, Bull. Amer. Meteor. Soc., pp. 1825–1830, 1994.

Held, I. M.: The Gap between Simulation and Understanding in Climate Modeling, Bulletin of the American Meteorological Society, 86, 1609–1614, https://doi.org/10.1175/BAMS-86-11-1609, 2005.

Hoskins, B. J. and Rodwell, M. J.: A Model of the Asian Summer Monsoon. Part I: The Global Scale, J. Atmos. Sci., 52, 1329–1340, http://dx.doi.org/10.1175/1520-0469(1995)052<1329:AMOTAS>2.0.CO;2, 1995.

Hsu, C. J. and Plumb, R. A.: Nonaxisymmetric Thermally Driven Circulations and Upper-Tropospheric Monsoon Dynamics, J. Atmos. Sci., 57, 1255–1276, http://dx.doi.org/10.1175/1520-0469(2000)057<1255:NTDCAU>2.0.CO;2, 2000.

Jeevanjee, N., Hassanzadeh, P., Hill, S., and Sheshadri, A.: A perspective on climate model hierarchies, Journal of Advances in Modeling Earth Systems, 9 (4), 1760–1771, 2017.

Jöckel, P., Sander, R., Kerkweg, A., Tost, H., and Lelieveld, J.: Technical Note: The Modular Earth Submodel System (MESSy) - a new approach towards Earth System Modeling, Atmospheric Chemistry and Physics, 5, 433–444, https://www.atmos-chem-phys.net/5/433/2005/, 2005.

Jöckel, P., Tost, H., Pozzer, A., Brühl, C., Buchholz, J., Ganzeveld, L., Hoor, P., Kerkweg, A., Lawrence, M. G., Sander, R., Steil, B., Stiller, G., Tanarhte, M., Taraborrelli, D., van Aardenne, J., and Lelieveld, J.: The atmospheric chemistry general circulation model ECHAM5/MESSy1: consistent simulation of ozone from the surface to the mesosphere, Atmos. Chem. Phys., 6, 5067–5104, 2006.

Jöckel, P., Kerkweg, A., Buchholz-Dietsch, J., Tost, H., Sander, R., and Pozzer, A.: Technical Note: Coupling of chemical processes with the Modular Earth Submodel System (MESSy) submodel TRACER, Atmospheric Chemistry and Physics, 8, 1677–1687, https://www.atmos-chem-phys.net/8/1677/2008/, 2008.

Jöckel, P., Kerkweg, A., Pozzer, A., Sander, R., Tost, H., Riede, H., Baumgaertner, A., Gromov, S., and Kern, B.: Development cycle 2 of the Modular Earth Submodel System (MESSy2), Geoscientific Model Development, 3, 717–752, https://www.geosci-model-dev.net/3/717/2010/, 2010.

Jöckel, P., Tost, H., Pozzer, A., Kunze, M., Kirner, O., Brenninkmeijer, C. A. M., Brinkop, S., Cai, D. S., Dyroff, C., Eckstein, J., Frank, F., Garny, H., Gottschaldt, K.-D., Graf, P., Grewe, V., Kerkweg, A., Kern, B., Matthes, S., Mertens, M., Meul, S., Neumaier, M., Nützel, M., Oberländer-Hayn, S., Ruhnke, R., Runde, T., Sander, R., Scharffe, D., and Zahn, A.: Earth System Chemistry integrated Modelling (ESCiMo) with the Modular Earth Submodel System (MESSy) version 2.51, Geoscientific Model Development, 9, 1153–1200, https://www.geosci-model-dev.net/9/1153/2016/, 2016.

Jucker, M. and Gerber, E. P.: Untangling the Annual Cycle of the Tropical Tropopause Layer with an Idealized Moist Model, Journal of Climate, 30, 7339–7358, https://doi.org/10.1175/JCLI-D-17-0127.1, 2017.

Jucker, M., Fueglistaler, S., and Vallis, G. K.: Maintenance of the Stratospheric Structure in an Idealized General Circulation Model, Journal of the Atmospheric Sciences, 70, 3341–3358, 2013.

Kerkweg, A., Sander, R., Tost, H., and Jöckel, P.: Technical note: Implementation of prescribed (OFFLEM), calculated (ONLEM), and pseudo-emissions (TNUDGE) of chemical species in the Modular Earth Submodel System (MESSy), Atmospheric Chemistry and Physics, 6, 3603–3609, https://www.atmos-chem-phys.net/6/3603/2006/, 2006.

Lindgren, E. A., Sheshadri, A., and Plumb, R. A.: Sudden Stratospheric Warming Formation in an Idealized General Circulation Model Using Three Types of Tropospheric Forcing. Atmospheres,, Journal of Geophysical Research:, 123(18), 10,125–10,139, 2018.

Liu, Y., Hoskins, B., and Blackburn, M.: Impact of Tibetan Orography and Heating on the Summer Flow over Asia, J. Meteorol. Soc. Jpn., 85B, 1–19, 2007.

Maher, P., Gerber, E. P., Medeiros, B., Merlis, T., Sherwood, S., Sheshadri, A., Sobel, A., Vallis, G., Voigt, A., and Zurita-Gotor, P.: The value of hierarchies and simple models in atmospheric research, Reviews of Geophysics, submitted, 2018.

Merlis, T. M., Schneider, T., Bordoni, S., and Eisenman, I.: Hadley Circulation Response to Orbital Precession. Part I: Aquaplanets, Journal of Climate, 26, 740–753, https://doi.org/10.1175/JCLI-D-11-00716.1, 2013.

Nützel, M., Dameris, M., and Garny, H.: Movement, drivers and bimodality of the South Asian High, Atmos. Chem. Phys., 16, 14 755–14 774, http://www.atmos-chem-phys.net/16/14755/2016/, 2016.

Pan, L. L., Honomichl, S. B., Kinnison, D. E., Abalos, M., Randel, W. J., Bergman, J. W., and Bian, J.: Transport of chemical tracers from the boundary layer to stratosphere associated with the dynamics of the Asian summer monsoon, Journal of Geophysical Research: Atmospheres, 121, 14,159–14,174, 2016JD025616, 2016.

Polvani, L. M. and Kushner, P. J.: Tropospheric response to stratospheric perturbations in a relatively simple general circulation model, Geophys. Res. Lett., pp. 40–43, 2002.

Polvani, L. M., Clement, A. C., Medeiros, B., Benedict, J. J., and Simpson, I. R.: When less is more: Opening the door to simpler climate models, Eos, 98, 2017.

Pozzer, A., Jöckel, P., Kern, B., and Haak, H.: The Atmosphere-Ocean General Circulation Model EMAC-MPIOM, Geoscientific Model Development, 4, 771–784, https://www.geosci-model-dev.net/4/771/2011/, 2011.

Randel, W., Udelhofen, P., Fleming, E., Geller, M., Gelman, M., Hamilton, K., Karoly, D., Ortland, D., Pawson, S., Swinbank, R., Wu, F., Baldwin, M., Chanin, M.-L., Keckhut, P., Labitzke, K., Remsberg, E., Simmons, A., and Wu, D.: The SPARC Intercomparison of Middle-Atmosphere Climatologies, Journal of Climate, 17, 986–1003, 2004.

Randel, W. J. and Park, M.: Deep convective influence on the Asian summer monsoon anticyclone and associated tracer variability observed with Atmospheric Infrared Sounder (AIRS), J. Geophys. Res., 111, D12 314, http://dx.doi.org/10.1029/2005JD006490, 2006.

Sander, R., Jöckel, P., Kirner, O., Kunert, A. T., Landgraf, J., and Pozzer, A.: The photolysis module JVAL-14, compatible with the MESSy standard, and the JVal PreProcessor (JVPP), Geoscientific Model Development, 7, 2653–2662, https://www.geosci-model-dev.net/7/2653/2014/, 2014.

Sander, R., Baumgaertner, A., Cabrera-Perez, D., Frank, F., Gromov, S., Grooß, J.-U., Harder, H., Huijnen, V., Jöckel, P., Karydis, V. A., Niemeyer, K. E., Pozzer, A., Riede, H., Schultz, M. G., Taraborrelli, D., and Tauer, S.: The community atmospheric chemistry box model CAABA/MECCA-4.0, Geoscientific Model Development, 12, 1365–1385, https://www.geosci-model-dev.net/12/1365/2019/, 2019.

Scheffer, M., Bascompte, J., Brock, W. A., Brovkin, V., Carpenter, S. R., Dakos, V., Held, H., van Nes, E. H., Rietkerk, M., and Sugihara, G.: Early-warning signals for critical transitions, Nature, 461, 53–59, 2009.

Schubert, W. H. and Masarik, M. T.: Potential vorticity aspects of the MJO, Dynamics of Atmospheres and Oceans, 42, 127 – 151, http://www.sciencedirect.com/science/article/pii/S037702650600039X, 2006.

Schulzweida, U.: CDO User Guide (Version 1.9.6), https://code.mpimet.mpg.de/projects/cdo/wiki/Cite, 2019.

Sheshadri, A., Plumb, R. A., and Gerber, E. P.: Seasonal Variability of the Polar Stratospheric Vortex in an Idealized AGCM with Varying Tropospheric Wave Forcing, Journal of the Atmospheric Sciences, 72, 2248–2266, 2015.

Siu, L. W. and Bowman, K. P.: Forcing of the Upper-Tropospheric Monsoon Anticyclones, Journal of the Atmospheric Sciences, 76, 1937–1954, 2019.

Son, S.-W., Gerber, E. P., Perlwitz, J., Polvani, L. M., Gillett, N. P., Seo, K.-H., Eyring, V., Shepherd, T. G., Waugh, D., Akiyoshi, H., Austin, J., Baumgaertner, A., Bekki, S., Braesicke, P., Brühl, C., Butchart, N., Chipperfield, M. P., Cugnet, D., Dameris, M., Dhomse, S., Frith, S., Garny, H., Garcia, R., Hardiman, S. C., Jöckel, P., Lamarque, J. F., Mancini, E., Marchand, M., Michou, M., Nakamura, T., Morgenstern, O., Pitari, G., Plummer, D. A., Pyle, J., Rozanov, E., Scinocca, J. F., Shibata, K., Smale, D., Teyssedre, H., Tian, W., and Yamashita, Y.: Impact of stratospheric ozone on Southern Hemisphere circulation change: A multimodel assessment, Journal of Geophysical Research: Atmospheres, 115, d00M07, 2010.

SPARC: SPARC Intercomparison of Middle Atmosphere Climatologies, Edited by W. Randel, M.-L. Chanin and C. Michaut, Tech. rep., SPARC Report No. 3, 2002.

Tan, Z., Lachmy, O., and Shaw, T. A.: The Sensitivity of the Jet Stream Response to Climate Change to Radiative Assumptions, Journal of Advances in Modeling Earth Systems, 11, 934–956, https://agupubs.onlinelibrary.wiley.com/doi/abs/10.1029/2018MS001492, 2019.

Turner, A. G. and Annamalai, H.: Climate change and the South Asian summer monsoon, Nature Clim. Change, 2, 587–595, http://dx.doi.org/10.1038/nclimate1495, 2012.

Vallis, G. K., Colyer, G., Geen, R., Gerber, E., Jucker, M., Maher, P., Paterson, A., Pietschnig, M., Penn, J., and Thomson, S. I.: Isca, v1.0: a framework for the global modelling of the atmospheres of Earth and other planets at varying levels of complexity, Geoscientific Model Development, 11, 843–859, https://www.geosci-model-dev.net/11/843/2018/, 2018.

Vogel, B., Günther, G., Müller, R., Grooß, J.-U., Hoor, P., Krämer, M., Müller, S., Zahn, A., and Riese, M.: Fast transport from Southeast Asia boundary layer sources to northern Europe: rapid uplift in typhoons and eastward eddy shedding of the Asian monsoon anticyclone, Atmos. Chem. Phys., 14, 12 745–12 762, 2014.

Vogel, B., Günther, G., Müller, R., Grooß, J.-U., and Riese, M.: Impact of different Asian source regions on the composition of the Asian monsoon anticyclone and of the extratropical lowermost stratosphere, Atmos. Chem. Phys., 15, 13 699–13 716, http://www.atmos-chem-phys.net/15/13699/2015/, 2015.

Wan, H., Giorgetta, M., and Bonaventura, L.: Ensemble Held-Suarez Test with a Spectral Transform Model: Variability, Sensitivity, and Convergence, Monthly Weather Review, 136, 1075–1092, 2008.

Wang, S., Gerber, E. P., and Polvani, L. M.: Abrupt circulation responses to tropical upper-tropospheric warming in a relatively simple stratosphere-resolving AGCM, Journal of Climate, 25(12), 2012.

Wei, W., Zhang, R., Wen, M., Rong, X., and Li, T.: Impact of Indian summer monsoon on the South Asian High and its influence on summer rainfall over China, Clim. Dynam., 43, 1257–1269, http://dx.doi.org/10.1007/s00382-013-1938-y, 2014.

Wei, W., Zhang, R., Wen, M., Kim, B.-J., and Nam, J.-C.: Interannual Variation of the South Asian High and Its Relation with Indian and East Asian Summer Monsoon Rainfall, J. Climate, 28, 2623–2634, http://dx.doi.org/10.1175/JCLI-D-14-00454.1, 2015.

Yano, J.-I. and L. McBride, J.: An Aquaplanet Monsoon, Journal of the Atmospheric Sciences, 55, 1373–1399, http://dx.doi.org/10.1175/1520-0469(1998)055<1373:AAM>2.0.CO;2, 1998.

Zhang, Q., Wu, G., and Qian, Y.: The Bimodality of the 100 hPa South Asia High and its Relationship to the Climate Anomaly over East Asia in Summer, J. Meteor. Soc. Japan, 80, 733–744, 2002.